POLITECNICO DI TORINO

Master's Degree in Electronic Engineering

Master's Degree Thesis

Hardware and Software sEMG-based Analyses for Stimulation Artifact Suppression

Supervisors

Prof. Danilo DEMARCHI

Ph.D. Paolo MOTTO ROS

M.Sc. Fabio ROSSI

M.Sc. Andrea MONGARDI

Candidate

Miriam ROCCAZZELLA

267520

TORINO, December 2021

Abstract

Functional Electrical Stimulation (FES) is currently one of the most used technique for muscle rehabilitation in order to help the patient in the recovery of voluntary movement by controlling muscle contraction and functional recovery.

A physiotherapist-patient system, such as the one used for this thesis, implies the presence of two subjects: the physiotherapist who performs a certain movement and the patient to whom the same movement is induced by electrostimulation. To obtain this result, the stimulation pattern derives from the analysis of the surface ElectroMyoGraphic (sEMG) signal, taken by the physiotherapist during the execution of the movement, which determines the amplitude of the FES impulse. Once extrapolated, the electrostimulation pattern is applied to the second subject (the patient) to induce movement replication.

Since the goal is to improve the acquisition front-end leading to a closed-loop application, it is necessary to record the sEMG signal also from the patient during the stimulation in order to be able to analyze the muscle response.
To achieve this is necessary to improve the interface between the acquisition device and the human body. As this device is aimed at rehabilitation and regular use during the day, the main features must be wearability, low power consumption being battery-powered, and high sEMG quality during movement execution to properly detect muscle activity and muscle fatigue resulting from electrical stimulation.

The first part of the thesis is aimed to investigate the performance of the device with and without the Driven Right Leg (DRL) circuit evaluating the Signal to Noise Ratio of both configurations.
Following different combinations of feedback and output resistors, evaluating the performances in terms of SNR in motion and in rest conditions, it emerged that the contribution of the DRL is useful to stabilize the signal taken in dynamic conditions. The SNR value using the DRL is equal to 23.03 dB, while without its use 19.56 dB were obtained. Therefore, the use of the DRL in the acquisition front-end has been confirmed.

The second part of the thesis concerns the detection of muscle voluntary response during electrical stimulation. To perform this analysis by sEMG it is necessary to find a way to minimize to minimize the impact on the acquired signal of stimulation artifacts (SA) that saturate the acquisition channel.
For this reason an hardware-based blanking technique has been investigated. This

technique involves switches on the input of the acquisition channel which allow to disconnect the body when the stimulation impulse is detected.
Following several tests, it is evident that the SA has been removed so the initial situation has certainly improved but not entirely as some artifacts continue to be present and do not allow effective analysis of the signal.

It was therefore necessary to face the issue by changing approach and moving to software-based SA removal techniques. In particular, it was decided to take the signal from the muscle adjacent to the stimulated one in order to remove the artifact.
The choice to analyze the adjacent muscle has been taken since the SA, even though is still present due to the cross-talk between nearby muscles, has a duration about ten times lower. For this reason the software SA removal, based on the subtraction of the SA from the sEMG signal combined with the ATC technique, it made it possible to effectively distinguish the moments of voluntary activation as the number of events above the threshold is greater (about 20) than the events identified during stimulation alone (about 10).

Summary

According to the World Health Organization just under 0.1% of the population has a spinal cord injury, this means that about 8 million people worldwide suffer from some form of paralysis whose severity and extent depend on the location of the spinal cord injury (SCI). In recent decades, various forms of rehabilitation have been investigated, among these the one that has obtained the best results is that based on functional electrical stimulation (FES). It is currently used in the rehabilitation field in order to help the patient in the recovery of voluntary movement and consequently of partial independence. It is not able to regenerate nerve tissues and does not represent a cure for neurological disorders but it is a muscle stimulation technique whose purpose is to control the contraction and functional recovery. FES uses impulses of low energy current safer than voltage pulses as any changes in impedance do not modify the charge injected into the tissue.

In practical applications it is of fundamental importance that the control of the FES and the processing of the surface EMG (sEMG) signal take place in real time since the stimulation patterns and the control of the stimulation itself depend on the features of the EMG signal.

The EMG signal is the graphic representation of the electrical functioning of the muscle, since it can also be taken from the surface of the skin from several decades it has become the preferred method for the study of the muscle as it allows to have an analysis detailed and non-invasive. The force exerted and the amplitude of the sEMG signal are closely related and for this reason it is possible to measure the force produced by a muscle and its behaviour by observing the characteristics of the sEMG signal.

A physiotherapist-patient system, such as the one used for this thesis, implies the presence of two subjects: the physiotherapist who performs a certain movement and the patient to whom the same movement is induced by electrostimulation. To obtain this result, the stimulation pattern derives from the analysis of the sEMG signal, taken by the physiotherapist during the execution of the movement, which determines the amplitude of the FES pulse. Once extrapolated, the stimulation

pattern is applied to the second subject (the patient) to induce movement replication.

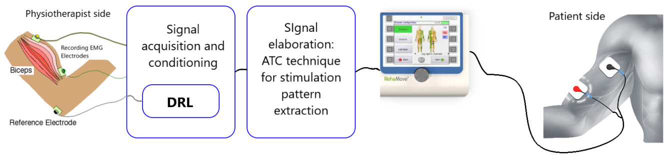

Figure 1: Schematic representation of physioterapist-patient system

Since the goal is to improve the front-end acquisition to the device leading to a closed-loop application it is necessary to record the EMG signal also from the patient during the stimulation in order to be able to analyze the muscle response. To achieve this is necessary to improve the interface between the acquisition board and the human body. Being a device aimed at rehabilitation and constant use during the day, the main features must be complete wearability, low power consumption as it is battery powered, the accuracy of the signal acquired during movement and the detection of signs of fatigue or voluntary response following electrical stimulation.

The first part of the work focused on optimizing the existing acquisition board. In particular, the board must amplify and filter the signal coming from the muscle in order to make it suitable for analysis and re-processing. In fact, the pure sEMG signal has an amplitude that varies between a few hundreds μV and tens of mV which, if left unchanged, would be difficult to interpret.
The acquired sEMG signal is sent in input to the hardware platform, which amplifies it with a gain of 500 or 250 in the band between 30 Hz and 400 Hz in order to eliminate high frequency noises and artifacts due to movements between the electrodes and skin. Finally, the processing of the event-driven signal is carried out using a hysteresis threshold comparator.
On the feedback branch, necessary to stabilize the signal, there is the Driven Right Leg (DRL) circuit which is often used in devices with biomedical applications for the measurement of biopotentials to reduce electromagnetic interference (EMI) due to the common mode signal. The basic configuration includes an operational amplifier with negative feedback and output resistance of a few kΩ connected to the reference electrode.
The performance of the device with and without the DRL circuit, whose connection was optional and obtained via solder bridge, was investigated.
Following different combinations of feedback resistors and output resistors, evaluating the performances in terms of SNR in motion and in rest conditions, it emerged that the contribution of the DRL is useful to stabilize the signal taken in motion

since the SNR value using the DRL is equal to 23.03 dB, instead the one without using the DRL is equal to 19.56 dB. The decision was made to keep it on the board with a fixed connection since an improvement in performance has been verified especially in a context of general movement of the patient and not only of the limb on which the sampling of the sEMG signal takes place.

The second part of the thesis concerns the detection of muscle fatigue or muscle voluntary response during electrical stimulation. To perform this analysis again by surface electromyography it is necessary to find a way to avoid the presence of stimulation artifacts (SA) that saturate the acquisition channel, without eliminating the M-wave component.
In particular, the SA is a short duration peak and 1-2V amplitude, after amplification, that can be observed in the EMG signal when the FES is applied during recording. Not having a physiological origin, they are not used for the study of the response to stimulation. In addition, the amplifiers used have a single power supply from 0V to 1.8V, consequently the SA causes the saturation. If we add the fact that each SA, however short, has a duration of tens of ms, the result is that at high stimulation rates it is not possible to see the EMG signal.
The M-wave, on the other hand, represents the response evoked by the muscle during stimulation and more specifically the excitability of the muscle membrane during fatigue.

For this reason an hardware-based blanking techniques has been investigated. This technique involves switches on the input of the acquisition channel which allow to disconnect the electrodes, and therefore the body, when the stimulation impulse is detected so as not to record the artifact and avoid saturation.

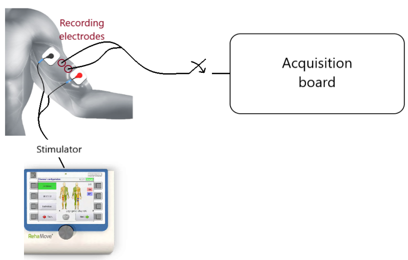

Figure 2: Schematic representation of blanking hardware type techniques

Following several tests, it is evident that the SA has been removed so the initial situation has certainly improved but not entirely as some artifacts continue to be present and do not allow effective analysis of the signal.

It was therefore necessary to find a new approach for muscle analysis during stimulation. Consequently, it was decided to exploit the correlation existing between adjacent muscles and to take the signal from the muscle next to the electrostimulated one. Clearly, precisely because of the existing correlation, the artifact is also present on the adjacent muscle, which in any case causes saturation of the acquisition channel but with a shorter duration of about ten times. For this reason the software SA removal, based on the subtraction of the SA from the sEMG signal, allows to maintain more information about the muscular response to the electrical stimulation.
The software removal technique combined with a filtering process to eliminate disturbances at the stimulation frequency equal to 40Hz and the following two harmonics and the ATC technique has proved effective for the recognition of the voluntary response of the antagonist muscle (ticeps brachii) during electrical stimulation of the biceps brachii. In the figure below are reported the results of this signal processing and it is possible to observe that for each current intensity different from zero 2 voluntary muscular activations are visible only in the third column, the one where the signal processing has been applied

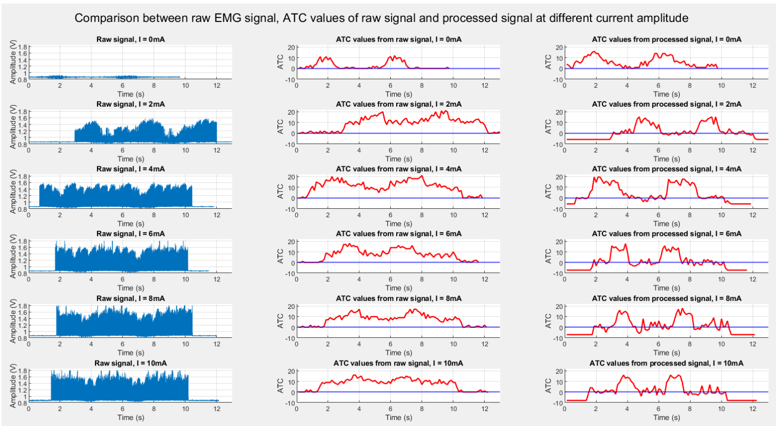

Figure 3: Comparison between ATC values evaluated at different stimulationcurrent intensity

Acknowledgements

Al professor Demarchi vanno la mia stima personale e i miei ringraziamenti per avermi permesso di lavorare a questo studio che mi sta particolarmente a cuore. Ringrazio inoltre Paolo Motto Ros, Fabio, Andrea e Andrea per avermi guidato e consigliato durante tutti questi mesi di lavoro.

Ringrazio particolarmente il professor Zamboni e con lui il professor Martina e il professor Piccinini per aver reso interessante e umanamente arricchente la mia esperienza da rappresentante degli studenti.

Ringrazio tutti gli amici del CLU, di Lavori in Corso, del Poli e di vecchia data per aver contribuito ognuno a modo suo a rendermi la persona che sono oggi e questi anni di studio una meravigliosa avventura.

Infine un grazie speciale va a tutta la mia famiglia e soprattutto a Mamma e Papà che mi hanno supportato e sopportato in tutti questi anni lasciandomi sempre libera di scegliere.

Table of Contents

List of Tables

List of Figures

Acronyms

AP
: Action Potential

K^+
: Potassium ion

Na^+
: Sodium ion

EMG
: Electromyography

sEMG
: Surface Electromyography

IAP
: Intramuscular Action Potential

Ca^+
: Calcium ion

MU
: Motor Unit

Au
: Gold

Ag
: Silver

AgCl
: Silver chloride

ATC
: Average Threshold Crossing

ADC
: Analog to Digital Converter

SNR
: Signal to Noise Ratio

DRL circuit
: Driven Right Leg circuit

FES
: Functional Electrical Stimulation

SCI
: Spinal Cord Injury

SA
: Stimulation Artifact

Chapter 1

Introduction

1.1 Description and functioning of muscular system

1.1.1 The muscular cell

In general, when a cell with intracellular ion concentrations (mEq/L) is placed in an environment with ionic solution of different concentration, an ionic gradient is formed depending on the diffusibility of the ions. In the particular case of the cells of the muscular apparatus, the membrane that separates the internal and external compartments is selectively permeable only to K^+, therefore the diffusion of this ion from the inside towards the outside of the cell begins immediately, with the consequent generation of a negative charge on the inner side of the cell membrane and a positive charge on the outside. As shown in fig.[1.1] an electrochemical equilibrium is established, in which the K^+ diffusibility gradient is of opposite sign with respect to the electric gradient and therefore the membrane is negatively charged.

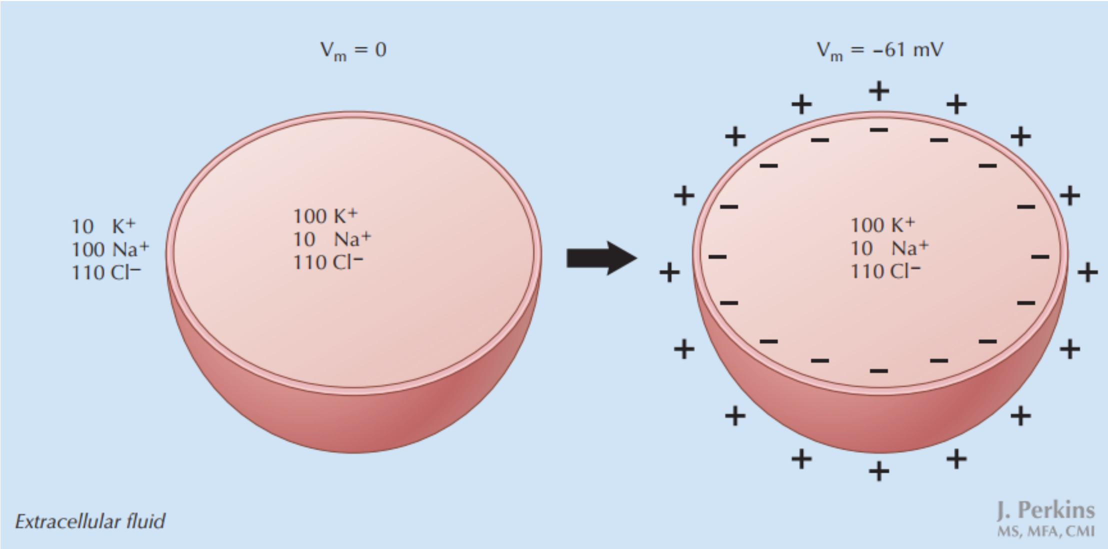

Figure 1.1: Membrane potential of a cell, adapted from [1]

In a simple system with only one permeable ion, the membrane potential V_m can be easily calculated by applying the Nernst equation [1.1].

$$E_x = \frac{RT}{ZF} \cdot \ln \frac{[X]_o}{[X]_i} \tag{1.1}$$

Where:

- E_x is the Nernst potential or equilibrium potential
- $ln\left(\frac{[X]_o}{[X]_i}\right)$ is the natural log of the ratio between the concentration of ion X outside the membrane ($[X]_o$) and the concentration of the ion inside ($[X]_i$)
- $R = 8.314\frac{J}{mol \cdot K}$
- T is the absolute temperature
- Z is the ion charge
- $F = 9.648534 \cdot 10^4$

Taking into account that in the human body the temperature T is about 37°C, the equation can be simplified as follows[1.2]

$$E_x = \frac{61mV}{Z} \cdot \log \frac{[X]_o}{[X]_i} \tag{1.2}$$

In a simple model with a single monovalent cation (e.g. K^+) such as that of the cell whose internal concentration is 10 times greater than the external one, it is possible to calculate the equilibrium potential:

$$E_{K^+} = \frac{61mV}{+1} \cdot \log \frac{0.1mM}{1mM} = 61mV \cdot \log(0.1) = -61mV \tag{1.3}$$

The difference in ionic concentration between the cytosol (intracellular liquid) and the extracellular liquid is due to the transport activity of the Na^+/K^+ ATPase protein, which pumps Na^+ ions out of the cell in exchange for K^+ ions which instead is pumped inside the cell.
Figure [1.2a] schematically represents the operation of the pumping system where the size of the rectangles indicates the relative concentration of ions.

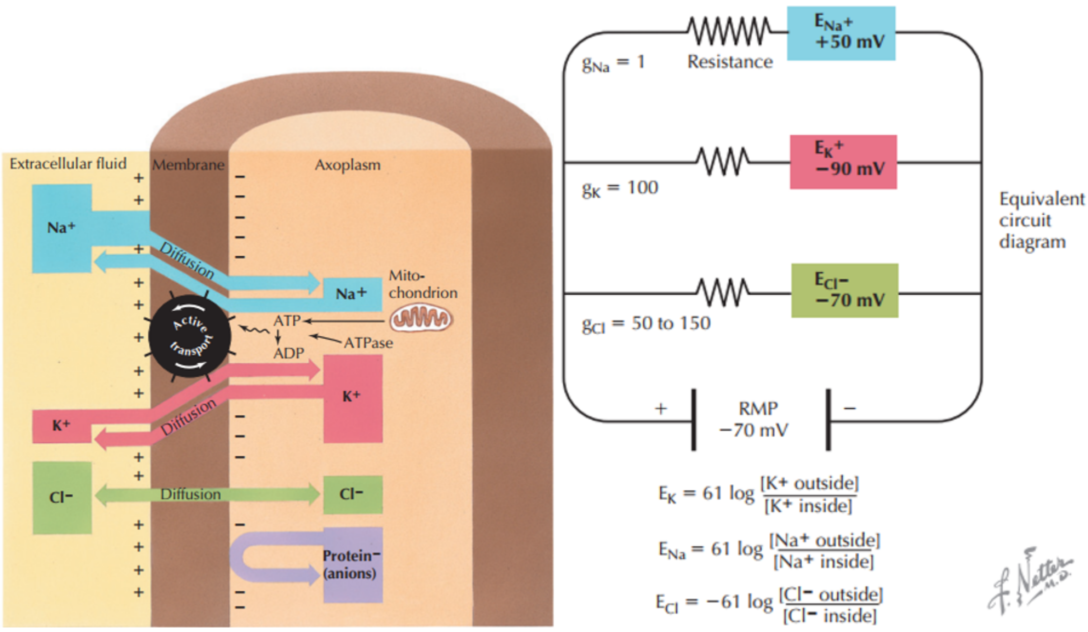

(a) Pumping system of a cell

(b) Equivalent electric circuit of the pumping system

Figure 1.2: Resting membrane potential, adapted from [1]

The loss of K^+ from the cell is the main factor in the genesis of the membrane potential at rest since it is the most permeable ion and therefore the one that has the greatest output speed. Added to this is the fact that the membrane is not permeable to proteins which are negatively charged and are mainly intracellular. In figure [1.2b] this passage of ions is schematized as an electric circuit to which the potential difference values of the ions (mV) and their permeability expressed in

terms of conductance have been added.
As in any circuit, the movement of charges determines a current flow whose direction depends on the potential differences of the system and on the resistance opposed by itself. In order to calculate this current it is convenient to first define the elements and laws used:

- the conductance G = $1/R$ measured in Siemens (S), is generally very small, the body offers a particularly high resistance, so the order of magnitude will be that of nano and/or pico Siemens. From the conductance value it is therefore immediate to derive that of the resistance used in Ohm's law.

- the Ohm law: $V = I \cdot R$ which will be used for the calculation of the ionic current based on membrane potential and conductance.

Given these premises, the ion current can be calculated as the difference between membrane potential and equilibrium potential (1.3):

$$I_x = G(V_m - E_x) \tag{1.4}$$

Then the positive ion K^+ continues to escape from the cell generating a positive current, while the sodium Na^+ enters the cell generating an opposite current. This activity keeps the potential difference constant and is called the sodium-potassium pump.

1.1.2 Action Potentials

Sudden changes in the polarization of the channels for the K^+ and Na^+ ions caused by an electrical or chemical stimulation cause an increase in the permeability of the cell and a consequent depolarization, so that it passes from a voltage of about -60mV to one of about 50mV very quickly and then return just as quickly to the equilibrium potential. This positive voltage peak is defined as Action Potential, the most important characteristics are:

- The **potential threshold**, i.e. the potential to be overcome for an AP to start.

- The **"all-or-none" answer**, which according to the cell type will have a fixed amplitude and shape.

- **Non-decremental propagation**, or the propagation of the AP from one cell to another. This characteristic is linked to the propagation speed which is greater in the largest and myelinated axons.

- The **Refractory Period** is a time interval following the start of the AP during which it is impossible to excite a second AP.

- **Relative refractory period** is a time interval after the absolute refractory period in which a second AP can be generated but requires a much greater stimulus than under normal conditions.

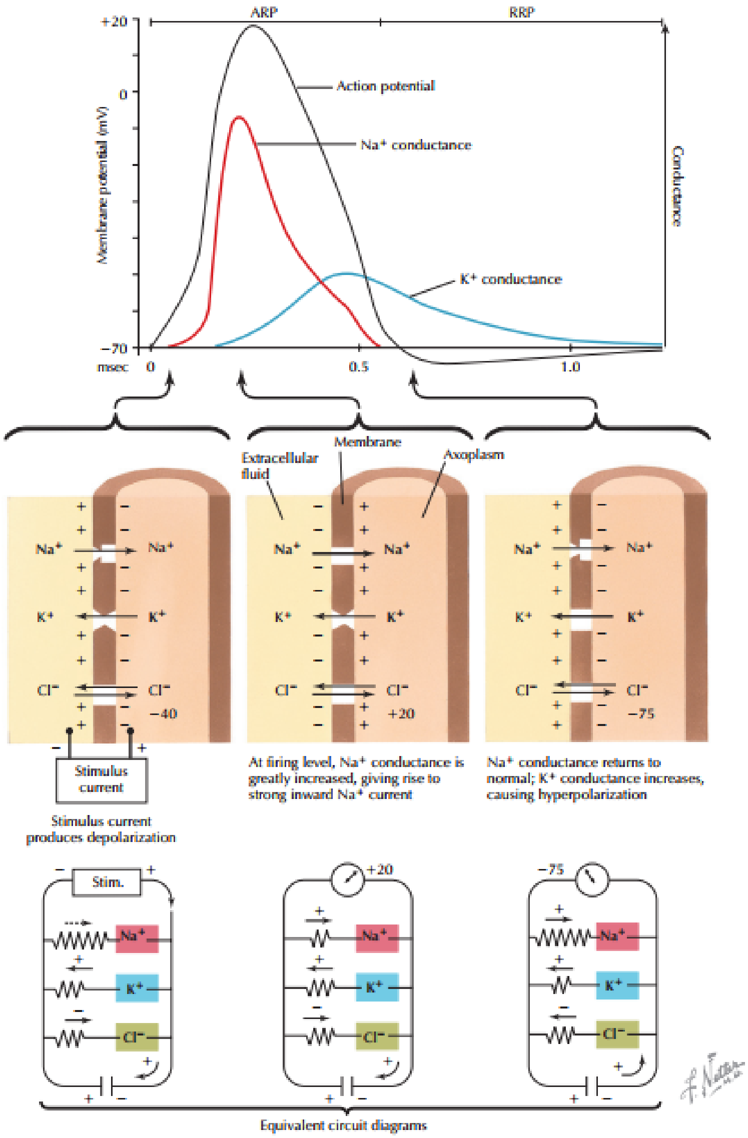

Figure 1.3: Action potential mechanism, adapted from[1]

The synoptic table represented in figure [1.3] illustrates the cellular AP mechanism starting from the electrochemical mode with the variations in conductance of the K^+ and Na^+ ions.
The action potential generated at the axon hillock propagates like a wave along the axon, opening gradually into adjacent Na^+ channels, the absolute refractory period ensures that the propagation of the AP is in a single direction along the axon.
The ionic current is carried by the cytoplasm and is sufficient to depolarize the first two following Ranvier nodes thus allowing rapid signal conduction.

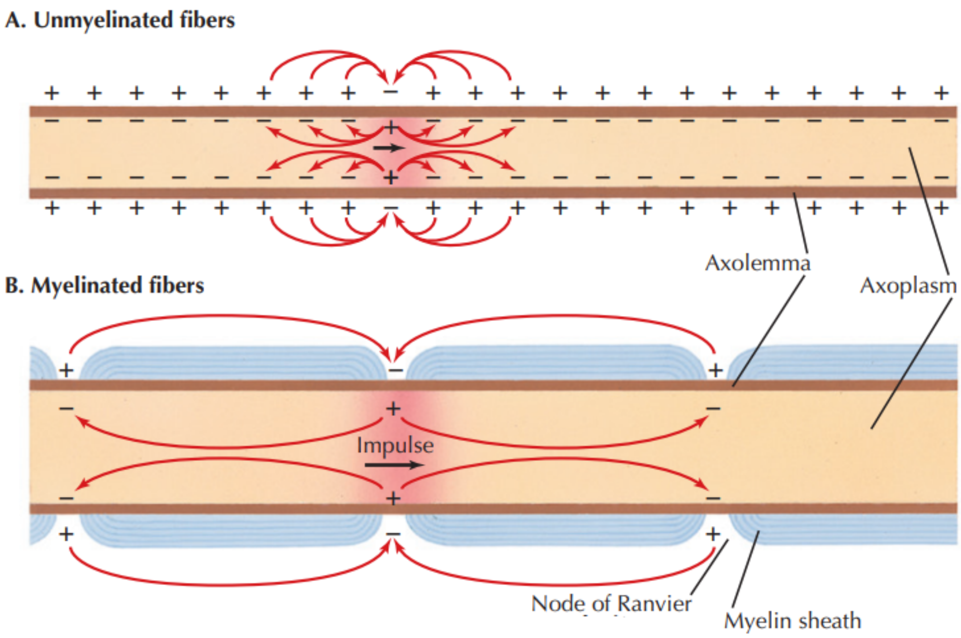

Figure 1.4: Axonal conduction in myelinated and unmyelinated fibers, adapted from [1]

1.1.3 The organization of the skeletal muscle

The basic unit of skeletal muscle is represented by the sarcomere, which is the site where the reciprocal sliding of the actin and myosin filaments produces contraction. The ordered succession of sarcomeres within it produces the characteristic striated appearance.
Figure [1.5] shows from the macro to the micro structure of the muscle and it is possible to observe the single fibers wrapped in a layer of connective tissue called endomysium and the multinucleated cells that compose it. These cells in turn consist of myofibrils which contain a succession of sarcomeres.

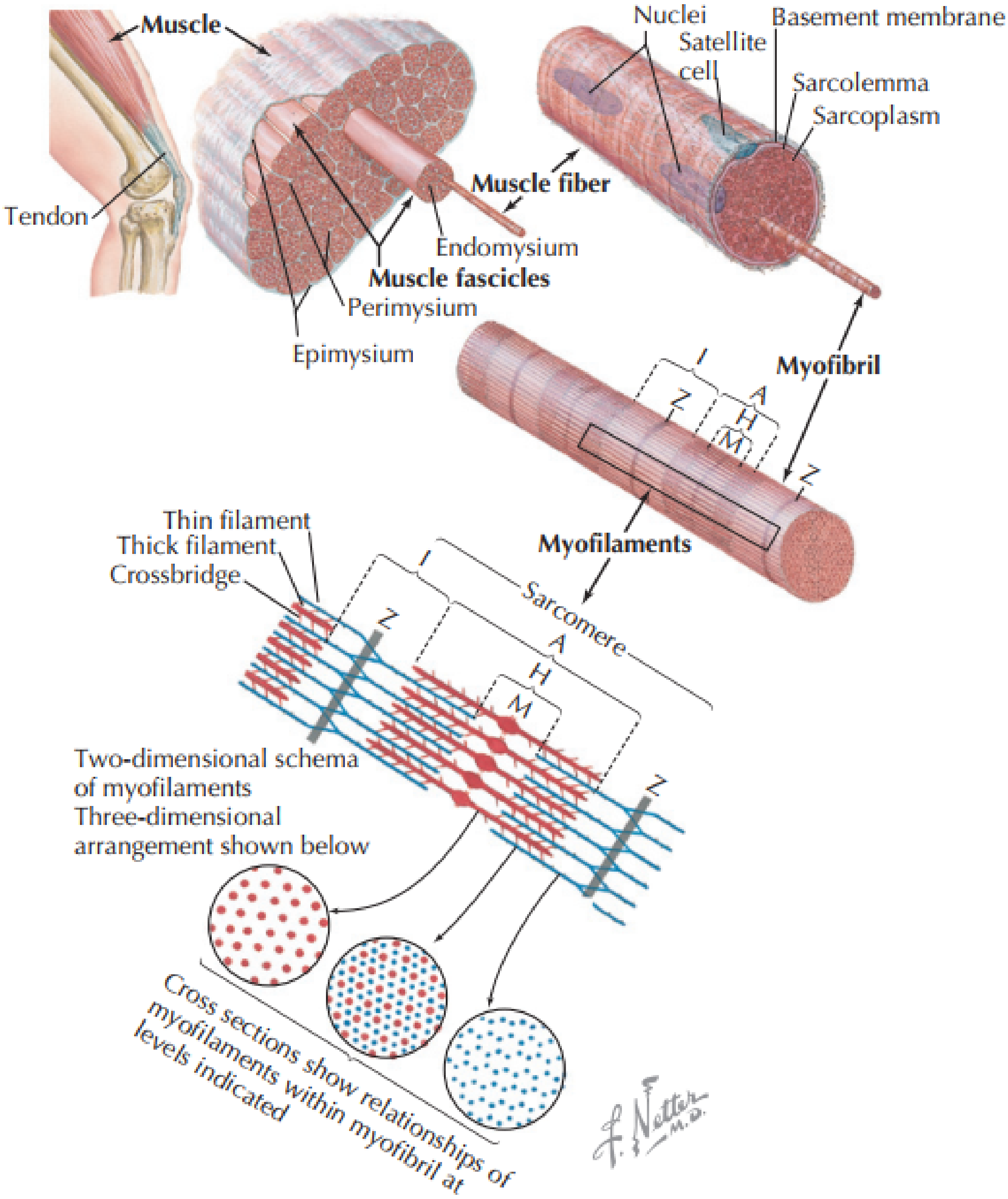

Figure 1.5: Organization of the skeletal muscle, adapted from [1]

The Z line marks the boundary between two sarcomeres. Band I contains only the thin actin filaments, which extend from the Z line towards the center of the sarcomere itself, while the thicker myosin filaments are found in band A, which is characterized by a darker color. The M line is located in the center of the sarcomere and is the site where the thick filaments are connected to each other. Zone H, on the other hand, is an area of the muscle fiber in which there is no overlap between actin and myosin.
Finally, the three cross sections at the bottom of figure [1.5] show the myofibrillar organization respectively in zone H where there are exclusively thick filaments, in zone A in which there are both thick and thin filaments and in zone I in which they are present exclusively the thin filaments.

1.2 The Electromyography

Electromyography is a technique that allows to investigate and graphically represent the potential electric field generated, as seen in section [1.1.1], by the depolarization of the external muscle membrane, the sarcolemma, and therefore to identify the action potentials mentioned in section [1.1.2]. Electrodes that can be intramuscular, needle-like, or surface electrodes are used for this type of analysis. The type of electrode used determines the type of electromyography, the accuracy and invasiveness of the investigation.
The tissue that separates the origin of the potential from the probing electrodes is defined as the conduction volume and its properties determine the characteristics of the recorded signal. In general, it acts as a low-pass filter on the electrical signal coming from the muscle, this effect is considerably less if an intramuscular analysis is performed while for surface electromyography (sEMG) this effect has a greater importance as it causes significant distortions on the signal.
Since all the work was done only with surface electrodes, only the behavior and characteristics of sEMG will be described below.
The schematics [1.6] represents the electrical approximation of a section along the z-axis of the muscle membrane.

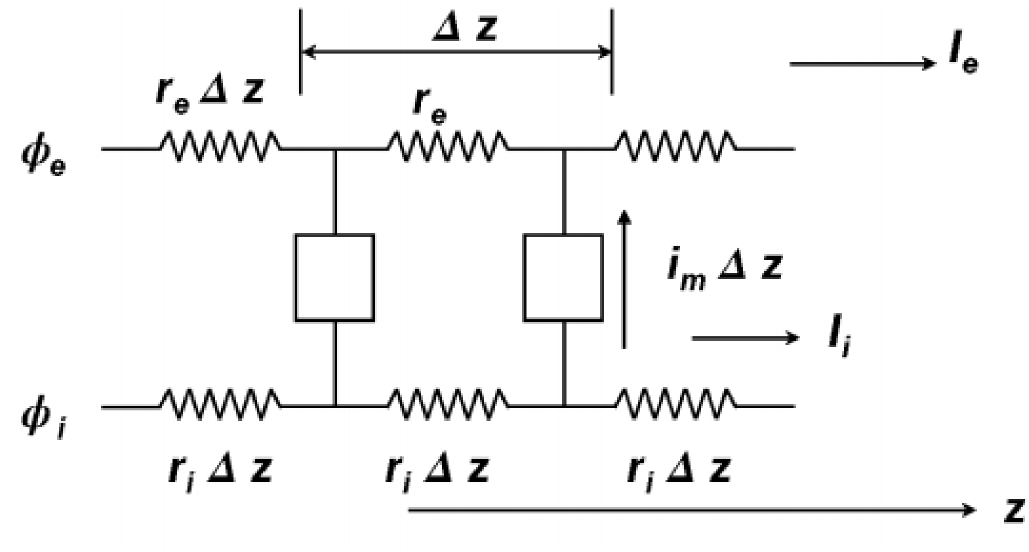

Figure 1.6: Electrical approximation of a muscle membrane, adapted from [2]

From here we can derive an analytical description that shows how the potential decreases according to the length of the fiber, in particular the decrease is given by the product between the resistance per unit length (r_e) and the current (I_e) flowing along the tissue.

$$\frac{\partial \Phi_e}{\partial z} = I_e r_e \tag{1.5}$$

As for the extracellular current, it could decrease as z increases for two reasons: the current flowing through the membrane could decrease or due to losses caused by the surface electrodes.

$$\frac{\partial I_e}{\partial z} = I_m + i_p \tag{1.6}$$

where i_m is the transmembrane current per unit length and i_p is the current flowing through the electrodes. Finally, the transmembrane voltage is given by the difference between the internal potential and the external potential.

$$V_m = \Phi_i - \Phi_e \tag{1.7}$$

The basic unit that is detected during an electromyography is the intramuscular action potential (IAP) in which three main phases can be recognized:

- **depolarization phase**: corresponds to the opening of the Ca-channels, the entry of Ca^+ ions and the consequent peak of potential

- **re-polarization phase**: corresponds to the opening of the K-channels, the entry of K^+ ions and the return of the potential to the starting value (resting potential)
- **hyper-polarization phase**: it precedes the stable return to the resting value in which the membrane has a more negative potential for a short period and then stably assumes the resting value.

The study of the variation in the shape of the IAP allows us to observe the muscle in various conditions, such as that of fatigue in which the amplitude decreases slightly.

Since the sources of EMG signals are not plane waves with constant velocity that travel from less to more infinity, it is necessary to consider some effects such as the one that occurs at the tendon junction where the potential runs out called the end-of-fiber effect.
It is important to emphasize that during application, in the case of surface electrodes, the distance between the source and the detection point and the positioning of the same are relevant issues.
To reduce the low pass filter due to the tissue separating the signal source from the electrodes, and to remove the common mode usually two electrodes are used, plus a third as a reference. The use of multiple electrodes allows you to extract the signal as a linear combination and to obtain more precise information, less affected by noise. The simplest form of bipolar mounting is the differential one in which there are two electrodes (+,-) at a distance of about 1-3cm as depicted in figure[1.7].

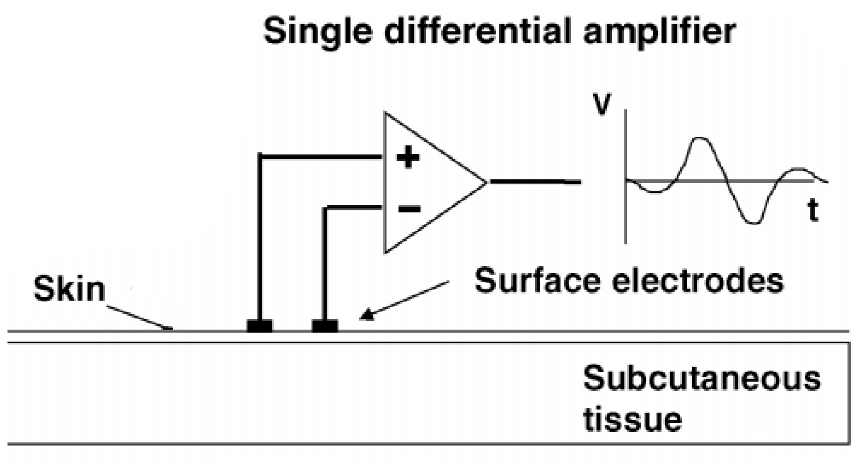

Figure 1.7: Bipolar configuration for EMG signal detection, adapted from [2]

1.2.1 Parameters that affect the EMG feature

The characteristics of an electromyographic signal depend on innumerable anatomical, physical and detection system factors. Those with a higher incidence are:

- the thickness of the subcutaneous tissue layer, the thicker it is and the smaller the amplitude and bandwidth of the signal
- the distance of the surface electrodes from the signal source and consequently the depth of the source
- the inclination of the system with respect to the muscle fibers and the positioning of the electrodes, it is always recommended to position the electrodes longitudinally with respect to the fibers.
- the length of the muscle fiber that is responsible for the end-of-fiber effect
- the inter-electrode distance which must be minimal to reduce spatial filtering
- size and shape of the electrode which, if not carefully chosen, can lead to a decrease in amplitude and frequency content
- the crosstalk between adjacent muscles, i.e. the signal recorded on a specific muscle but generated by the adjacent one.

Crosstalk is a problem that occurs exclusively with surface EMG as the distance between the detection point and the source is of the same order of magnitude for different muscles. To measure the impact of this effect on the measurements, the cross-correlation coefficient is calculated.

1.2.2 Signal amplitude and muscle strength

The strength used and the amplitude of the EMG signal both depend on two factors:

- the recruitment of multiple motor units (MU)
- the increase in the firing rate of the motor units already recruited

For this reason, it is possible to measure the force produced by a muscle by observing the amplitude of the EMG signal. It follows that, again by analyzing the variation in amplitude, it is possible to identify any signs of fatigue.

1.2.3 The electrodes

A fundamental choice concerns the electrodes to be used, in fact, as mentioned in the paragraph [1.2.1], shape, materials, positioning and inter-electrode distance have an important influence on the quality of the signal taken from the muscle. Normally the favored materials for the manufacture of good electrodes are Ag/AgCl (silver/silver chloride), Au (gold), AgCl and Ag since they are materials with high conductivity and consequently allow to better detect the electrical activity of the muscle. In particular, in surface electromyography it is possible to choose mainly between two types of electrodes:

- Wet
- Dry

Wet electrodes are currently the most used since they provide excellent adhesion to the skin and therefore easy application. They are identified as wet as they use an electrolytic gel as an interface between the skin and the metal part of the electrode which allows for a very low electrode-skin impedance. For the metal part Ag-AgCl is usually used which allows a better passage of the current from the muscle through the electrolyte-electrode junction and this means that less noise is introduced during the measurements.

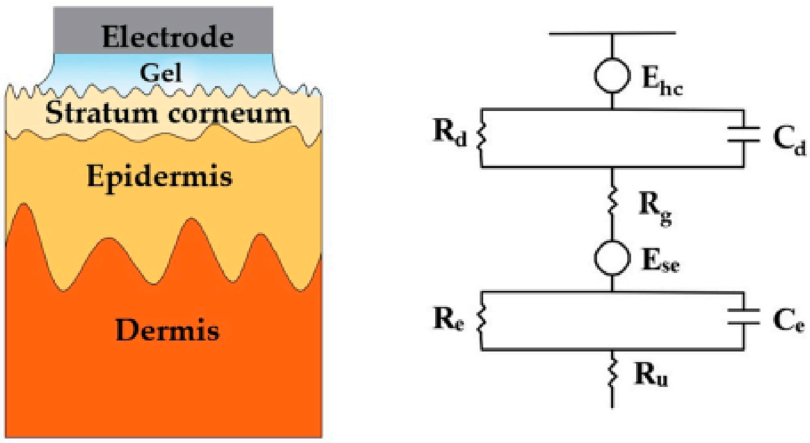

Figure 1.8: Schematic and electrical equivalent of wet electrodes, adapted from [3]

As previously mentioned, the electrode simply represents an interface between the ionic charge generated in the body and the electron flow of the external detection device. Looking at the circuit model in the image [1.8] on the right, starting

from the top it is possible to notice how the interface created when the electrode is attached to the body is of the electrochemical-electrolytic type and generates a half potential cell E_{hc} while the the electrode itself can be modeled as an impedance where C_d is the capacitance and R_d is the resistance.
Continuing we find the resistance R_g which represents the actual resistance due to the effects of the contact between gel and skin. Going forward we have the potential E_{se} caused by the difference in ionic concentration that is generated through the stratum corneum and calculable with the Nernst equation ([1.1]), the entire epidermis is usually modeled as a further impedance with a resistance R_e and a capacitor C_e. Finally we have the resistance R_u which represents the dermis and the subcutaneous layers, a capacitive component is not added as its contribution can be ignored.
The gel electrodes can be reusable but disposable ones are preferred since they are very light and there is no risk of interference due to residues of skin or hairs remaining attached following previous use. There are various shapes and sizes of wet electrodes and often depend on the manufacturer, in any case with a correct application it is possible to have a perfect adhesion to the skin which drastically reduces the risk of displacement even during particularly rapid movements.
Despite everything they have disadvantages that cannot be ignored. First of all, it is not possible to use them for long-term acquisitions since the gel is slowly absorbed and, combined with the effect of the glue on the edge, can cause skin irritation and allergic reactions in particularly delicate subjects. Furthermore, the absorption of the gel causes a significant deterioration in the quality of the recordings.

Dry electrodes are recently finding a wide use in long-term applications as they do not have problems of signal degradation over time and do not cause skin irritation, and they can also be reused.
On the other hand, they are decidedly heavier than wet electrodes and have a much higher electrode-skin impedance that can no longer be ignored. Due to the lack of gel, fixing on the skin is also more complicated: they must be pressed to the skin to have a good contact and in any case they are much more subject to displacement during movements.

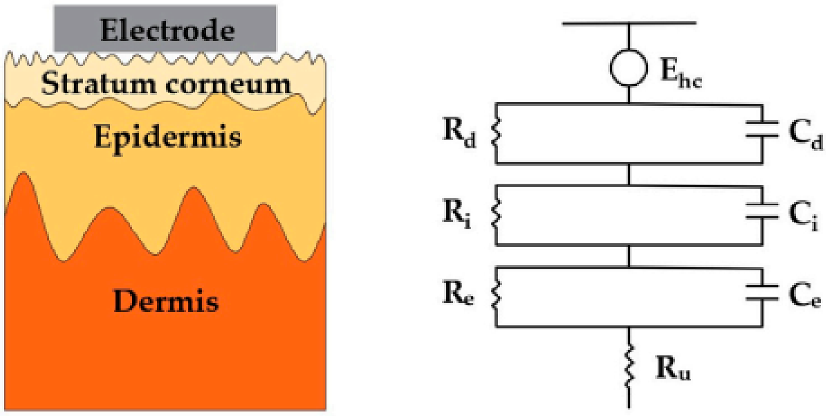

Figure 1.9: Schematic and electrical equivalent of dry electrodes, adapted from [3]

In dry electrodes, since there is no conductive gel, the resistance R_g is replaced by a resistance R_i and a capacitor C_i connected in parallel as shown in figure [1.9].

1.2.4 The Average Threshold Crossing technique (ATC)

A new technique called Average Threshold Crossing (later ATC) was used to delineate the stimulation profile, presented and extensively discussed in [4], [5], [6] and [7].
This allows to considerably reduce the amount of data to be processed and therefore have a lower circuit complexity and lower power consumption, all fundamental aspects for obtaining an increasingly integrated device.
The ATC allows for a quasi-digital conversion without the need for an analog-to-digital converter (ADC) as the entire muscle signal is simply compared with a previously set threshold. The result is the generation of digital pulses whenever the sEMG signal exceeds the threshold.

The sequence of impulses obtained exploits only the temporal dimension and not the amplitude thus reducing the information to be transmitted while maintaining a high correlation with the firing rate of the motor units of the muscle in question and therefore with the force generated. In particular, the information relating to the strength is contained in the time that the sEMG signal takes to return below the threshold. This way of evaluating it is precisely what allows us not to consider the amplitude of the signal.

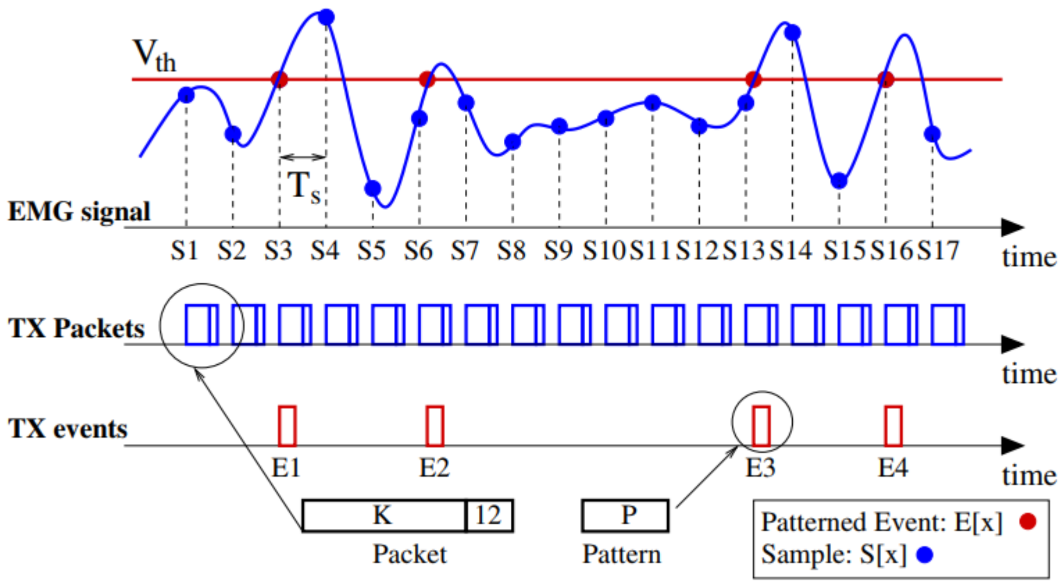

Figure 1.10: Standard EMG signal in comparison with the quasi-digital conversion obtained with ATC technique, adapted from [4]

The stimulation pattern is obtained by dividing the signal into time windows, for each one the suprathreshold events are counted and finally they are summed up to obtain a vector in which each cell contains the total number of suprathreshold events in a time window.
The uniqueness of the activation paths of the muscle fibers that avoid cross-talk interference between different muscles, combined with the robustness of the ATC, allows for a signal-to-noise ratio (SNR) of 5-6 dB.

The generated pulses can be transmitted asynchronously using an RFCMOS Impulse-Radio UWB transceiver chipset, this implies the transmission of a single bit at a time with an unfixed pulse-rate which further simplifies the components, reduces the active silicon area and the power consumption.
Thanks to the reduced complexity, it is possible to easily switch from a single channel to a multi channel system composed of multiple channels with incoming EMG signals that generate ATC events, an "arbiter" to regulate concurrent events, an encoder to form data packets coming from the same channel and finally a transmitter.
In general, with ATC the number of pulses transmitted is considerably lower as the information is represented only by the delay between one trigger event and the next one, this means that no further compression techniques are required to

minimize the data to be transmitted.

1.3 The Mechanomyography

Mechanomyography is another technique for detecting muscle activity which, instead of recording electrical activity, records mechanical activity using MEMS condenser microphones and the information derives from the sum of the pressure pulses detected on the surface of the skin and its trembling. This different type of analysis avoids many of the limits imposed by electrical detection such as the positioning of the electrodes, the preparation of the skin and above all the problem of the stimulation artifact is no longer present as it is not detected.
Clearly, the use of microphones introduces other problems such as noise, the need to design particular cases that allow detecting even the slightest displacement of the skin, the positioning of the transducers is not relevant but their pressure on the skin yes because, if excessive, it could suppress the pressure waves generated by the muscle.

Sofia Milanese in her thesis [8] investigated the use of different types of microphones and the quality of the recorded signals. In general, MEMS condenser microphones are useful in muscle detection of dynamic movements and show greater reliability during daily rehabilitation exercises. The main components are:

- a movable plate, usually made of silicone, free to move if pressure waves are present
- a fixed plate always of silicone

At the output, there will be a variation of the capacitive value provided as a sequence of bits (digital) or as a waveform (analog) based on the type of microphone used.

An analog microphone is best for low-frequency responses and the output values vary between GND and the supply voltage in a band between 10 and 100 Hz.

A digital microphone, such as the one designed by S. Milanese [8] is made up of two modules:

- a $\Sigma\Delta$ modulator that digitizes the signal using a 1-bit ADC converter and a DAC
- a digital filter for decimating the signal, it generates a clock pulse at each rising edge in order to reduce the sampling rate

The digital microphone is able to detect low frequencies but with much greater attenuation than the analog one. However, excluding the question of frequency detection, the digital microphone proved to be more reliable during recordings.

1.4 Topics covered: DRL circuit and SA removal

A physiotherapist-patient system, such as the one used for this thesis, implies the presence of two subjects: the physiotherapist who performs a certain movement and the patient to whom the same movement is induced by electrostimulation. To obtain this result, the stimulation pattern derives from the analysis of the sEMG signal, taken by the physiotherapist during the execution of the movement, which determines the amplitude of the FES pulse. Once extrapolated, the electrostimulation pattern is applied to the second subject (the patient) to induce movement replication.

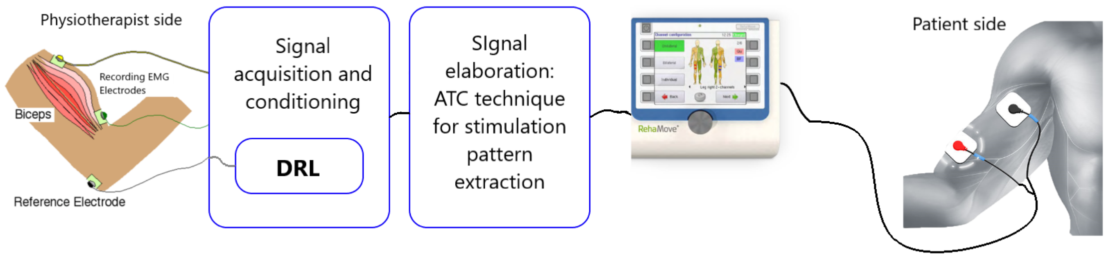

Figure 1.11: Schematic representation of physioterapist-patient system

The main goal is to improve the interface between the acquisition board and the human body in order to upgrade the front-end acquisition of the device to arrive to a closed-loop application.
Being a device aimed at rehabilitation and constant use during the day, the main features must be the complete wearability and therefore reduced dimensions and wireless connections, low energy consumption as it is battery powered, the accuracy of the signal acquired during movement and the detection of any signs of fatigue following electrical stimulation.

The first part is dedicated to the study and analysis of the data acquired by the brachial biceps muscle using two different configurations of the circuit mounted on the breadboard relating to the Apollux3 board and in the final stages the board itself. The two configurations concern in particular the presence or absence of the Driven Right Leg (DRL) circuit and the comparison between the two sEMG output signals was made in terms of signal to noise ratio (SNR).

The second part, on the other hand, is dedicated to the study and design of a circuit part capable of eliminating the stimulation artifacts present in the sEMG signal coming from an electrostimulated muscle (in this case always the brachial biceps).The idea of removing this type of disturbance derives from the desire to also analyze the muscle signal during the electrostimulation phase to detect signs of fatigue or voluntary response.

Chapter 2

State of the art on Functional Electrical Stimulation

According to the World Health Organization ([9]) just under 0.1% the population has a spinal cord injury, this means that about 8 million people worldwide suffer from some form of paralysis whose severity and extent depend on the location of the spinal cord injury (SCI).
In order for the condition of paraplegia or quadriplegia to occur it is necessary that there is an interruption of the signal through the spinal cord since the nerve endings that allow the movements start from there. SCI can be of a traumatic nature (falls, road accidents,...) or non-traumatic (infectious diseases, tumors, congenital problems).
To the paralysis due to SCI are also added those due to strokes.

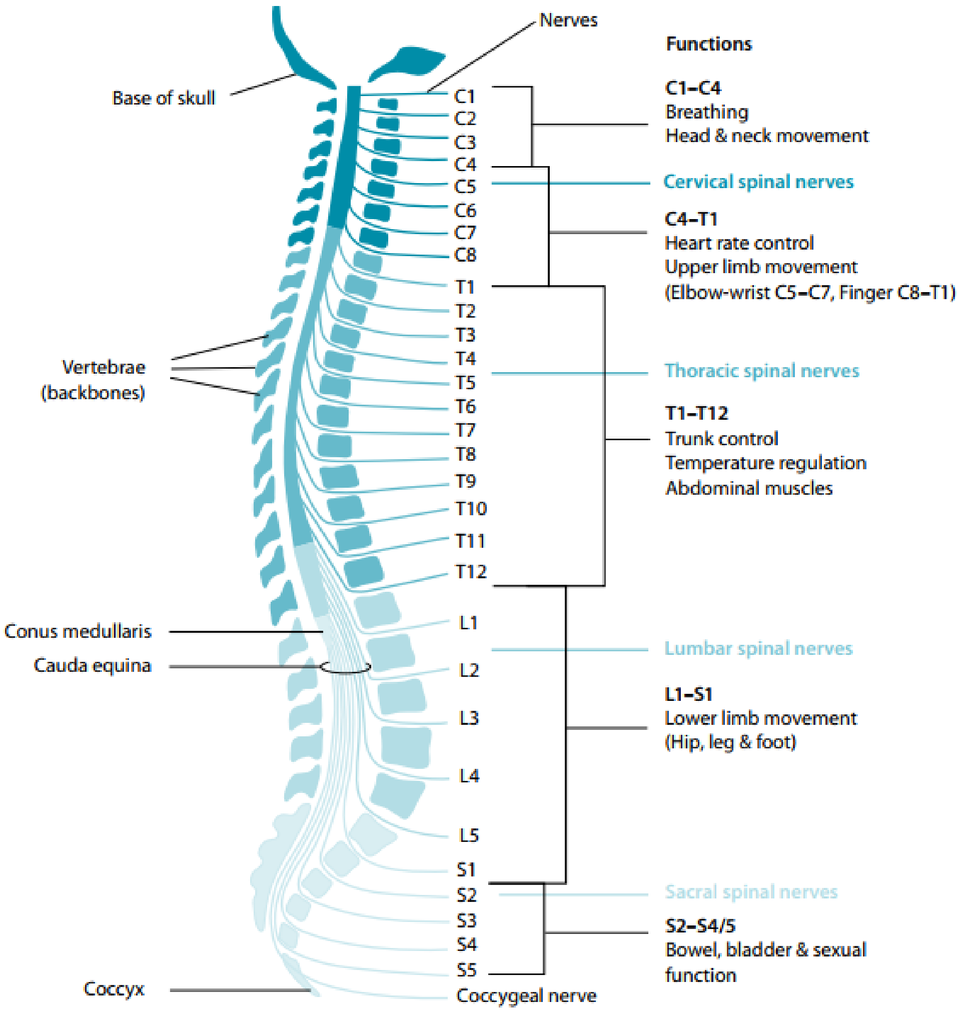

Figure 2.1: Spinal cord and its innervations, adapted from [9]

Bearing in mind that the human body does not have the ability to regenerate nerve tissues, functional electrical stimulation (FES) is a valid solution to allow movement in people suffering from paralysis as it allows you to skip the point where nerve transmission is interrupted and directly stimulate the muscle.

The first application of FES dates back to the 1960s with the aim of correcting foot drop in hemiplegic patients by stimulating the common peroneal nerve when the patient's heel was not in contact with the ground during walking.

Currently the FES is used in the rehabilitation field in order to help the patient in the recovery of voluntary movement and consequently of a partial independence.

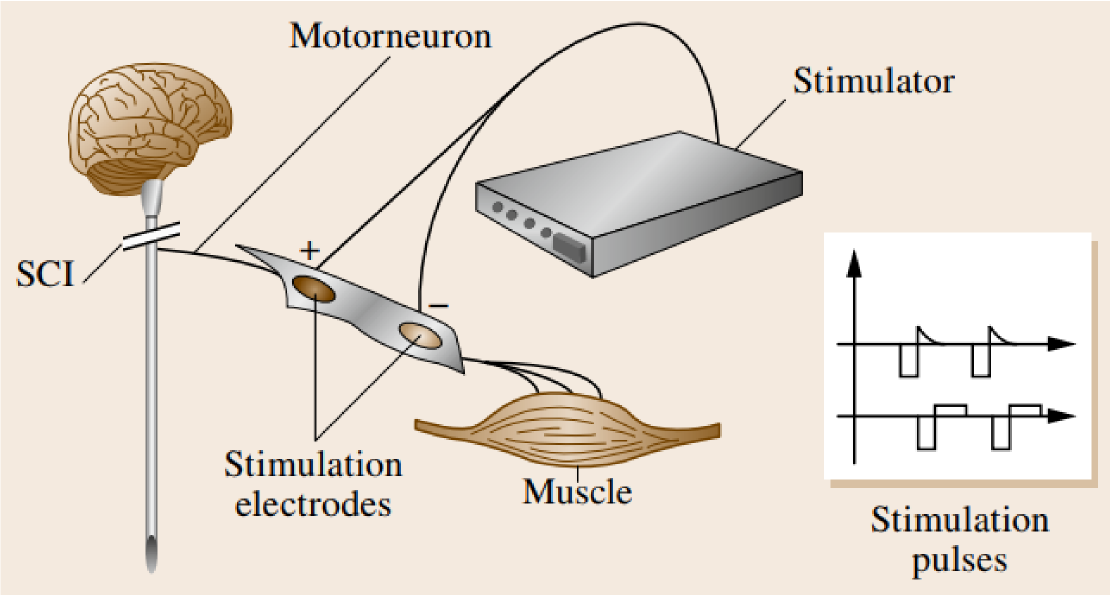

Figure 2.2: Application of FES using surface electrodes, adapted from [10]

FES is unable to regenerate nerve tissues and does not represent a cure for neurological disorders even though it can be integrated with neuroprostheses that permanently replace the physiological mechanisms of movement.

It is a muscle stimulation technique whose purpose is to control contraction and functional recovery as physiologically as possible, for this reason it uses low-energy current pulses. One of the conditions necessary to maintain low current values is to apply the stimulation directly on the motor nerve (i.e on the bundle of motor axons) instead of on the muscle, which would require energies up to three orders of magnitude higher. For this reason it is necessary that the muscle in question is well innervated, if it is not it is possible to intervene surgically to replace it with an innervated one.
Stimulation occurs by injecting a train of rectangular impulses into the nerve as shown in fig.[2.2] and contraction occurs if the membrane potential is high enough to generate an action potential. The pulse can be both monophasic or biphasic, in this case there will be a positive and a negative phase with the aim of removing the charge injected from the tissue. Generally the two impulses are balanced in such a way as to prevent an accumulation of charge in the tissue and the ionization of the electrodes thus avoiding that part of the material of the latter is deposited on the tissues.

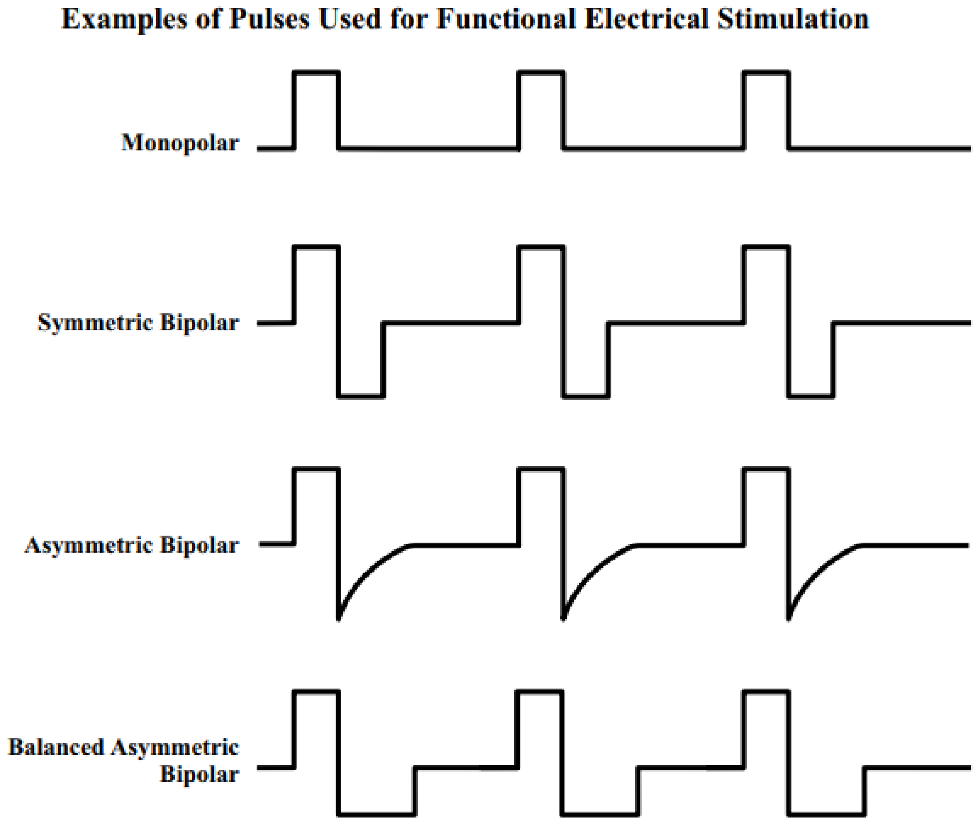

Figure 2.3: Different shape of pulses used in FES, adapted from [11]

Normally the electrodes used are the surface ones which make the technique much more accessible and non-invasive but present some problems related to placement on the skin and greater variability between the subjects which makes the calibration phase fundamental.
Muscle contraction can be achieved with both voltage and current regulated pulses, in both cases the fundamental parameters established during the calibration phase are the pulse width and the stimulation frequency (fig.[2.4]). Current regulation is preferred as it is safer since the impedance variation does not modify the charge injected into the tissue and therefore does not require the continuous adjustment of the stimulation parameters.

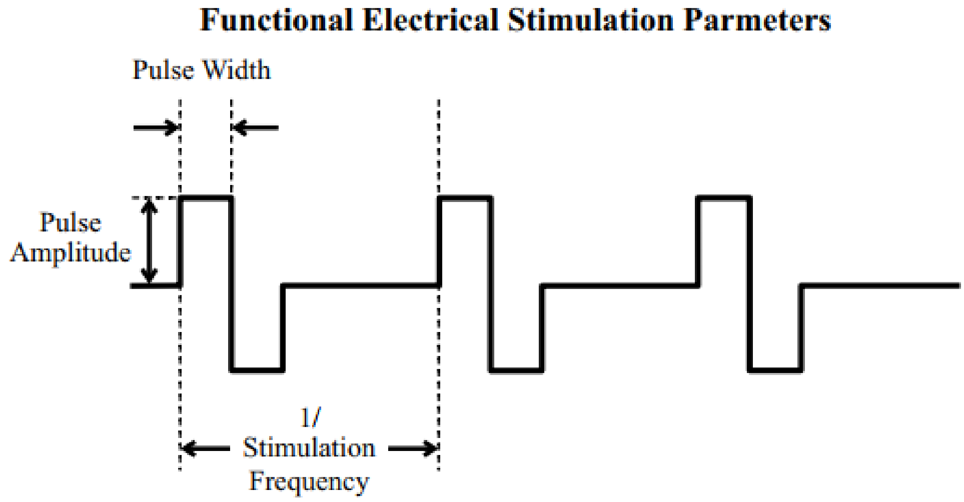

Figure 2.4: Fundamental parameters of FES pulses, adapted from [11]

In practical applications it is of fundamental importance that the control of the FES and the processing of the electromyographic signal take place in real time and therefore it becomes necessary to replace the general purpose computer for the control of the FES with a dedicated integrated system. In this thesis work for the muscle stimulation part an integrated bio-mimetic system based on Functional Electrical Stimulation (FES) was used in combination with the ATC technique applied on the sEMG signal as depicted in [7].

In the particular case of a physiotherapist-patient system, such as the one used for this thesis, the stimulation pattern derives from the analysis of the sEMG signal using the ATC technique and the FES pulse amplitude depends directly on the ATC values. Once the electrostimulation program has been extrapolated, it is applied to the second subject (the patient) to induce the replication of the same movement.

2.1 Differences between physiological muscle contraction and that induced by FES.

The contraction induced with FES has several disadvantages that lead to muscle fatigue much faster than a physiological contraction. The main differences are as follows:

- The first fibers to be stimulated are those innervated by a motor neuron with a larger axon diameter, since they offer a lower electrical resistance [12] allowing them to be excited with a lower current. This means that the fibers are excited in an inverse way to the physiological one and, since we start with the most fatiguing ones, this type of contraction causes greater muscle fatigue. The advantage of the contraction induced by the FES is that the fibers in question are the ones most prone to atrophy in patients with motor difficulties, the continuous recruitment therefore allows to prevent this effect.

- Since the stimulation current is injected through the electrodes which have a fixed position, the recruited fibers are always the same and this leads to greater muscle fatigue [10].
- In a physiological contraction the motor units are stimulated asynchronously so as to be able to distribute the muscular effort and reduce fatigue. During artificial stimulation (FES), on the other hand, the motor units are recruited synchronously, this leads to the need to use higher stimulation frequencies, greater than 20 Hz, to obtain continuous muscle tension. Of course, this factor also causes increased muscle fatigue [10].

2.2 System architecture description

The system used for the acquisition of the EMG signal and its reprocessing with the ATC technique can be divided into three macro areas starting from the acquisition and ending with the stimulation [7]:

- input
- control
- output

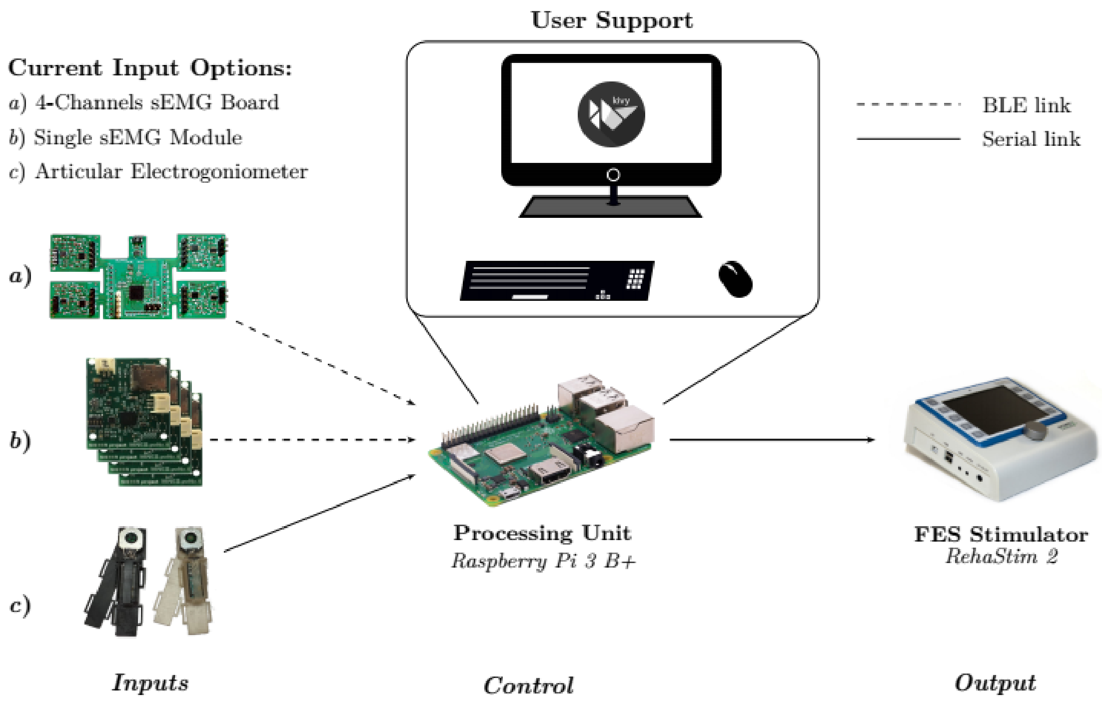

Figure 2.5: System architecture and user interface, adapted from [7]

Once acquired, the data is processed in the control unit that is to say a generic device on which a software ,written in Python, is started and flexible enough to be able to adapt to the machine, which analyzes and processes the acquired signal according to the ATC technique.

2.2.1 The input: the hardware platform

The input devices used are exclusively the wet electrodes described in section [1.2.3] which allow to take the sEMG signal. The acquisition board is also able to receive signals deriving from articular electrogoniometers useful for detecting variations in the angles assumed by the joints during the movement of the limbs but, since they have not been used, they will not be described below.

In the case of wet electrodes, the acquisition board must amplify and filter the signal from the muscle in order to make it suitable for analysis and re-processing. In fact, the pure sEMG signal has an amplitude that varies between a few hundred μV and tens of mV which, if left unchanged, would be difficult to interpret.
The gain factor cannot be too high in order to comply with the constraints related to the power supply of the amplifiers used in the device which are of the single-supply

type between 0V and 1.8V.

The sEMG signal acquired in a differential way using three electrodes (two explorers and one reference) is sent to the input of the hardware platform, which amplifies it with a gain of 500 or 250 in the band between 30 Hz and 400 Hz in order to eliminate high frequency noise and artifacts due to even minimal movements between the electrodes and the skin. The desired bandwidth was obtained with a cascade of a first order high pass differential filter and a second order low pass filter of the Sallen-Key type. In addition, a protection diode has been added for each input channel for overvoltages that could damage the device during coupling with the FES stimulator.

Event-driven signal processing begins with the extraction of TC events using a threshold comparator with hysteresis set to 30mV to avoid detecting even spurious glitches. The second step is to count the events using a digital interface with a microcontroller whose task has been reduced to a GPIO interrupt that detects the TC event and a timer that calculates the activation window set to 130 ms. The value of the window was evaluated as an optimal compromise between the temporal resolution of muscle activation and the differentiation of the various levels of muscle strength.

Two solutions are available for this board which differ in the number of input channels: the first has four acquisition channels and is useful for controlling multiple muscles in the same limb, the second is a single channel board useful for single acquisitions. Since multiple acquisitions were not necessary for the purposes of the thesis, the platform used is the one with a single acquisition channel.

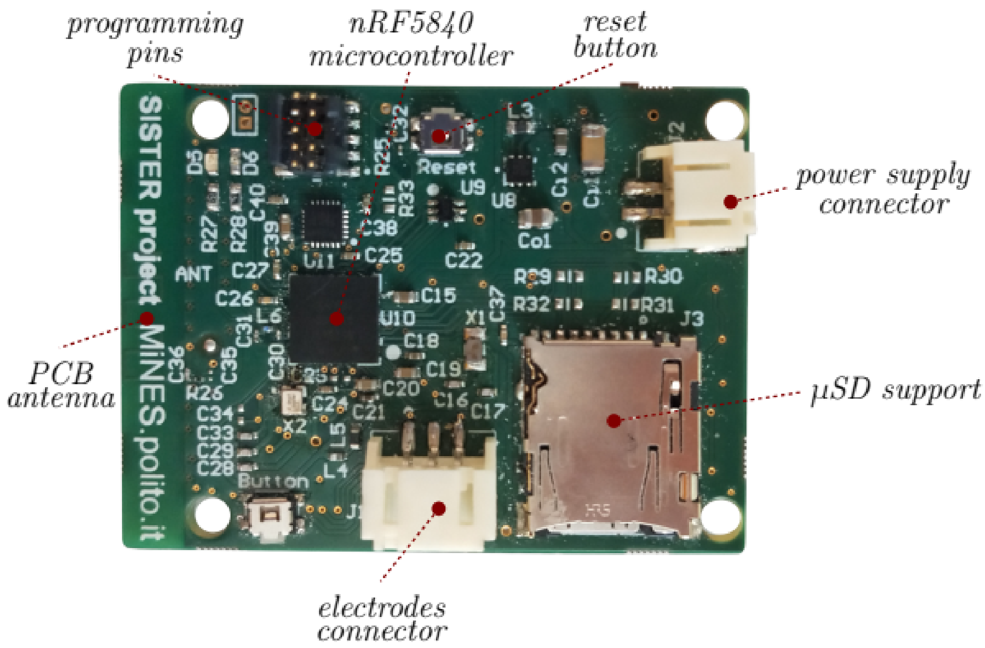

Figure 2.6: Single channel module, adapted from [7]

In any case, both solutions are equipped with wireless connectivity for maximum freedom of movement and a Bluetooth Low Energy (BLE) protocol for data transmission necessary for the stringent requirements on the power supply of the device. Finally, the last feedback stage of the device consists of a voltage follower and the DRL circuit on which the first part of this thesis will focus.

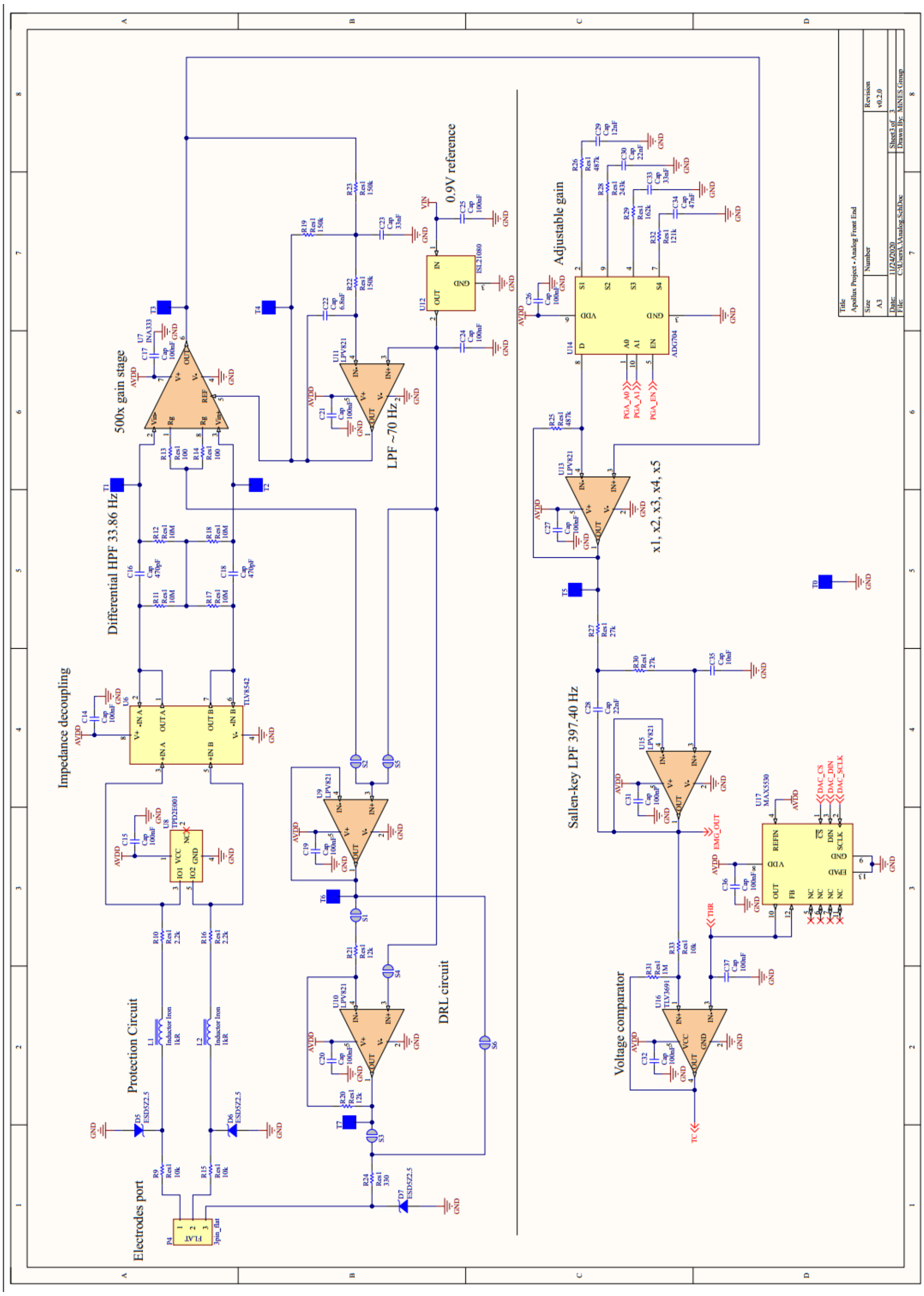

Figure 2.7: Apollux schematics, adapted from Apollux Project by MiNES group

2.2.2 The output: FES stimulator

Overview of a typical FES stimulator

The first electrical stimulators were designed for specific applications while for more generic applications that allow different types of configuration by the user it is necessary to consider only the devices of the last decades. An accurate description of a configurable device can be found in the work of M. Ilic et all [13] in which there is the design of a stimulator whose main features are:

- two operative modes: Setup Mode (SM), which involves setting specific parameters to be able to program different stimulation patterns, and Autonomous Mode (AM) which instead generates pre-set patterns
- at least four programmable channels
- portable and battery-powered
- generation of bipolar and monophasic compensated stimulation pulses
- availability of synchronized input and output pulses
- low power consumption
- galvanic isolation
- low price
- control unit suitable for non-expert users of the sector

In particular, as regards the stimulation patterns, to obtain wide applicability of the system, it is necessary to have the greatest possible freedom on the greatest number of parameters, therefore, in the case of M. Ilic et all citeIlic:FESstim the device has been designed to respect the following characteristics:

- pulse duration between 10 and 500 μs
- stimulation frequency between 5 and 99 Hz with an increase in 2 Hz steps
- positive stimulation current between 0 and 140 mA with 2 mA incremental steps

Obviously, these parameters are specific to the device which is one of the first general purpose designed, at the moment some devices allow you to act on a greater number of parameters and with less stringent limits. In any case, to give a complete and explanatory view of a generic electrical stimulator, the treatment of M. Ilic et all is more than sufficient.

Taking the above specifications as a reference, the necessary system requirements are:

- the possibilities to use different analogic and digital transducers as inputs
- the ability to flexibly program all the channels present to adapt the stimulation to the application area (training, rehabilitation ...)

From the block diagram in figure [2.9] it is possible to see the main stages that make up the architecture of the stimulator.

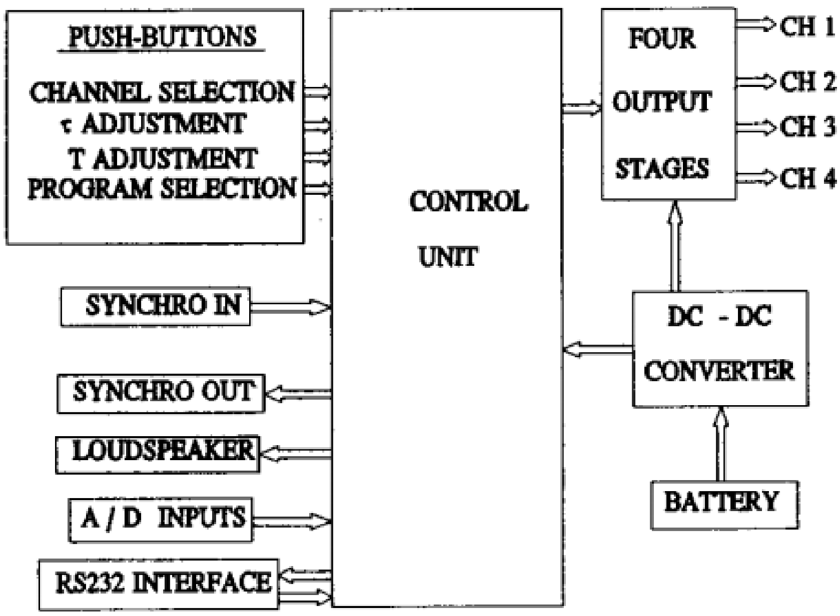

Figure 2.8: Block diagram of typical stimulator, adapted from [13]

The output stage

The output stage consists of 4 channels and must be able to generate constant positive and negative current pulses, to control their duration, the delay between one pulse and the next, the frequency with which they are generated and must allow manual correction amplitude.

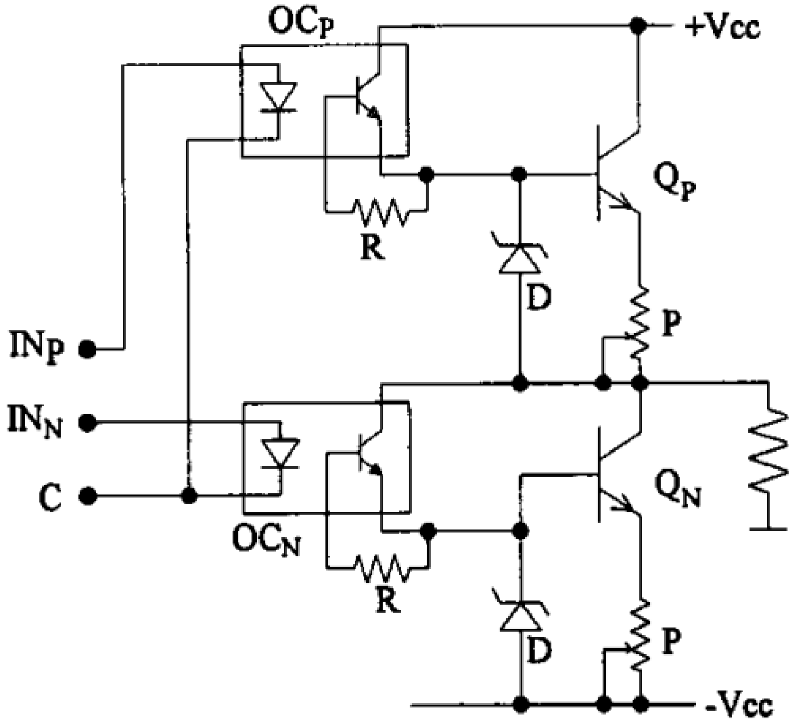

Figure 2.9: Output stage circuit, adapted from [13]

This stage is made using two high voltage transistors in push-pull configuration Q_P and Q_N which act as constant current generators whose amplitude is limited by the breakdown voltage of the Zener diodes D and by the variable resistances of the potentiometers P. The negative current depends exclusively on the collector current of the transistor Q_N while the positive one depends both on the collector current and on the current flowing through the Zener diode. This second component is not constant due to the Early effect of the OC_p and OC_n photocouplers, for this reason, the current received by the muscle tissues with different resistance varies with respect to the set value.

The circuit does not consume power when the load current is equal to zero, the thermal stability is ensured by the presence of the Zener diodes and the measurements taken during the circuit test have confirmed the values expected from the simulations for which the pulses can have an amplitude between 0 and 140 mA, frequency between 5 and 100 Hz, duration between 50 and 100 μs. Timing accuracy is ensured by the presence of a quartz oscillator.

The power source stage

The battery power unit is made using a DC / DC converter that guarantees high voltages, galvanic isolation, high efficiency and small size. The circuit and the block diagram are shown in figure [2.10]

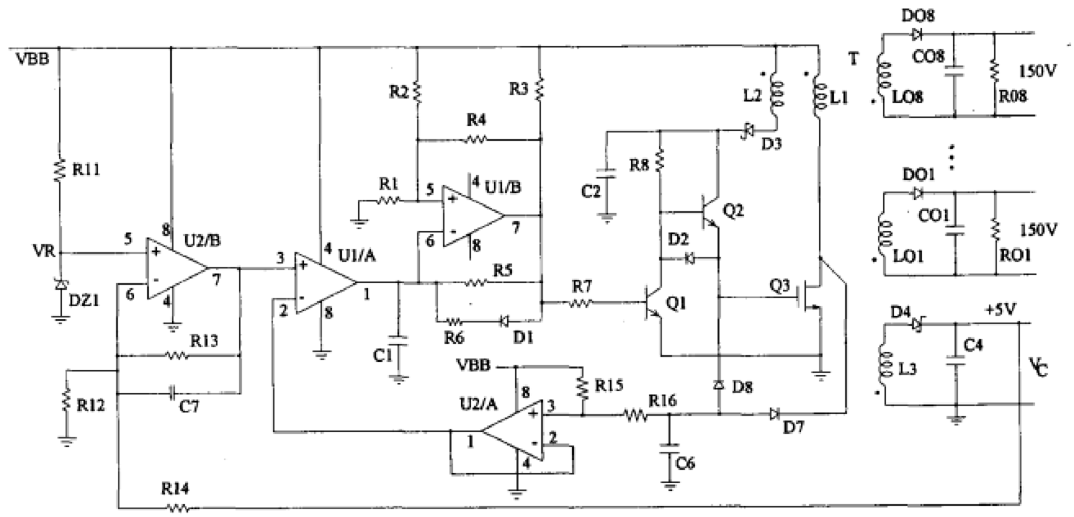

Figure 2.10: Power source stage circuit, adapted from [13]

The square wave voltage with variable frequency $f = \frac{1}{T}$ where T= t_{ON} + t_{OFF} is generated by the oscillator, the pulse time t_{ON} is limited internally to protect the converter from any voltage peaks.

The entire DC/DC converter is made using single power supply operational amplifiers and comparators of which two (U1/A and U1/B) behave as passive elements and constitute the oscillator whose output controls the transistors Q_1, Q_2 and Q_3. In general, the power consumption is low but in any case, the diode D2 has been added to have a faster shutdown of the MOSFET Q_3.
The operational U2/A and U2/B are used to compensate (U2/B) the errors in output from the amplifier and increase the current detection voltage (U2/A).

The control unit

The control unit is mainly based on the use of a microcontroller and must be able to control the output stage according to the duration and frequency parameters set. To obtain the same result, several possibilities can be implemented: the generation of a periodic pulse at the desired frequency, the generation of pulses by calling a subroutine, the usage of sensors that control the generation of pulses by sending signals to the control unit.

Finally, the use of the device by the user is facilitated by the implementation of buttons and a graphical interface.

FES stimulator used

The control of the functional electrical stimulation impulses depends, as mentioned in section [2], on the parameters set at the beginning and during the stimulation session. For this reason, the RehaStim 2 stimulator already chosen in the paper [7] was used throughout the work. In fact, it allows advanced control of all parameters relating to the impulse, can be easily interfaced with other external devices and is provided with a medical certification that classifies it as suitable for muscle stimulation.

Taking into account the dependence of ATC on muscle strength, the intensity of the impulses was calibrated on the basis of TC events while all other parameters were set following the physiotherapy manual provided by the manufacturer of the stimulator. In this way it is possible to excite the muscle fibers correctly for a wide range of movements without running the risk of tissue damage.

Figure 2.11: FES stimulator RehaMove2, manufacturer: Hasomed GmbH

Chapter 3

Design and validation of the DRL circuit

3.1 Introduction on DRL circuit

From the literature [14] it emerges that the Driven Right Leg circuit is useful during biopotential measurements to reduce electromagnetic interference (EMI) due to the common mode signal. Theoretically, the use of three electrodes in differential configuration should already lead to a significant reduction of the common mode, but the connection of the third electrode (the reference one) directly to the common should be avoided mainly for two reasons:

1. if the circuit is not well insulated there could be a current flow through the third electrode potentially dangerous for the human body.

2. the risk of a bad contact of the electrode is higher with respect to the one present with the DRL circuit and can lead to very high resistance (about 100 kΩ) between the patient and the common.

For these reasons the best and most used method is to connect the third electrode directly to the DRL circuit.

A generic circuit diagram is shown in figure [3.1] and comprehends an amplifier (number 3) with negative feedback connected in input to two equal resistances which act as voltage divider (R_3) and in output to a resistor R_0. Furthermore, on the feedback branch there is a third resistance R_f.

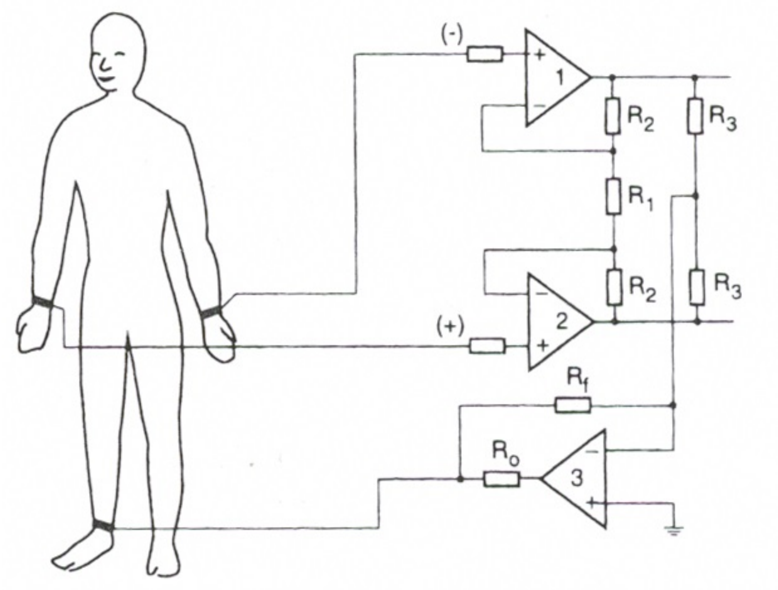

Figure 3.1: Example of DRL circuit, adapted from [15]

The resistor R_0, as widely described in [14], has the task of limiting the flow of current from external sources and protecting the patient from any current transients, for this reason it assumes a value between a few kΩ and the MΩ.
Usually the input resistances (R_3 of figure [3.1]) and the feedback resistance (R_f) assume values such that the gain of this amplification stage is greater than 1 but, not being a necessary condition, the designer has the possibility to choose, also bearing in mind that a too high gain (greater than 100) introduces other types of interference due to the instability of the circuit.

Also according to [14] it is possible to replace the feedback capacitance with a capacitor of a few tens of nF. This allows to have a decidedly greater overall gain while maintaining good circuit stability.

Another possibility, theorized by Spinelli et all [16], which allows for a common mode rejection at higher frequencies, involves replacing the classic operational amplifier with one of transconductance. In this way we would obtain:

- the independence of the stability of the system from the impedance of the electrode

- a band in the order of MHz

3.2 Initial DRL circuit

At the beginning of the revision the DRL circuit used in the acquisition board was connected through solder bumps (S1-S5 in figure [3.2]) leaving the actual decision on the use to a moment after the design and production as it could be connected by stagnating solder bumps or left unconnected. The main reason for this choice depends on the fact that in this specific case the DRL circuit did not seem to provide obvious advantages in terms of interference rejection and in general of signal to noise ratio (SNR).

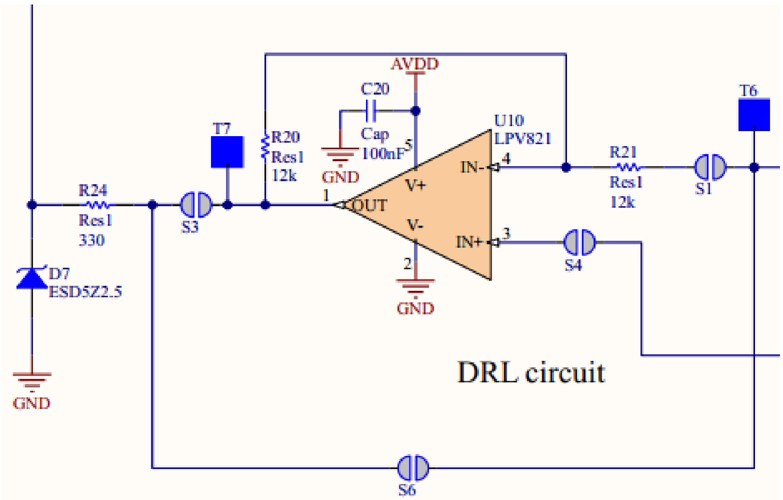

Figure 3.2: DRL circuit designed for the Apollux Project by MiNES group. The branch of R_{24} is connected to the reference electrode and the non-inverting input of the amplifier is connected to th reference voltage equal to 0.9V

Furthermore, the addition of the operational amplifier U10 which constitutes the DRL circuit involves two disadvantages which for the final application of the device can be particularly problematic. In fact, being an extra component on the PCB (printed circuit board), it implies the need for additional space and power consumption. Both factors are in contrast with the main requirements of the device such as the small size to allow a complete wearability and the lowest possible power consumption to avoid having to change the supply battery too often.

For these reasons, an in-depth analysis of the performance of the device was started in the two configurations (with and without DRL circuit), quantified in terms of SNR, applying changes to the same to verify any improvements and using both dry and wet electrodes.

The initial DRL circuit shown in figure [3.2] has several aspects that differ from the configurations suggested in the literature:

- the gain is equal to 1 while it is recommended to have a gain with a factor of 10 or 100 [14]
- the output resistance from the operational amplifier is only 330 Ω and therefore much lower than the hundreds of kΩ reported in the literature

Furthermore, a further performance analysis was performed by replacing the feedback resistance with a capacitor as proposed in [16] and [17].

3.3 Improvements to the circuit and performance analysis

Taking into account the proposals found in the literature ([14],[16],[17]) and the initial circuit, various configurations were tested, the performances of which were reported and analyzed through Matlab to verify the situation with a higher SNR and therefore a lower sensitivity to electromagnetic noise or due to movement.
All the changes made will be presented below, then the acquisition method and finally the main phases of the analysis performed on Matlab.

3.3.1 Changes to the circuit

Taking into account what has emerged from the literature, the feedback configurations that have been tested are mainly the three listed below.
Furthermore, a modification independent of the feedback has been applied concerning the output resistance of the operational amplifier, in fact the resistance R_{24}, as shown in the figure [3.2], has a starting value of 330Ω which has been increased up to 100 kΩ.

Gain equal to 100

The first test was that relating to the gain for which the two resistors R_{21} and R_{22} shown in figure [3.2] and equal to 12 kΩ were replaced with two others respectively equal to 10 kΩ and 1 MΩ in such a way as to obtain a gain factor equal to 100. This modification should allow a better rejection of the common mode without compromising the stability of the circuit.
Summarizing, the variations of this first configuration are:

- R_{24} = 100 kΩ
- R_{21} = 10 kΩ
- R_{22} = 1 MΩ

Gain equal to 1

The second test was made on the initial circuit with a gain equal to 1 and the only change is that related to the resistance at the output of the operation amplifier. In this case the aim is to verify whether a circuit with a low gain but certainly stable or one with a higher gain but less stable is more sensitive to noise.
Summarizing, the variations of this first configuration are:

- R_{24} = 100 kΩ
- R_{21} = 10 kΩ
- R_{22} = 10 KΩ

Capacitive feedback

The third test consists in completely changing the type of feedback passing from a resistive to a capacitive type, for this reason the R_{20} resistor has been replaced with a 10 nF capacitor. This should allow for high gain and at the same time maintain good circuit stability.
The choice of the capacitor value was made keeping in mind the values reported by Spinelli et al.[17].

3.3.2 Matlab analysis

The signal to be analyzed contains ten muscle activations alternating with as many moments in a situation of rest, moreover, the recording begins and ends in a situation of rest. All moments of muscle activation were obtained by flexing the left forearm on the upper arm and taking the signal from the brachial biceps muscle.

To evaluate the signal-to-noise ratio at the output of the acquisition circuit in the various configurations, a Matlab code was written whose main steps are schematically presented in the image [3.3] and will be fully described below.

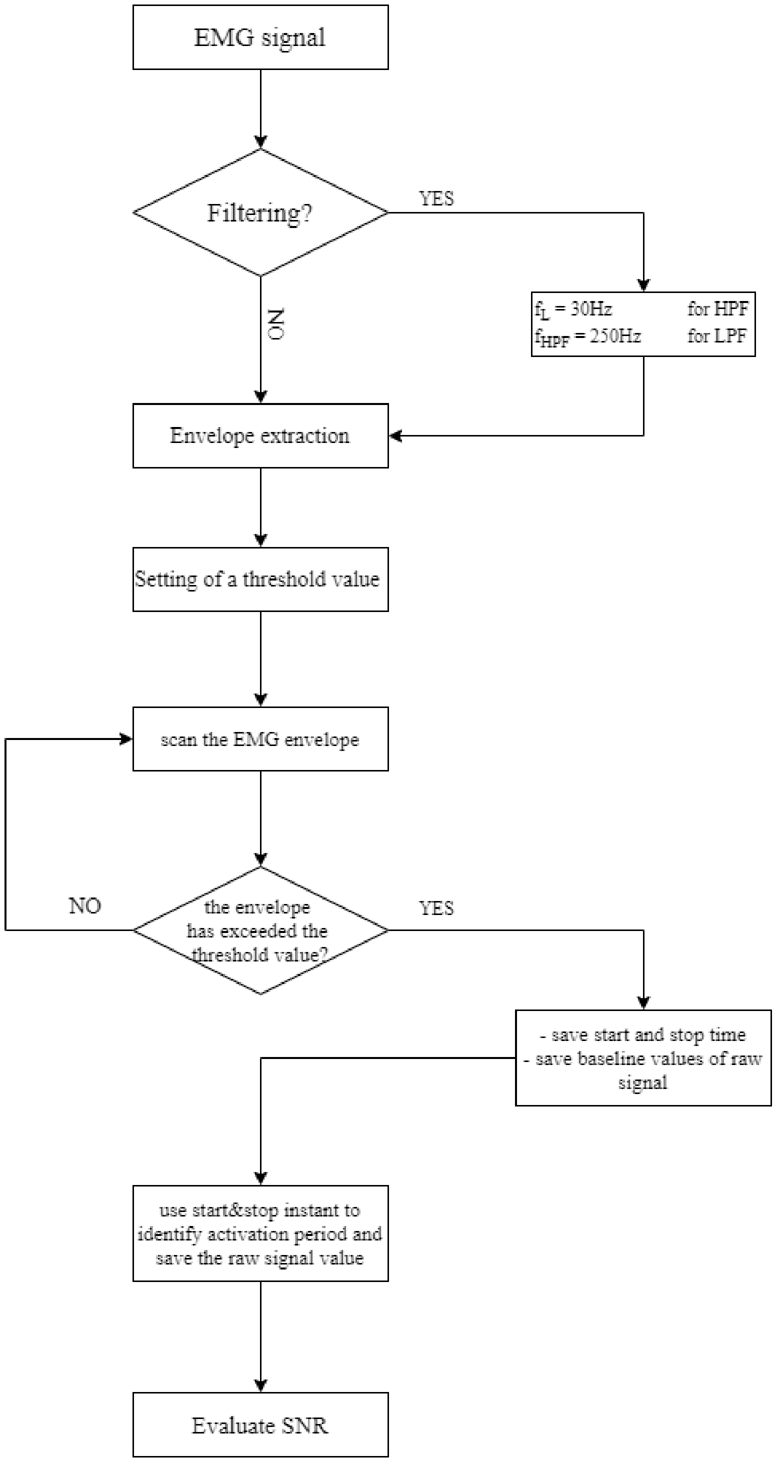

Figure 3.3: Block diagram of the Matlab code written to evaluate the SNR

First of all, it is possible to choose whether to further filter the signal or not. Band-pass filtering is obtained by first executing a high-pass filter and then a low-pass filter, if this option is chosen, the lower (for II-Order Chebyshev HPF) and upper (for II-Order Chebyshev LPF) cut-off frequency values must be entered from the keyboard. The choice of these values is made on the basis of the spectral density of the signal power, that is, by evaluating in which frequency range the main component of the signal falls.
In the case of the EMG signal taken from the brachial biceps, the frequencies that were found to be appropriate are:

- $f_L = 30$Hz for the HPF
- $f_H = 250$Hz for the LPF

Subsequently, whether it is decided to filter the signal or whether you prefer to keep the raw signal, we proceed by calculating the envelope of the signal useful to clearly distinguish the moment in which muscle activation is present.
To obtain the envelope of the signal it was necessary to rectify the signal using the Matlab abs(x) function which returns the absolute value of the function and then applying a low pass filter with a very low cutoff frequency as the main interest was the general behavior of the signal. Cutoff frequency:

$$f_L = \frac{1}{500Hz} \tag{3.1}$$

where 500 Hz is the Nyquist frequency calculated as:

$$f_N = \frac{f_{sampling}}{2} = \frac{1kHz}{2} = 500Hz \tag{3.2}$$

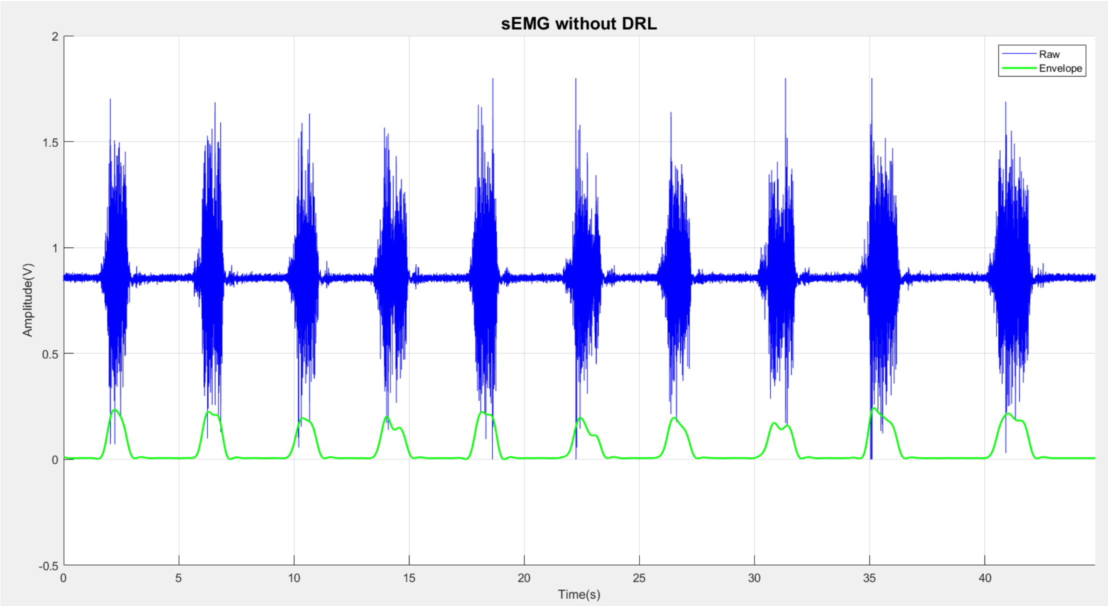

Figure 3.4: Raw EMG signal without DRL circuit and its envelope

Once the envelope was obtained (green graph in the image [3.4]), a threshold value was entered from keyboard (figure [3.5b]) to recognize when muscle activation begins and ends.

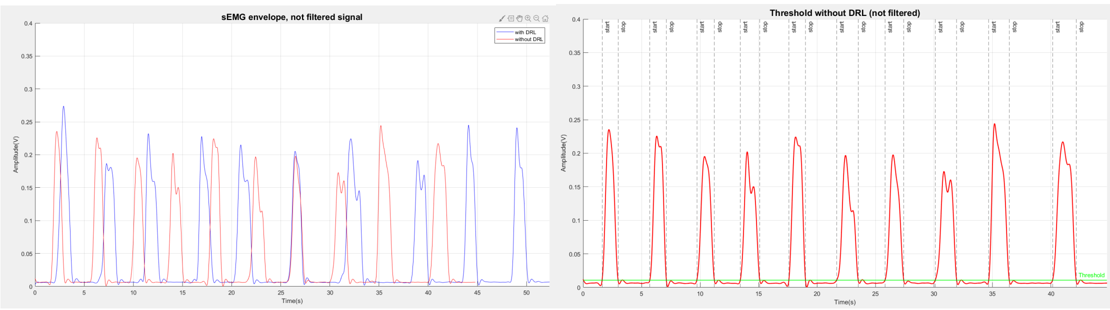

(a) Envelope of not filtered signal with and without DRL

(b) Activation windows

Figure 3.5: Envelope signal and recognition of start and stop activation time

Whenever the envelope exceeds the threshold it means that we are at the beginning of the muscle activation window and the raw signal values relating to those instants of time are saved in a new vector called *"activation"*. When the envelope returns to having values below the threshold and therefore there is a rest situation, the raw signal is stored in a second vector called *"baseline"*.

At this point it is possible to proceed to the determination of the signal to noise ratio (SNR) by calculating the standard deviation of the activation and baseline vectors. Subsequently, the standard deviation of the baseline is subtracted from that of the activation and finally the SNR is calculated as per definition:

$$SNR = 20 \cdot \log\left(\frac{signal}{noise}\right) = 20 \cdot \log\left(\frac{std_{active}}{std_{baseline}}\right) \tag{3.3}$$

This cycle is repeated for all the activation periods and therefore allows to have an estimate, averaged over 10 repetitions, of the SNR value.

3.3.3 Results comparison

All the tests relating to the feedback branch and the output resistance were first performed on the circuit mounted on the breadboard, using the wet electrodes described in the section [1.2.3]. The use of a circuit mounted on a breadboard implies the fact that the components used are not integrated and therefore, having greater tolerances, they provide less precise results, furthermore the connections do not all have the same length so there may be, albeit minimal, some transmission delays between one branch and another which also make the measurements less precise.
It is also necessary to emphasize that all SNR values were obtained by choosing not to further filter the signal via software.

However, table [3.1] shows the SNR values for the various combinations of feedback and output resistance.

	R_{out}=100 kΩ	R_{out}=330 Ω	R_{out}=4.7 kΩ
Without DRL	25.968 dB	25.498 dB	29.154 dB
DRL gain = 100	18.050 dB	14.851 dB	20.718 dB
DRL gain = 1	24.878 dB	25.681 dB	29.985 dB
DRL capacitive feedback	26.504 dB	26.191 dB	30.857 dB

Table 3.1: SNR results of the circuit mounted on breadboard

From a first analysis it is evident that the circuit with the high gain DRL, equal to 100, is the configuration that gives the worst results, while the one with the capacitor on the feedback branch would seem the most promising. In addition, it is useful to highlight how the results without DRL are similar or even better than the others.

Taking these results into account, we moved on to experimentation on the Apollux boards present in the laboratory. Since it is a printed circuit board (PCB) it wasn't particularly practical to modify the value of the resistances on the feedback and output branch so the resulting SNR values are related exclusively to the configuration without DRL and with DRL with unity gain and output resistance $R_{out} = 330\ \Omega$. Furthermore, the measurements were taken with wet electrodes which are the best case and which introduces less noise due to the displacement of the electrodes on the skin, and with dry electrodes which instead represent the worst case as they are not fixed on the skin but always subject to some shift.
As last test, the muscle signal was acquired using the dry electrodes and while performing a walk simultaneously with the flexion and extension movement of the arm.

	WET electrode	DRY electrode	DRY electrode and walking
Without DRL	23.010 dB	24.228 dB	19.562 dB
DRL gain = 1	22.602 dB	25.603 dB	23.035 dB

Table 3.2: SNR results of the Apollux board

From table [3.2] it is possible to see how the DRL has a fundamental stabilizing function if the acquisition of the signal occurs during the performance of other motor activities.

It is important to underline that the tests with capacitive feedback were not carried out with the Apollux board since the advantage in terms of SNR shown in table [3.1] was not so high and, moreover, and furthermore, by introducing an RC circuit, there would have been a very high risk of introducing a delay that would have led to a phase shift of the signal.

3.4 Conclusion

Taking into account that the main intent is to use the device in the rehabilitation field and with constant use during the day, which includes the need to be able to acquire a sufficiently stable signal even when the patient performs other movements (see table [3.2]) and considering the results obtained which indicate that the most favorable configurations are those with an output resistance equal to 4.7 kΩ and DRL with gain 1 or with capacitive feedback (see table[3.1]), it was decided to keep as the definitive configuration the one that involves:

- R_{out} = 4.7 kΩ
- DRL gain = 1

Furthermore, since it is no longer necessary to choose whether or not to connect the DRL circuit based on use, solder bumps have been eliminated, leading to a reduction in the size of the board.

Therefore the final circuit is the one shown in figure [3.6].

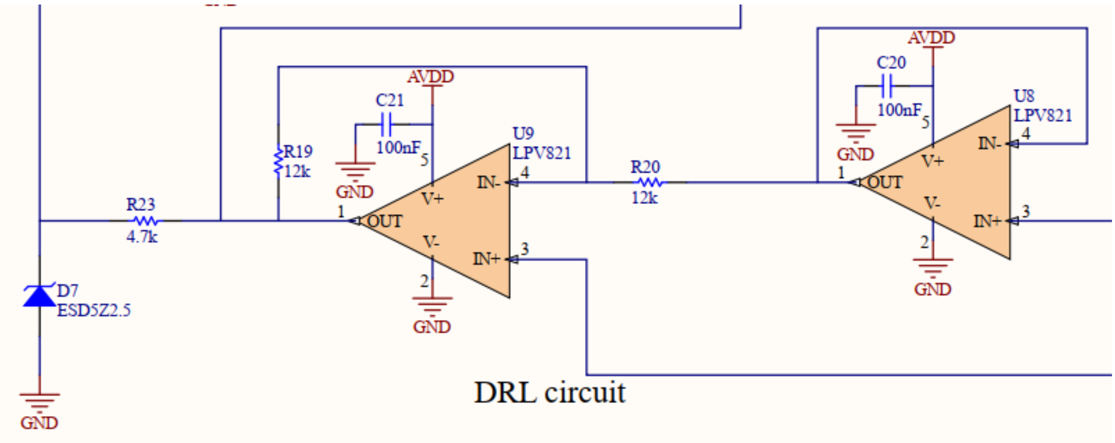

Figure 3.6: Final DRL configuration implemented on the Apollux board. The non-inverting inputof the amplifier is connected to th reference voltage equal to 0.9V

Chapter 4

Stimulation Artifact Suppression

The main objective of this thesis, as anticipated in the [1.4] section, is to improve the front-end acquisition of the device in order to be able to use it in closed-loop applications. For this, it is necessary to be able to record the sEMG signal also from the electrostimulated muscle. The recording of the signal during stimulation is anything but trivial since, due to the electric current that runs through it, there are two types of artifact that make the analysis complex:

- the stimulation artifact
- the M-wave

4.1 The Stimulation Artifact

The stimulation artifact is a voltage peak of about 1-2V (post-amplification value) and short duration caused by the rapid, as well as passive, depolarization of muscle tissues following electrical stimulation. This type of artifact is characterized by three different components:

- the peak whose amplitude depends on the intensity of the stimulation current
- the fast decay tailing part
- the slow-decay tailing part, depends on the electrode-skin impedance which discharges slowly.

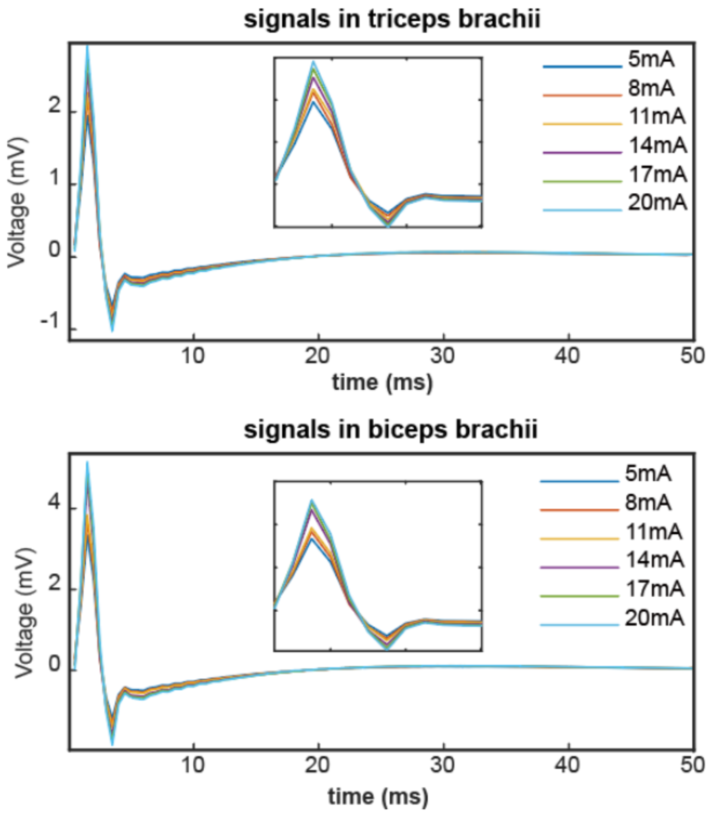

Figure 4.1: The typical form of a stimulation artifact and peak variation with increasing current intensity, adapted from [18]. The values are taken without amplification

Not being a response of physiological origin, it is recommended to eliminate it as it does not provide useful information on the muscle response. In addition to having no relevance for the muscular response, the presence of this type of artifact does not allow the correct visualization of the sEMG signal for two reasons related to its intrinsic characteristics. First of all, having an amplitude of the order of magnitude of volts, it causes the saturation of the acquisition channel (see section 2.2.1). Secondly, the duration of the queue component, despite being quite short, is still several tens of ms. This implies that, at high stimulation frequencies, and therefore very short distances between one electrical impulse and the next, it is no longer possible to obtain an adequate representation of the sEMG signal since the SAs appear at such close distances that it is no longer possible the visualization of a large part of the muscle signal between one and the other.

4.2 The M-wave

The M-wave represents the evoked response of the muscles during electrical stimulation, more specifically it provides information regarding the excitability of the muscle membrane in situations of fatigue.

It is a wave that, based on the stimulation current, can have amplitudes up to 2-3 times greater than the sEMG signal and can also be prolonged for an entire stimulation period, thus superimposing itself on an sEMG that represents a possible voluntary response of the muscle.

The properties of the wave such as amplitude and duration depend in general on the stimulation current acting on the muscle therefore if we want to go more specifically, it is possible to find the explanation for these characteristics in the reaction of the motor units.
In particular, the waveform is influenced by the number of motor units that are activated, by the dispersion of their innervation areas and by the thickness of the subcutaneous layers.

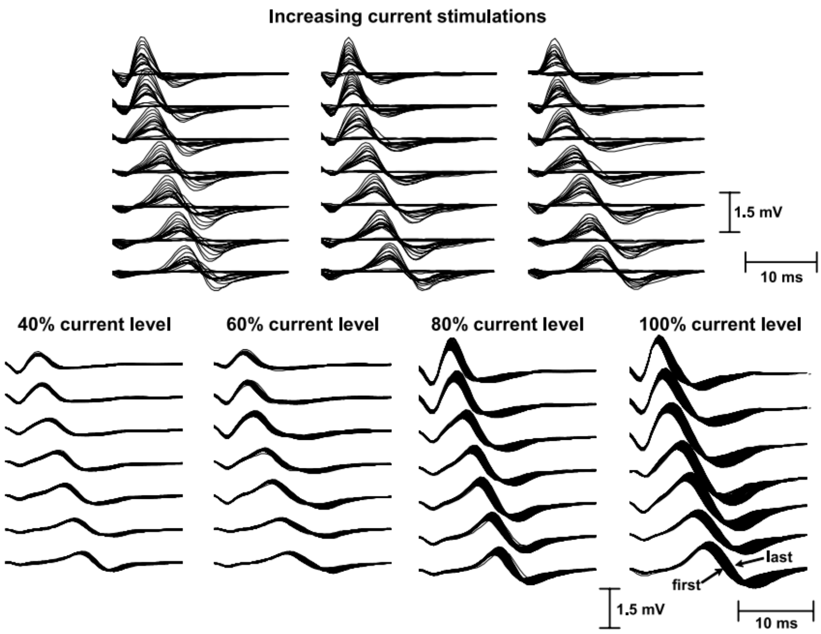

Figure 4.2: Variation of M-wave amplitude due to different stimulation current, adapted from [19]

However, since it is a physiological response of the muscle to stimulation, even if it prevents the graphic display of information relating to the voluntary response, it may be useful to analyze it if you want to know the fatigue state of the muscle. To extract it, however, it is necessary to be able to remove the SA since the M-wave, in accordance with the literature [18], is visible after the peak of the SA and therefore in correspondence of its tail.

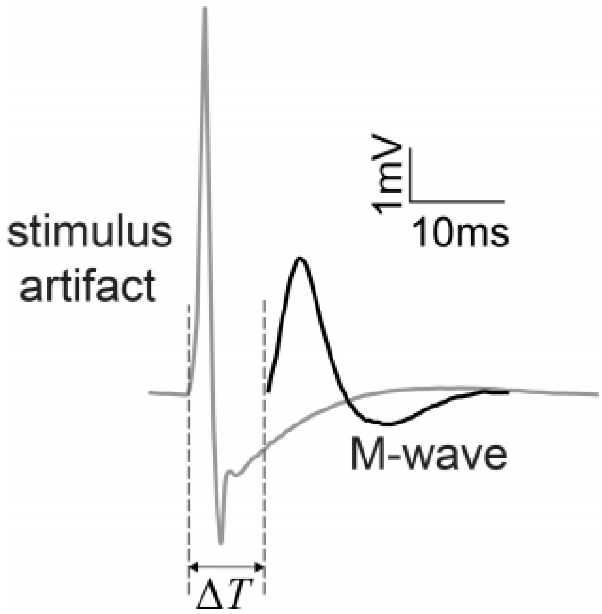

Figure 4.3: Combination of stimulation artifact followed by the M-wave, adapted from [18]

4.3 Introduction on Stimulation Artifact suppression

In recent decades, research has focused on the study of the stimulation artifact, its characteristics and the most effective techniques for removing it. In particular, there are two possible ways of removing: hardware removal with blanking circuits or software removal with subtractive methods. Given the diversity in terms of duration and amplitude of the SA components, the two techniques are often used together to obtain better results.

4.3.1 Hardware removal techniques

The most used hardware removal techniques are those that involve signal blanking with Sample Hold circuits activated by a trigger signal sent in advance or when the start of the stimulation phase is detected. It is good practice to filter the signal afterwards to eliminate the residual frequency components, however, it is often not necessary to add a filter as those present on the acquisition channel are enough. The disadvantage of this strategy is certainly the loss of all information during the blanking phase which, however, is balanced by good signal robustness for the rest of the acquisition.

In literature [18],[20],[21] there are several examples of blanking circuits that generally use bidirectional switches, placed at the input of the circuit, which have the task of short-circuiting the electrodes to ground when they receive the trigger signal sent by the computer or microcontroller used to control the circuit.
What varies, also based on the project specifications, are how the electrodes are short-circuited and which can be distinguished into two macro-strategies:

- the first is to not short-circuit directly to the ground but to add a resistance of a few tens of Ohms to help the decay of the current peak ([21])
- the second is to short-circuit the electrodes directly to ground ([18])

Furthermore, Bi et al. [20] proposed not only to disconnect the electrodes during stimulation but also to disconnect them from the electrostimulator to help remove the SA. To improve the rapid recovery of the baseline, they added an integrator on the branch of the reference voltage of the instrumentation amplifier that also helps to filter out movement artifacts. In particular, the resistance R_6 remains connected for the entire duration of the stimulation pulse and for a subsequent time interval and is then disconnected, thus helping the elimination of movement artifacts.

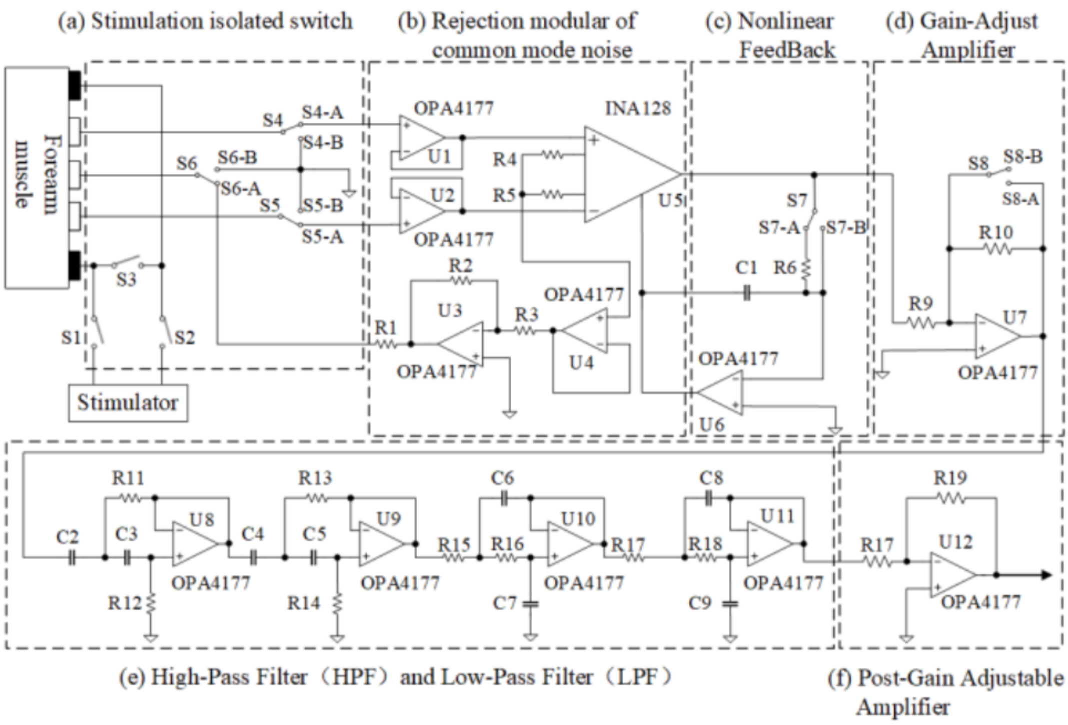

Figure 4.4: Circuit proposal for stimulation artifact removal with non linear feedback, adapted from [20]

However, blanking techniques have not always given exhaustive results for two reasons: the first is that there is a loss of information throughout the blanking period, the second is that they often only eliminate the SA peak and not even the tail parts. For this reason, hardware filtering techniques adapted to this type of problem have been introduced. For example, A.Crema in his master thesis [21] has obtained promising results using a filtering method proposed by Thorsen [22] which involves the use of a rapid recovery instrumentation amplifier with the addition of non-linear feedback on the baseline.

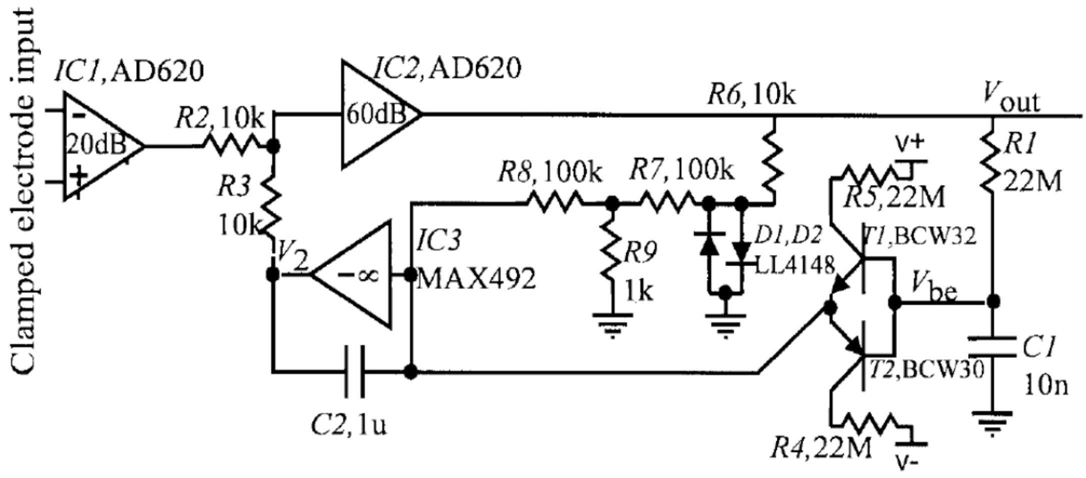

Figure 4.5: Simplified circuit of myoelectric amplifier used for fast artifact suppression, adapted from [21]

This circuit allows for continuous acquisition through the electrodes, which always remain connected, limiting the potential difference thanks to the protection diodes. The IC2 amplifier amplifies the signal while the IC3 amplifier is the one responsible for the removal of offsets and the suppression of artifacts. Finally, the two transistors T_1 and T_2 compensate for the drift of the system. The two transistors never enter the active region during stimulation as the time constant R_1C_1 maintains $|Vc_1| > V_{be}$. Compensation occurs only when

$$V_{be} = V_{out}\Big(1 - e^{\frac{-t}{R_1C_1}}\Big) \tag{4.1}$$

In this situation the capacitor C_2 is charged, evaluating the time constant

$$R_{4,5}C_2 = \frac{V_{R_{4,5}}}{\Delta V_2/t_r} \tag{4.2}$$

where t_r is the compensation time, we obtain that the only components that can pass through the $T_{1,2}$ network are those with a frequency lower than 0.72 Hz.

4.3.2 Software removal techniques

The hardware removal of the stimulation artifact is not always the best technique for several reasons, including the increase in the circuit complexity of the acquisition board, the introduction of other types of disturbances due to new components, or the sudden variation of the impedance values due to the disconnection from the human body and, last but not least, the fact that it is not always possible to obtain a total removal of the SA.

For all these reasons, software-level SA removal techniques have been developed in recent years. This methodology allows not to further complicate the circuitry and does not involve the loss of information as the acquisition is constant. On the other hand, are techniques that do not allow the real-time removal of artifacts and require devices with greater computing capacity.

It is possible to divide the software methods into two groups:

- filtering of the sEMG signal
- subtraction of a previously modelled artifact from the sEMG signal

For what concern the signal filtering, it is applied only in certain bands and some also include frequencies that belong to the spectrum of M-wave and voluntary EMG. This means that the signal, after processing, will not be particularly faithful to the starting one and therefore not useful for identifying voluntary responses from the muscle.

On the subtractive methods, on the other hand, there are different strategies applicable in particular for the extraction of a model of the artifact. For example, Keller and Popovic [23] propose to evaluate the artifact model by performing a weighted average of several previously recorded artifacts and to apply an IIR filter only in the 12.5 ms following the stimulation pulse.

A second possibility is described by Y.Li [18] and considers the idea of deriving the SA template from a pre-stimulation phase in which a subthreshold current is used. Once this phase has been completed, the model is calculated using an autoregressive process.

Regardless of the methodology with which the SA model is obtained, the next step is to subtract it from the raw sEMG signal. In this way, in addition to the peak, the tail components are also eliminated.

4.4 Initial assesment

Before applying techniques for the removal of the stimulation artifact, a test was performed to verify that the voluntary activity of the muscle is not actually visible during the electrical stimulation. For this, the sEMG signal was taken directly

from the electrostimulated muscle and the ATC technique was applied to observe if the muscle activity was still recognizable.
For these trials during the recording of the signal, in addition to applying the electrical stimulation, two voluntary flexion movements of the arm were performed. The stimulation current values used are 2mA and 10mA to have limit cases and, for each intensity, five recordings were taken.
The results obtained, as visible from the images [4.6],[4.7],[4.8], are not satisfactory as it is not possible to distinguish the moments of voluntary activation.

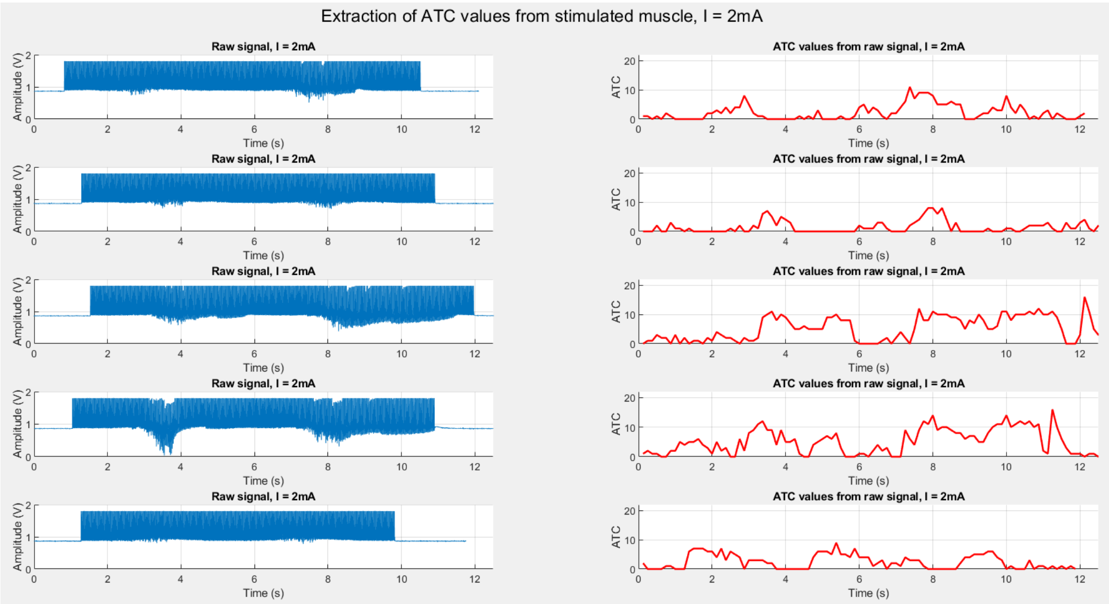

Figure 4.6: ATC values extracted from stimulated muscle with current intensity equal to 2mA

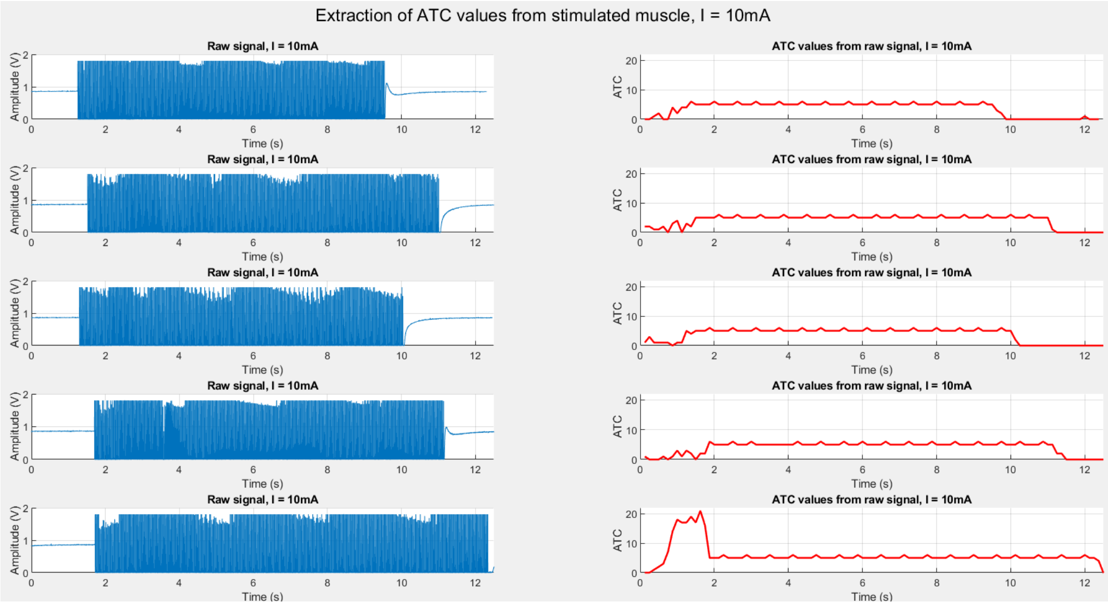

Figure 4.7: ATC values extracted from stimulated muscle with current intensity equal to 10mA

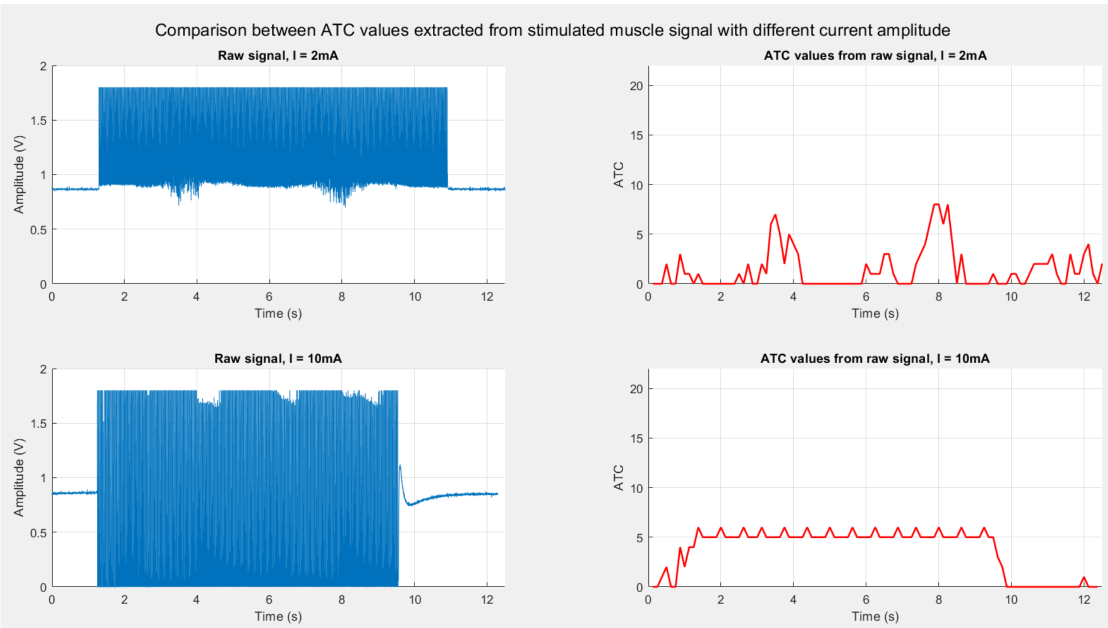

Figure 4.8: Comparison of ATC values extracted from stimulated muscle with different current intensity

It is also useful to underline how the ATC values for low stimulation currents, e.g. 2mA, assume a value of 0 in some points despite the stimulation current applied. This is because the threshold, calculated as

$$threshold = mean(baseline) + 3 * std(baseline) \tag{4.3}$$

in some cases, it is lower than the stimulation peaks which therefore, in certain time windows, are not detected and thus leading to an ATC value equal to 0.

This does not occur at high stimulation currents since, as visible from the image [4.7], the sEMG signal taken brings the acquisition channel to complete saturation and therefore the above-threshold events will always be detectable but however it is impossible to distinguish the voluntary activation signal from the stimulation one.

4.5 Preliminary tests with the instrumentation amplifier

The first test performed for the removal of the stimulation artifact concerns a modification to the feedback branch of the acquisition board and in particular the branch that supplies the reference voltage to the INA 333 instrumentation amplifier. In the original circuit, the reference voltage is supplied through a low-pass filter with a cut-off frequency at 70 Hz which takes the voltage of the inverting input, from the INA333 output as shown in figure [4.9].

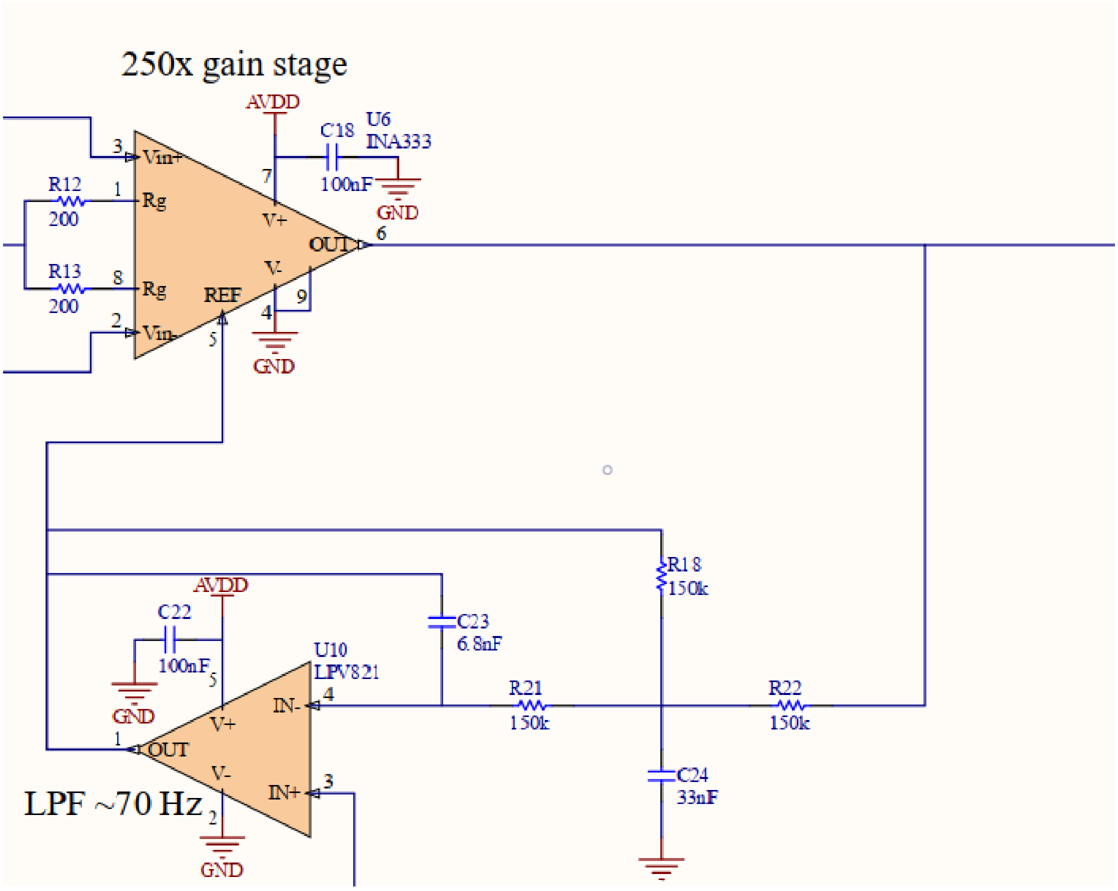

Figure 4.9: Low pass filter on feedback of INA333, adapted from Apollux Project by MiNES group. Positive and negative input of INA333 are connected to the differential HPF visible in figure 2.7, the non-inverting input of the LPF at 70Hz is connected to reference voltage.

The idea for this test comes from the study carried out by Bi et al. [20] where the low pass filter has been replaced with an integrator (fig. [4.4) whose resistance R_6 is excluded from the circuit after the stimulation interval to facilitate rapid recovery of baseline values.

Before mounting the circuit on the breadboard, the functioning of the circuit was simulated with LT-Spice on which the entire circuit of the acquisition board, reported in figure [4.10] was implemented excluding only the last stage consisting of the threshold comparator. Furthermore, to have results as similar as possible to the real case, three RC parallels have been added that reproduce the behaviour of the electrodes and a current generator with 2 other capacitors in parallel to recreate the impedance of the body. The additions to get closer to the real case are shown in figure [4.11]

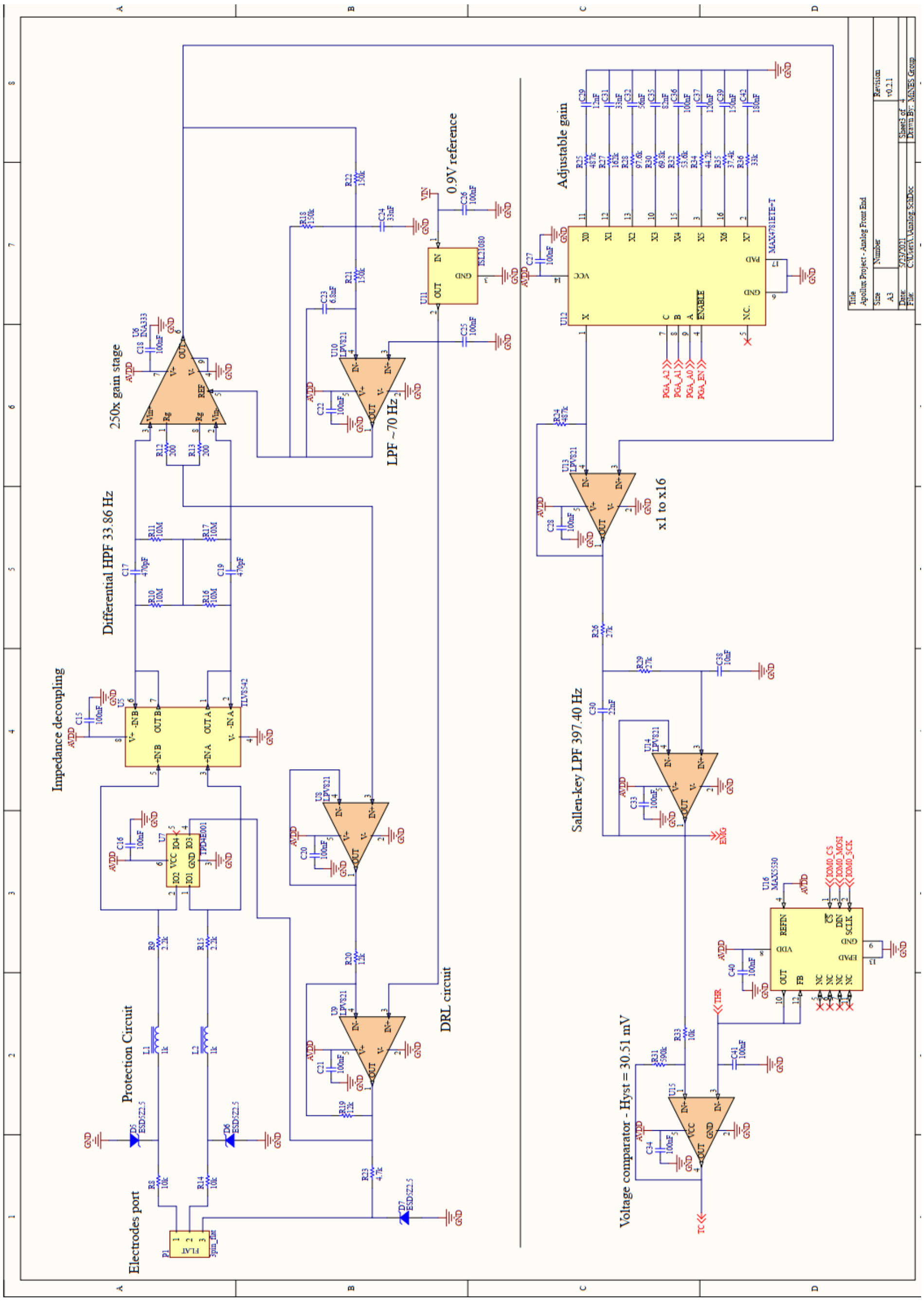

Figure 4.10: Apollux schematics, adapted from Apollux Project by MiNES group

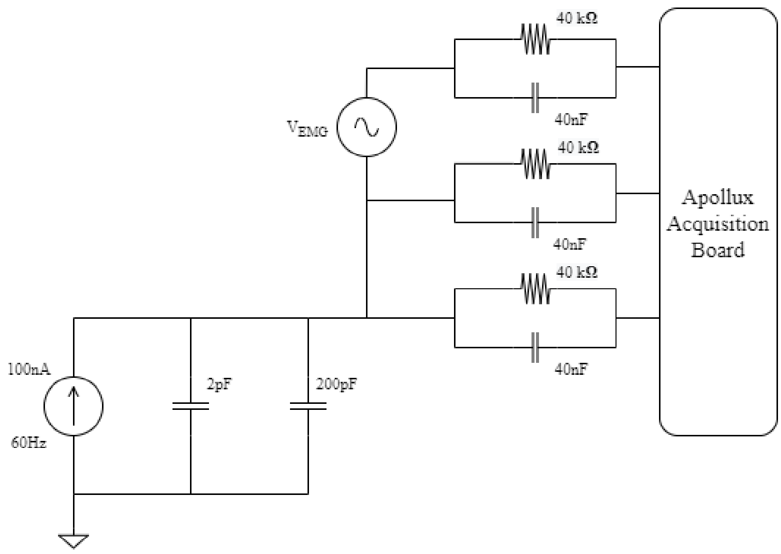

Figure 4.11: Circuit to recreate contribution of body impedence and electrode impedences

Where:

- the current generator supplies a sinusoidal current at 60Hz and 100nA of direct current (DC value)
- the capacitors C_1 and C_2 are respectively 2 pF and 200 pF
- the three RC parallels are composed of a resistance R equal to 40 kΩ and a capacitor C equal to 40 nF
- the voltage generator placed between the first two RC parallels represents the electromyographic signal, initially the signal, previously recorded, which was used for analysis on the DRL circuit was given as input

The first step was to verify that the modifications on the reference voltage of the INA333 did not modify the output signal, for this reason, both the low pass filter shown in figure [4.9] and the integrator, shown below in figure [4.12], were implemented on the LT-Spice.

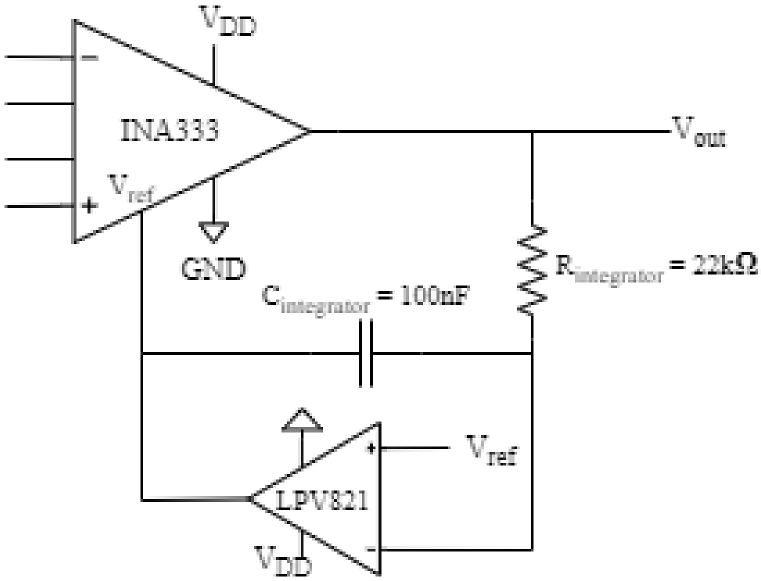

Figure 4.12: Integrator on feedback branch to provide reference voltage to INA333

Initially, the simulations were performed in static conditions for which the sEMG signal was observed without the intervention of the switch to disconnect the R_6 resistor. From the results obtained it is evident that this modification has no effect on the recorded signal, in fact the green signal, which represents the EMG signal on only one branch of the acquisition channel, and the orange signal, which instead represents the differential signal obtained by the difference between the upper and lower branches, shown in figures [4.13a] and [4.13b], have the same width and the same shape.

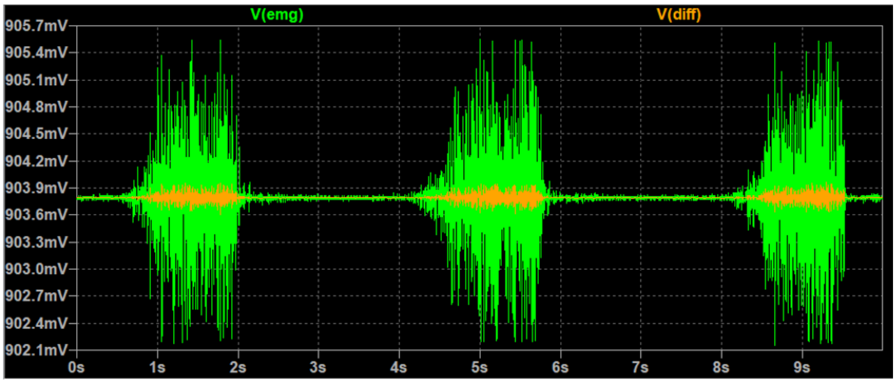

(a) Integrator

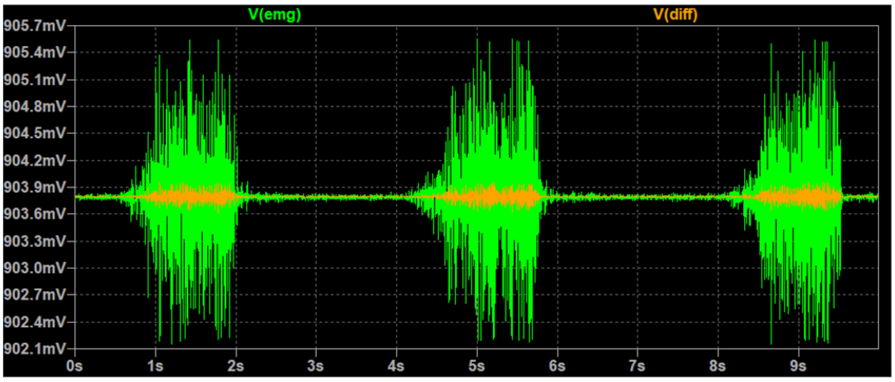

(b) Low Pass Filter

Figure 4.13: Simulation results on LT-Spice

This allowed us to continue on this way by introducing the switch for rapid baseline recovery, so the second step was to simulate, with the same input signals used previously, the circuit with the switch on the feedback of the integrator used to disconnect resistor $R_{integrator}$ and accelerate baseline recovery.

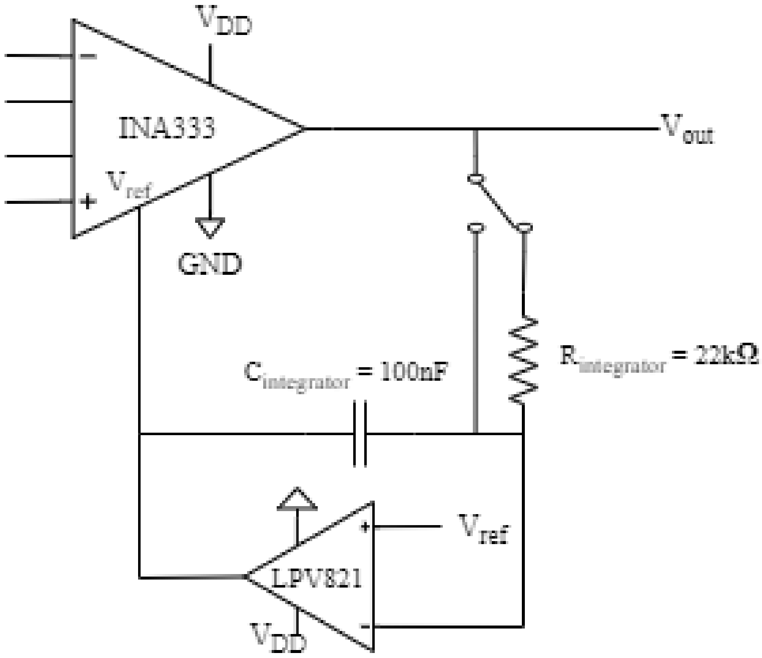

Figure 4.14: Integrator on feedback branch to provide reference voltage to INA333 with addition of a switch to disconnect the resistor $R_{integrator}$ to accelerate baseline recovery

The recovery of the baseline is possible since the output voltage from the integrator is negative and, adding to the positive input voltage to the INA333, should lower it and bring it closer to the baseline value.

The results obtained from this second simulation are not so promising as the reference voltage supplied is outside the amplifier dynamics and causes it to be completely saturated. From image [4.15] it is possible to observe the behaviour of the signal at the output of the acquisition board (red), at the integrator output (green) and the step signal which determines the switching instants of the switch so that if once the resistance $R_{integrator}$ is disconnected, complete saturation is obtained.

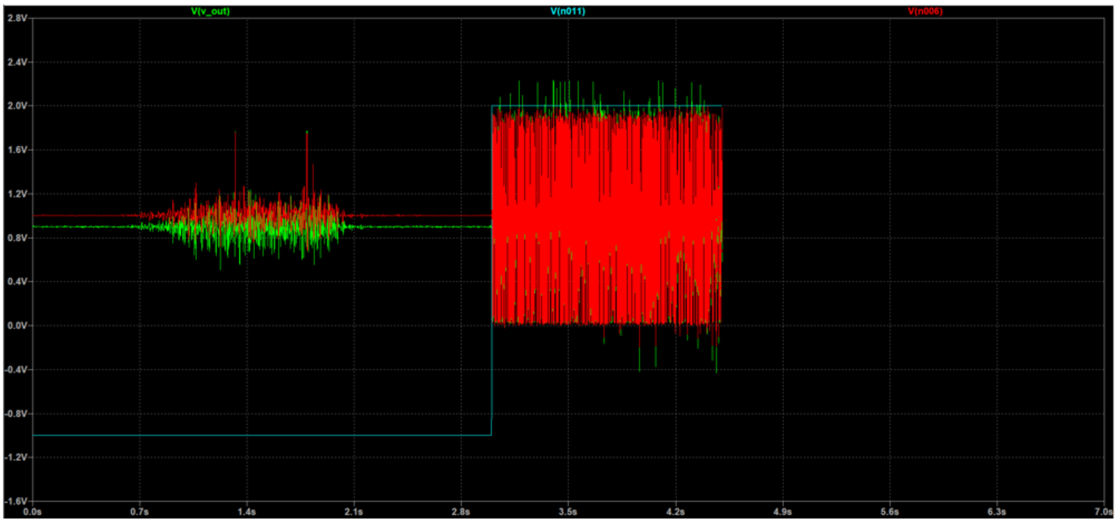

Figure 4.15: Saturated output signal of the INA333

This effect is caused by the fact that the specifications of the device in use are decidedly more stringent than those of the device presented in the paper, in particular as regards the power supply voltage which is dual between + 5V and -5V while the Apollux board is single power supply between 0V and 1.8V.
The differences in supply voltage are also the reason why all the circuit proposed by Bi et al. [20] has not been implemented.

4.6 Improvements on the input stage: simulation on LT-Spice

Excluding the possibility of changes to the feedback line, the attention was shifted to the board inputs connected to the two recording electrodes. Since the ultimate goal is to avoid stimulation artifacts, it was decided to implement a hardware blanking of the input signal and therefore not to absolutely record the instants in which the artifact is present. As regards the positioning of the SW and the switching instants, the work of Bi et all [20] was taken as an example , while, as regards the signal supplied in input during the LT-Spice simulation, it was created on Matlab starting from an sEMG signal previously recorded during the analysis of the DRL circuit.

4.6.1 Circuit design

The circuit used for the simulation on LT-Spice is exactly the one shown in the schematic [4.10], once again excluding the stage of the threshold comparator and

applying the changes between the 10kΩ input resistances showed in figure [4.10] and the RC parallels that simulate the impedances of the recording electrodes reported in figure [4.11], and between the output of the DRL circuit and the reference electrode. To carry out the signal blanking the SPDT switch must commutate at a determined instant, which in the real case coincides with the arrival of the stimulation pulse while during the simulations it is decided a priori, disconnect the electrodes from the rest of the circuit and carry them to GND.
In order not to leave the two branches of the recording electrodes floating, other two SPDT switches have been added which, under normal conditions, connect the circuit to the electrodes and when the control signal arrives they switch and connect the circuit to the reference voltage V_{ref} equal to 0.9 V which is also the baseline value. This should achieve two useful results: the first is to avoid unwanted voltage spikes due to the unconnected branches and the second is a faster baseline recovery. As for the branch connected to the reference electrode, since it is not an input, it can remain disconnected without creating the risk of voltage peaks.
The whole circuit is reported in figure [4.16]

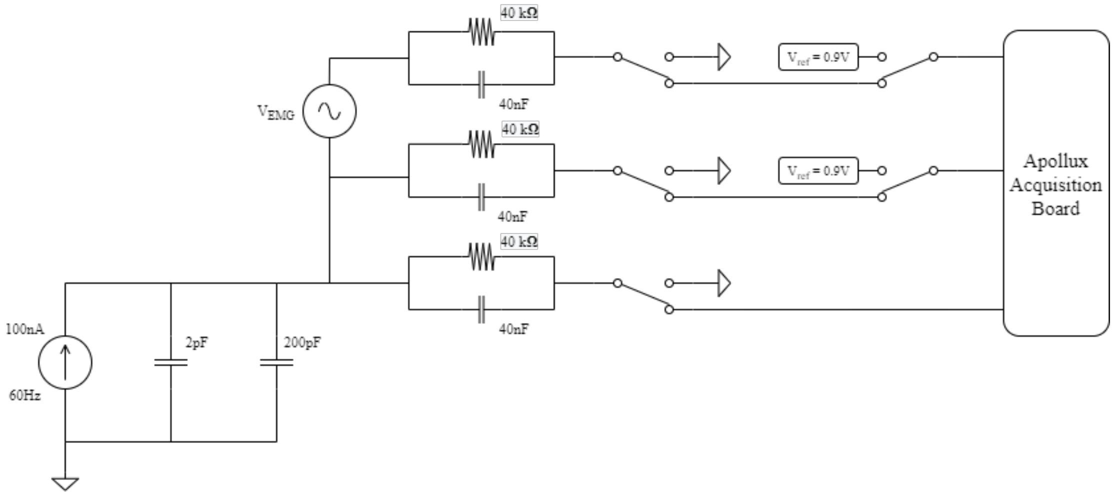

Figure 4.16: Circuit implemented on LT-Spice for the simulation

4.6.2 Processing of the input signal on Matlab

In order to evaluate the behaviour of the circuit through simulation in the LT-Spice environment, it was necessary to reprocess a previously extracted sEMG signal, using the Apollux board with a gain set at 500. The goal is to obtain a 100ms signal in the middle of muscle activation and add a sequence of 3 SA at a distance of 25 ms and 2 M-waves also at a distance of 25 ms, in this way it is possible to simulate the stimulation frequency of 40Hz with which the impulses arrive. The choice to add only 2 M-waves is determined by the fact that about 25 ms pass from the beginning of each M-wave to the end of the tail part, having to distance them by 25ms to respect the stimulation frequency and leaving an initial 20 ms of the pure signal without other components and delaying the arrival of the M-wave by 5ms compared to the beginning of the SA, the third M-wave could not be summed as it would have been longer than the remaining part of the sEMG signal. The delay concerning the start of the SA is necessary to reproduce the real case for which the M-wave is detected at the end of the SA which normally lasts about 5 ms. Figure [4.17] shows the duration and intervals of the signals that will be generated on Matlab.

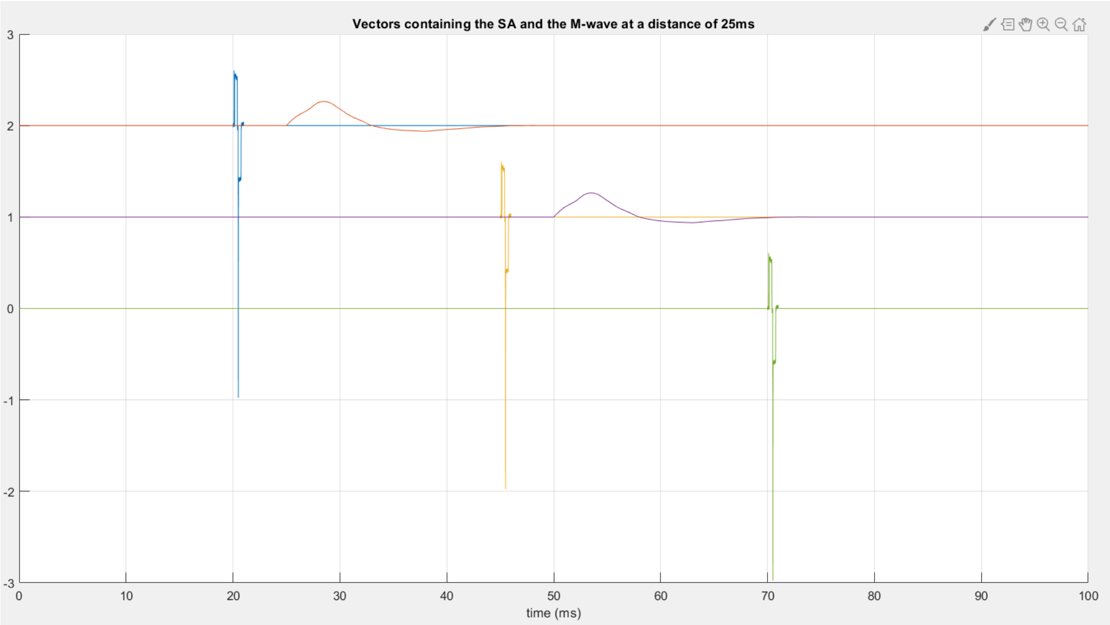

Figure 4.17: Composition of the input signal used for the LT-Spice simulation. The values reported on the vertical axis are not indicative as the positioning of the signals was done purely for the purpose of demonstrating how they are summed over time, so the only indicative axis is the x axis which reports the times. also to make it visible in comparison to the SA, the M-wave has been multiplied by a factor of 100.

The starting sEMG signal had a duration of about 60s, contained 10 muscle activations, the sampling frequency with which it was taken was 1kHz and the acquisition board introduced a gain factor of 500.
The first action was to high pass filter with a cutoff frequency equal to 15Hz to eliminate low-frequency noise. Subsequently, the signal was resampled to have 8000 samples per ms to have the same sampling of the stimulation artifact already provided in digital format. The last steps were the division by 500 of the signal in order to bring it back to a situation before amplification and finally a large number of samples were removed before and after the portion of the interesting signal in such a way as to have a 100ms track in the middle of muscle activation.

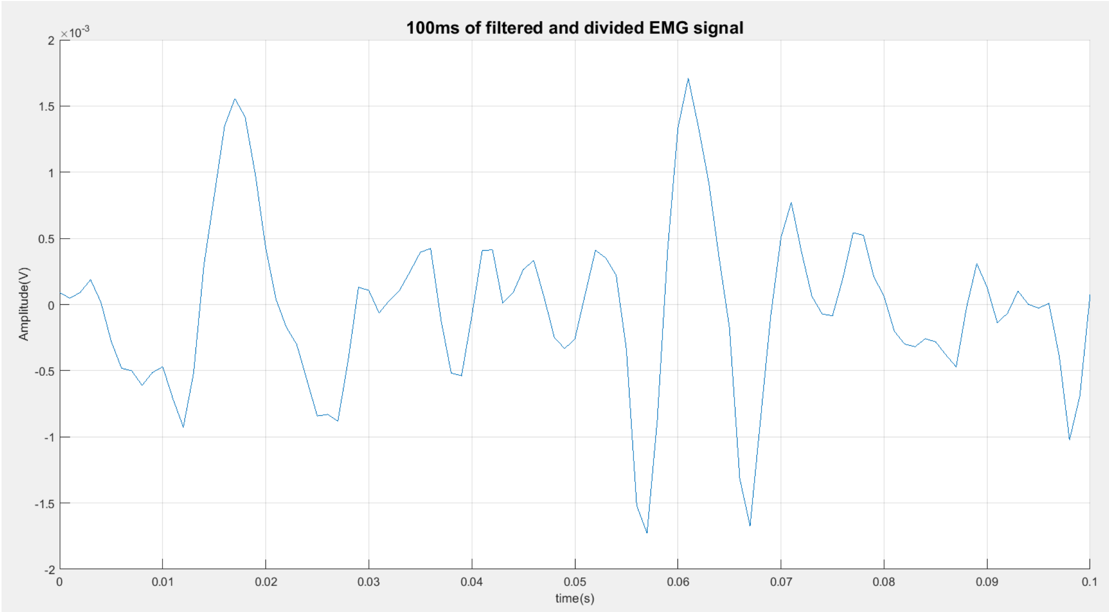

Figure 4.18: 100ms signal extrapolated in the middle of a muscle activation

Once the noise-free signal was obtained, the processing on Matlab continued with the creation of the SA and M-wave sequences.

The first sequence to be carried out was that relating to stimulation artifacts, as the signal of the single artifact was already available, so the actions were to resample it to 8000 samples per ms and to concatenate the signal three times. In order to maintain the distances of 25ms between one and the other imposed by the stimulation frequency at 40Hz, and to leave the first 20 ms of sEMG signal free of any additional noise, the three vectors containing the artifact signal all have the same total length but a different number of zeros before and after the points that actually make up the SA.

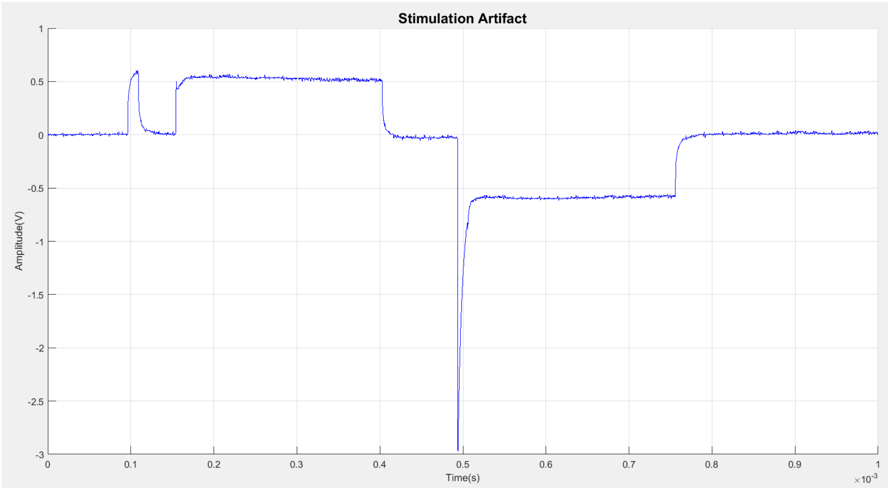

(a) Single stimulation artifact

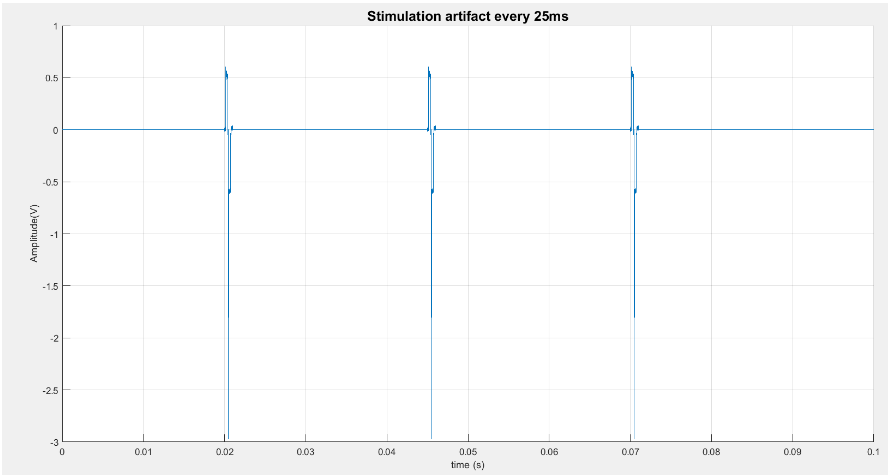

(b) Sequence of three stimulation artifacts

Figure 4.19: Stimulation artifacts signal

Once the artifact sequence was added to the sEMG signal, the work focused on the realization of the M-wave sequence. The single signal was obtained by recreating its shape point by point taking as a reference the image [4.3]. In particular, a point was taken every ms and, once the vector with all the points was formed, a cubic interpolation was applied to obtain a smoother line and with the same number of samples per ms (8000 samples/ms). Subsequently, as for the stimulation artifact, two vectors of the same length but with a different number of zeros before and after the points defining the M-wave were created and finally they were added together obtaining the result shown in the figure [4.20b].

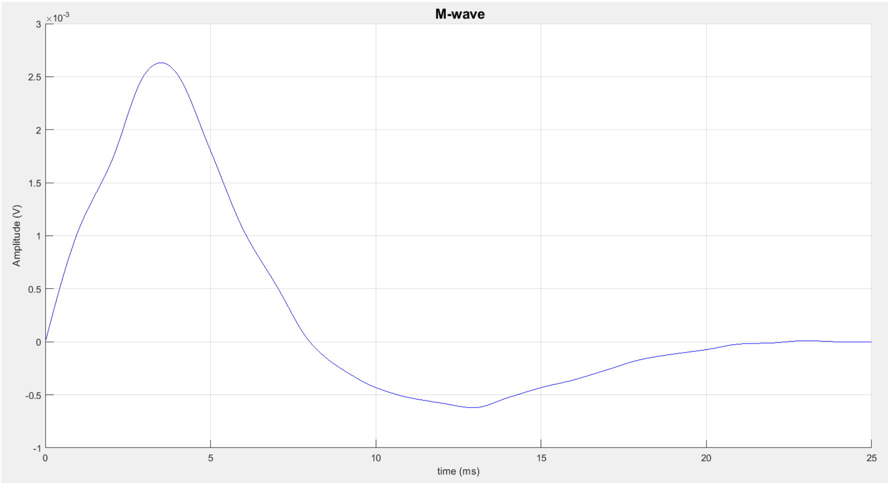

(a) Single M-wave

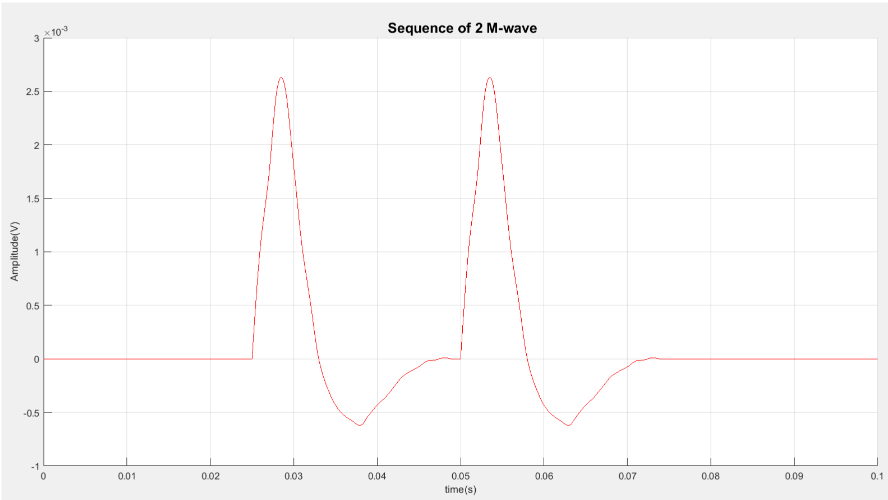

(b) Sequence of two M-wave

Figure 4.20: M-wave signal

Finally, both sequences were added to the 100ms of sEMG signal obtaining the result shown in figure [4.21] from which the problem related to the stimulation artifact is clearly noted, in fact, when it is present, it has an amplitude such large compared to the sEMG signal to make it extremely difficult to visualize and recognize the M-wave or any other muscular signal.

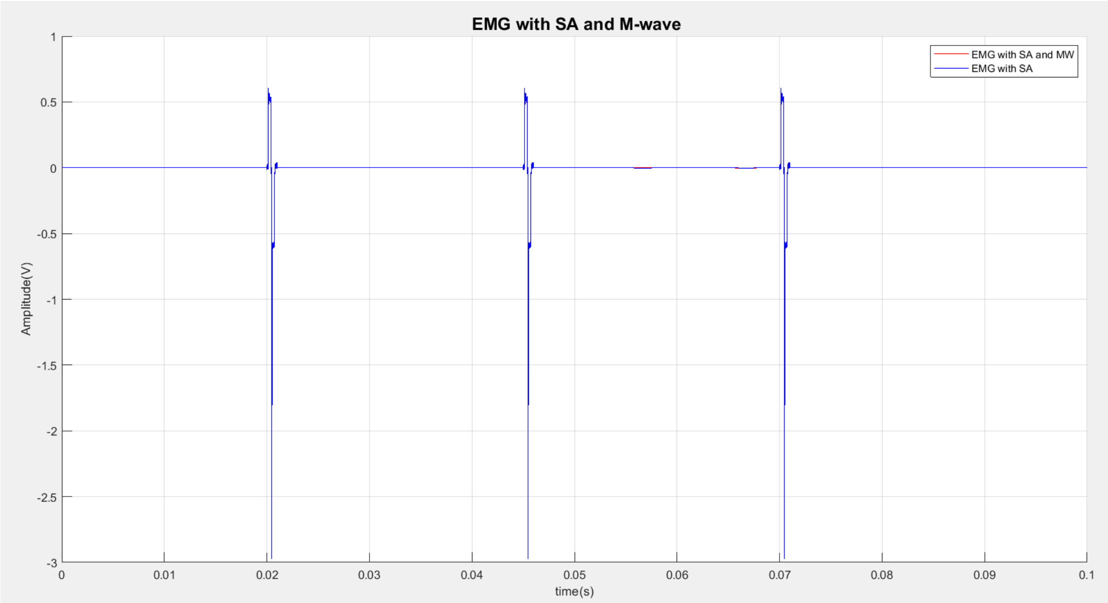

Figure 4.21: 100ms signal with superimposition of SA and M-wave sequences

All the signal processing is shown schematically in the image below [4.22].

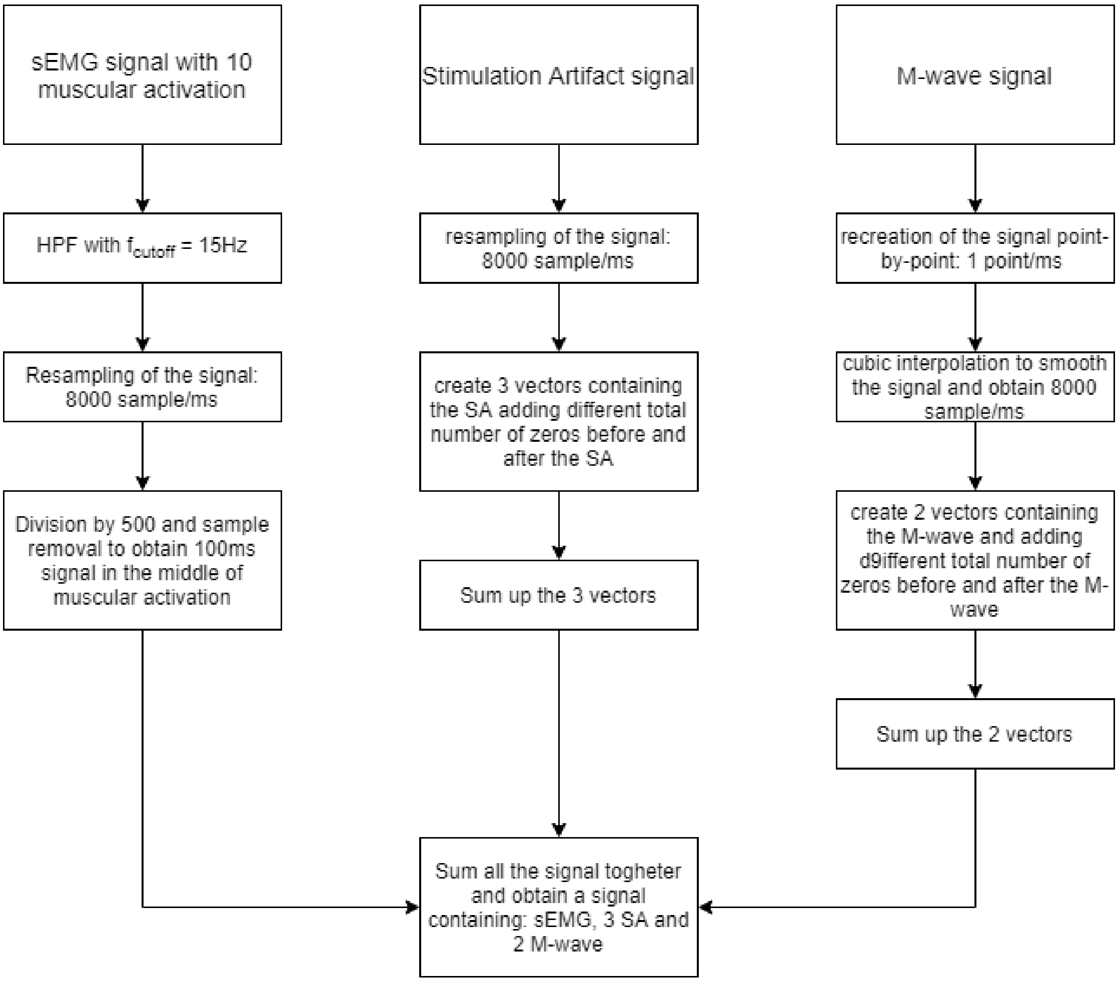

Figure 4.22: Block diagram of signal processing performed to obtain a 100ms signal containing both SA and M-wave

4.6.3 LT-Spice simulation

The whole circuit described in section [4.6.1] has been reported on LT-Spice to proceed with the simulation of the behaviour. To verify the operation of the SA blanking by the switches, the signal processed on Matlab and described in section [4.6.2] is given as input to the differential branches of the board.
The power supply voltage equal to 1.8V and the reference voltage equal to 0.9V are generated by voltage generators external to the circuit, the switches are controlled using a square waveform that every 25 ms assumes a high logic value for 1 ms. Furthermore, an initial delay of 20ms has been added to the command signal of the switches, which coincides with the duration of the initial portion of the sEMG signal free of disturbances due to stimulation.

The signal taken out of the circuit at the end of the simulation was reported on Matlab and plotted to observe the behaviour of the entire circuit more easily. In order to make a comparison as truthfully as possible, the original EMG signal with no artifacts and without switching the switches, the EMG signal with only the SA and switching of the switches and finally the EMG signal with SA, M-wave and switch switching were plotted together.
From the graph below (image [4.23]) it can be seen that in correspondence with the switching of the switches (dashed lines) the artifact is effectively removed without eliminating the M-wave (blue signal) which retains its contribution in amplitude but not the shape. Furthermore, it is necessary to underline how the contribution of the switches leads to small variations of the signal in the 3-4 ms following the return to the initial position of the switches.

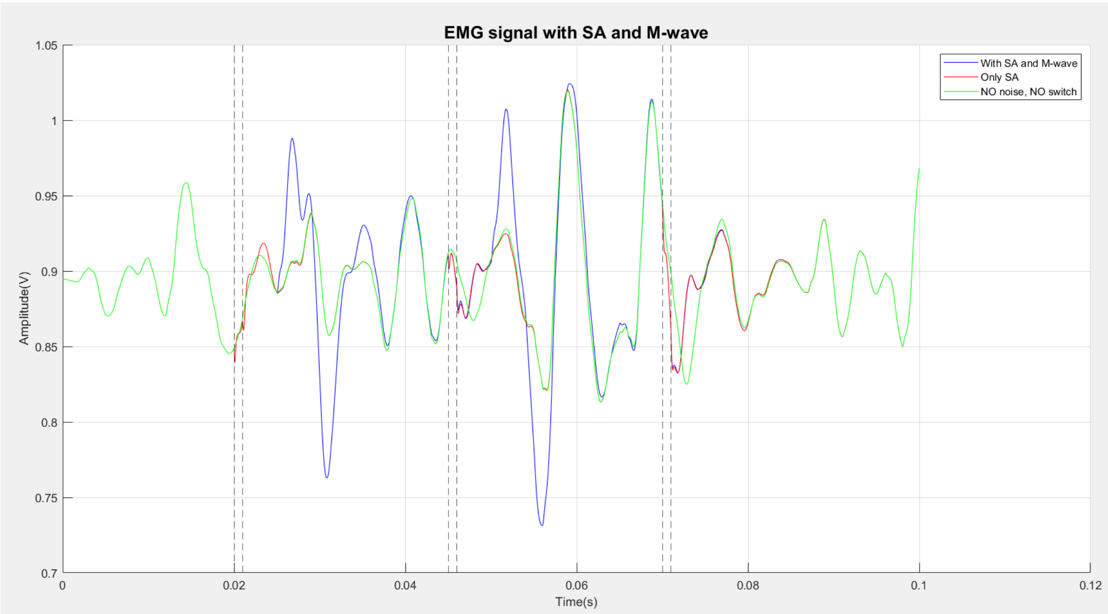

Figure 4.23: Comparison between three signal: pure sEMG signal without the contribution of the switches, sEMG with the SA and the contribution of the switches, sEMG with SA, M-wave and the contribution of the switches

4.7 Implementation and experimental results

Given the promising results provided by the LT-Spice simulations the physical device was tested using:

- an Apollux board as the one shown in the figure [4.10], used to acquire the sEMG signal
- the Apollo3 EVB microcontroller to drive the switching of the SPDT switches
- a circuit mounted on a breadboard that includes: the switches to disconnect the body during stimulation, a voltage divider to supply the reference voltage equal to 0.9V to the switches, a push-button to simulate the arrival of an impulse and a last stage useful for the recognition of the initiation of stimulation.

4.7.1 Implemented circuit

The switches used are of two different types due to the availability of components, an ADG734 was used for the recording electrodes since it includes four SPDT switches which then go through between two positions connected to different branches, while for the reference electrode it was used an ADG811 composed of four SPST switches of which only two were used.
The operation is the same as previously described for which all the electrodes, in normal conditions, are connected to the acquisition board while in stimulation conditions they are carried to GND. As regards the Apollux device, the acquisition channels, when they are disconnected from the electrodes, are brought to the reference voltage equal to 0.9V, obtained using a voltage follower with a voltage divider on the non-inverting input, while the branch feedback remains floating.
The circuit diagram with which the switches and connections were mounted is shown below [4.24]

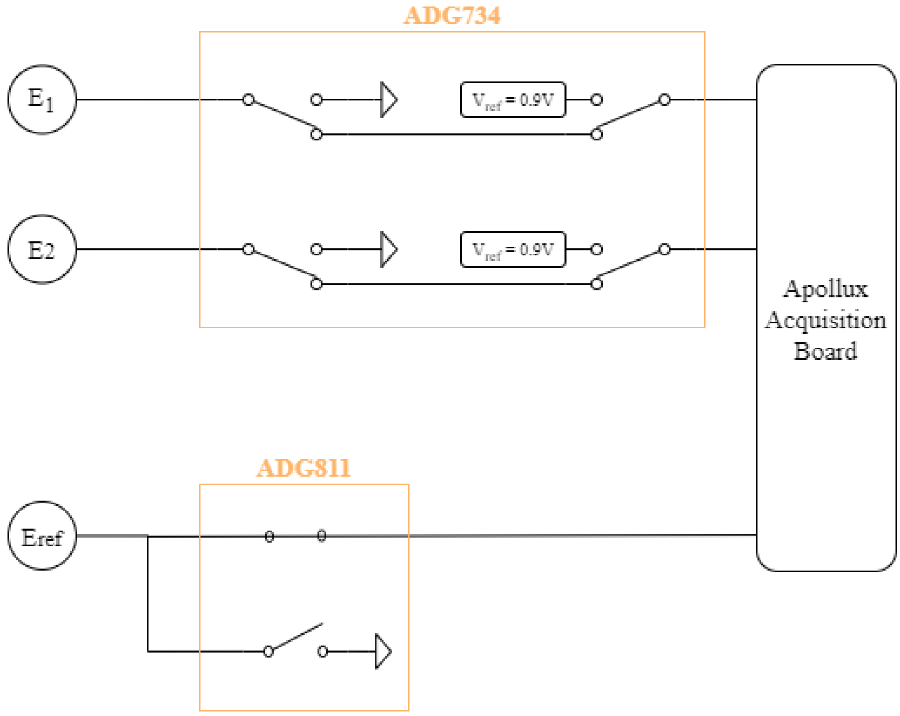

Figure 4.24: Real circuit mounted on breadboard

To what concern the push-button used to simulate the arrival of an electrical stimulation pulse, it was connected between ground and power supply by adding a pull-up resistor for the correct functioning. The signal taken between the button and the resistor assumes a high or low logic value and is directly connected to a GPIO of the microcontroller.

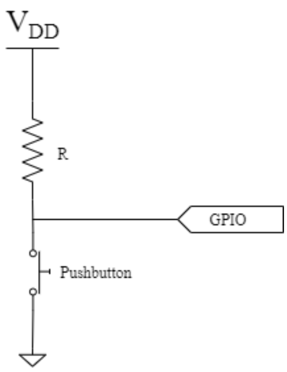

Figure 4.25: Circuit for the push-button

In the real case, where electrical stimulation is present, it is necessary to have a circuit for pulse recognition and thus generate an interrupt on the microcontroller. In this case, two operational amplifiers were used to generate a signal which, from a low logic value, passes to a high logic value when there is a stimulation impulse. The operational, whose output is connected to a GPIO of the microcontroller different from the one used for the push-button, has the two probing electrodes as inputs and the reference voltage generated by the second operational in voltage follower configuration with a voltage divider on the non-inverting terminal.

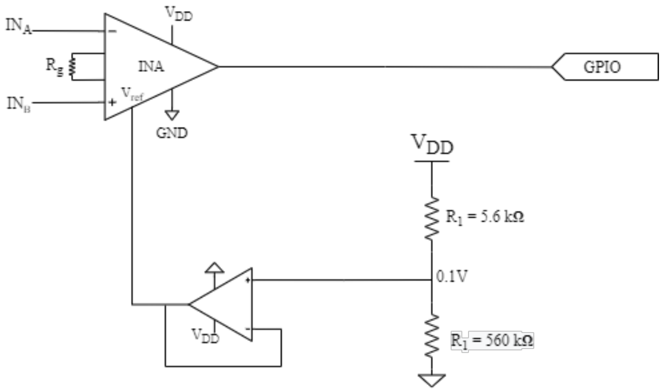

Figure 4.26: Circuit for electrical stimulation pulse recognition. The input IN_A and IN_B are connected to the recording electrodes

To conclude, figure [4.27] shows the block diagram of the entire circuit.

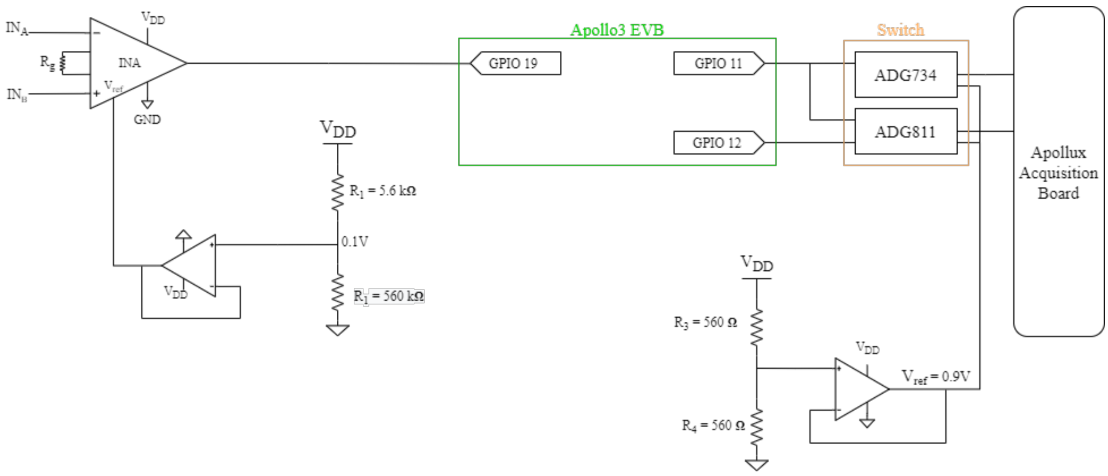

Figure 4.27: Block diagram of the whole circuit mounted on breadboard

4.7.2 Programming of the microcontroller

The microcontroller used is an Apollo 3 EVB of the Apollo MCU family, they are ultra-low-power microcontrollers, highly integrated and based on Ambiq Micro's patented "Subthreshold Power Optimized Technology" platform.

The C code written to program the microcontroller is based on the use of interrupt service routines and timers. In particular, based on the active GPIO at the input, the microcontroller will recognize the transition from high to low in the case of the GPIO connected to the push-button, or from low to high in the case of the GPIO connected to the circuit that recognizes the arrival of the electrical impulse. Once the transition has been recognized, an interrupt is triggered which calls two functions simultaneously: the first relating to the timer set to count up to 1.2ms and the second which takes care of driving the GPIOs connected to the switches to make them switch and disconnect the body from the device . After the set time interval is elapsed, the timer function generates a second interrupt that calls the function to bring back the switches to their initial state.

It is necessary to underline that for the switches two different GPIOs were used, normally set with opposite values, so the one that controls the ADG734 and a single SPST switch of the ADG811 in static conditions has a high logic value, while the one that controls the other SPST switch used by the ADG811 initially has a low logic value. This solution was adopted for two reasons:

- the ADG734 component is equipped with an inverter on the command signal inputs, so in order not to have a position change of the switches already at the beginning, it is necessary to supply a signal with a high logic value which, once inverted, will be perceived as low and not will cause commutations.
- the switches used on the ADG811 component must open and close alternately so that two different command signals are required.

4.7.3 Circuit testing

The entire circuit, consisting of Apollux, Apollo3 EVB and components mounted on breadboard, was tested using the Rigol MSO5000 digital oscilloscope to take the output signals from the Apollux board. All the acquisitions have been digitized and reported on Matlab to allow a correct visualization.

The tests were performed by varying the stimulation current, starting from 2mA up to 26mA, with a fixed increase of 8mA and sending only one pulse at a time in such a way as to be detected by the dedicated GPIO of the microcontroller and causing only one cycle of commutation of the switches.

The results reported on Matlab are shown in figure [4.28] from which it is possible to notice how the peak of the SA has been partially removed and partially replaced by another type of noise whose amplitude and duration depend, in a directly proportional way, by the intensity of stimulation current.

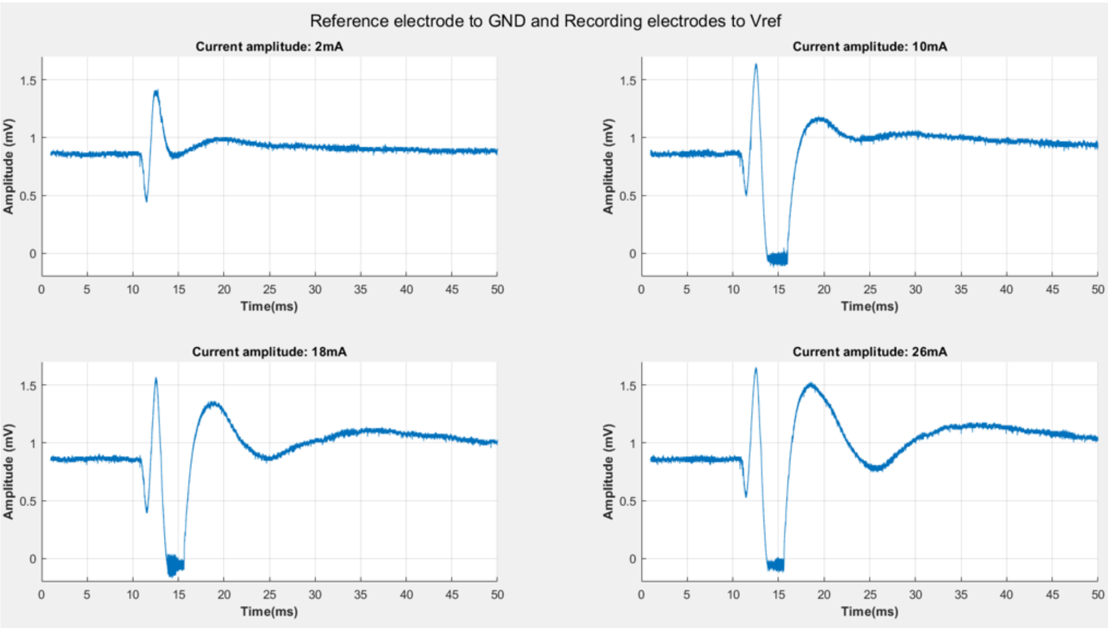

Figure 4.28: Measurements from the circuit mounted on breadboard

It was therefore necessary to investigate the origin of these voltage peaks.

4.8 Investigation on alternative input stages

Before investigating the origin of the spikes, tests were carried out to reduce the phenomenon using an RC circuit, commonly used for the removal of spikes generated by the commutation of switches, but did not give positive results. For this reason, it was essential to understand its origin and in this regard, several tests were carried out with related changes to the circuit and programming of the microcontroller aimed at excluding each one a different cause.

4.8.1 Test 1: commutation of the switches on identical paths

The first test performed has the purpose of verifying the correct functioning of the switches. Being solid-state components they should not introduce noises during switching but wanting to perform an accurate study they were equally tested in two different configurations and keeping the reference electrode always connected to avoid circuit instability.

The first configuration involves the use of all four switches of the ADG734 which commutate simultaneously between two identical paths connected to the recording electrodes.

The second configuration is similar but instead of using all four switches, only two are used, which commutate on identical paths connected to the recording electrodes.

The circuits are shown in figure [4.29a] and [4.29a], while the test result is shown in image [4.30].

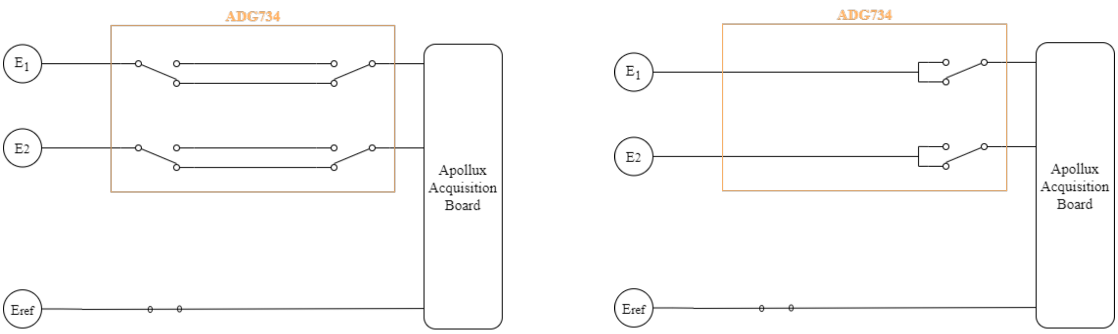

(a) Four switches **(b)** Two switches

Figure 4.29: Test 1: switch commutation between two identical path

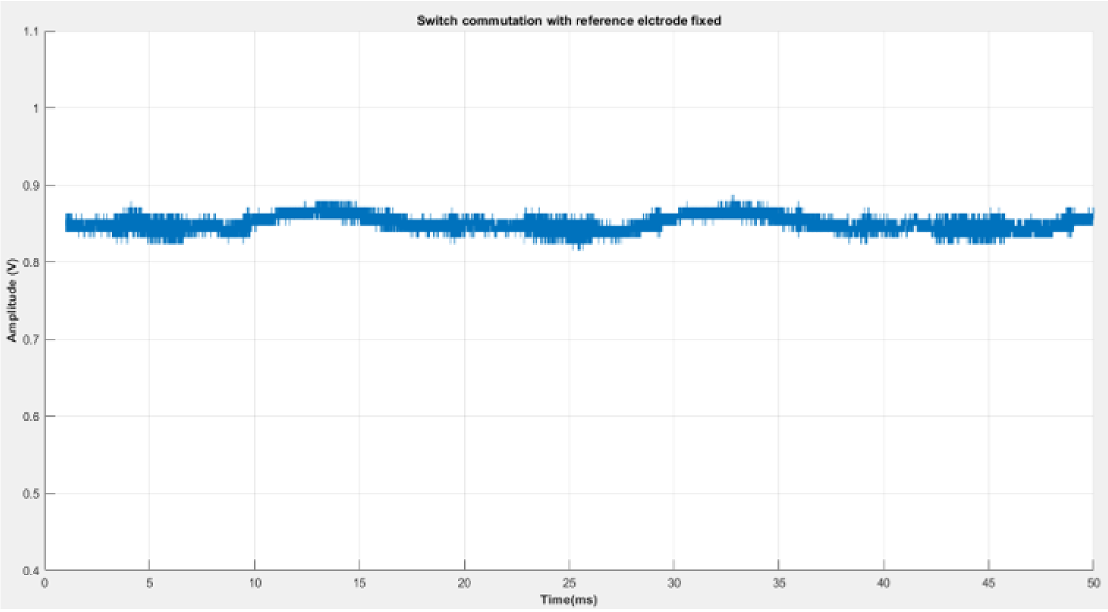

Figure 4.30: Simulation results of test performed by commutating the switches between two identical path

4.8.2 Test 2: commutation of the switches with early and late closing

This second test aims to verify if the too rapid variation of the common mode, deriving from the variation of the input signal on the two branches of the acquisition board, first coming directly from the body, and then equal to the reference voltage at 0.9V, may be the cause of the spikes.

Also in this case two types of the same test were tried by changing the opening and closing times of the switches that are connected to the reference voltage by adding a timer in the programming code of the microcontroller.

For the first try, a delay ΔT was added with respect to the opening of the switches connected to the electrodes, so the body is first disconnected, the input branches remain floating for a period equal to ΔT, and then they are connected to the reference voltage.

In the second case, instead of introducing a delay, the switches related to the reference voltage are closed with an advance ΔT, so before disconnecting the body there will be a time interval in which the input branch is connected both to the body and at the reference voltage.

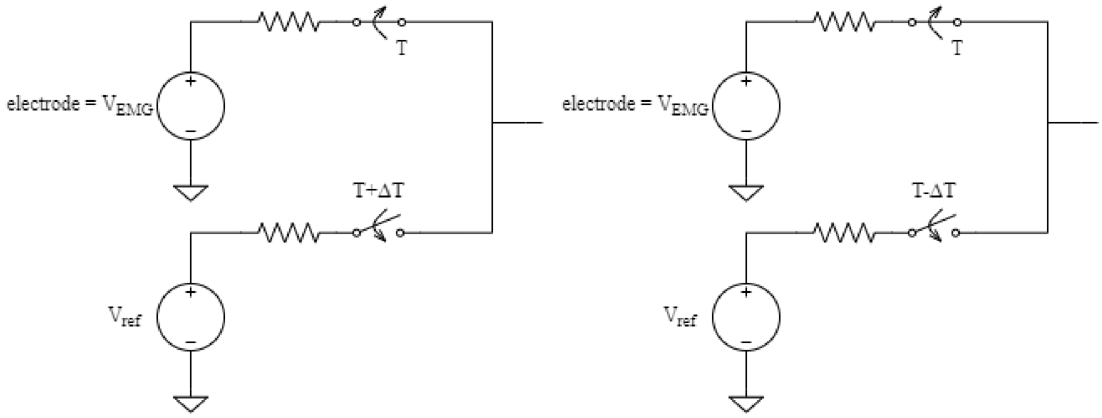

(a) Delay **(b)** Advance

Figure 4.31: Test 2: switch commutation with early and late closing of switch towards reference voltage

Both tests introduce an intermediate state between the common-mode generated by the voltage taken from the body and the reference voltage which should stabilize the response of the circuit.

The ΔTs set are equal to 300, 600 and 900ns both when a delay is introduced and when closing is anticipated. The results are shown in figure [4.32a,5.2b] from which we can see that the voltage spike is always present and variable based on the time interval used.

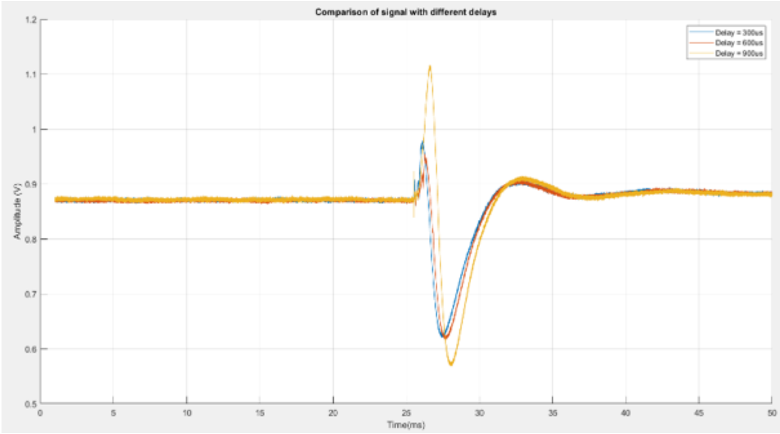

(a) Delayed commutation

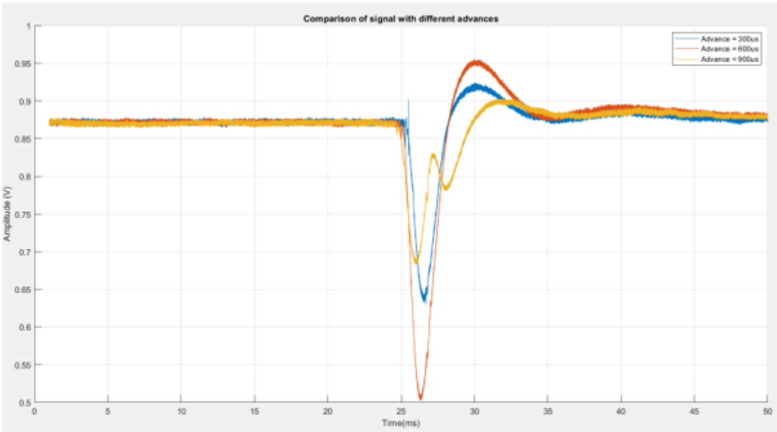

(b) Advanced commutation

Figure 4.32: Simulation results of test performed by adding a delay or an advance in the commutation of the switches

From here it is also reasonable to exclude the rapid variation of the common mode from the causes of the origin of the spikes.

4.8.3 Test 3: four switches for each recording electrode

The last test was carried out by making the variation between body voltage and reference voltage as gradual as possible to verify if this strategy could contribute to the cancellation of the spikes coming out of the circuit.

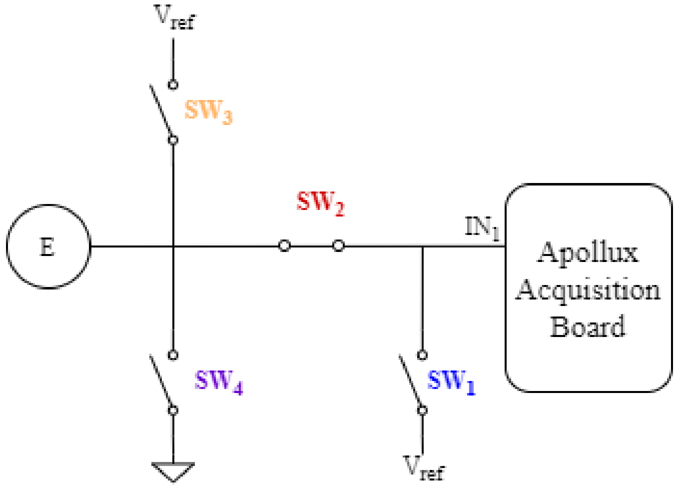

Figure 4.33: Test 3: use of four switches for each recording electrode

To perform this test it was necessary not only to modify the circuit by adding switches but also to modify the code substantially in order to introduce two new timers (100ns and 1μs) in addition to the one already present (1.2ms) and finally also the actions related to the number of times the interrupt is generated by the timer that has finished counting. Specifically, two functions have been added, both containing a switch-case that returns different commands to the GPIOs that drive the switches.

The execution sequence for closing and opening the switches is as follows:

1. Closing switch 3 and calling the 100ns and 1.2ms timers
2. Closing switch 1 and calling the 1μs timer
3. Opening switch 2 and calling 1μs timer
4. Opening switch 3 and calling 100ns timer
5. Closing switch 4

At this point it is necessary to wait for the 1.2 ms timer to finish counting, once this interval has elapsed, we have:

6. Opening switch 4 and calling 100ns timer
7. Closing switch 3 and calling the 1μs timer
8. Closing switch 2 and calling the 1μs timer

9. Opening switch 1 and calling 100ns timer

10. Opening switch 3 and end of execution.

For clarity below (image [4.34]) the timing of the signals taken by the digital oscilloscope with which the switches are driven is shown and where the high logic signal indicates the opening of the switch while the low logic signal indicates its closure. It should be noted that the switching intervals of less than 1ms, declared in the code written for the microcontroller, in reality, are not fully respected due to the physical limits of the device, in any case, they have been kept in the order of hundreds of μs.

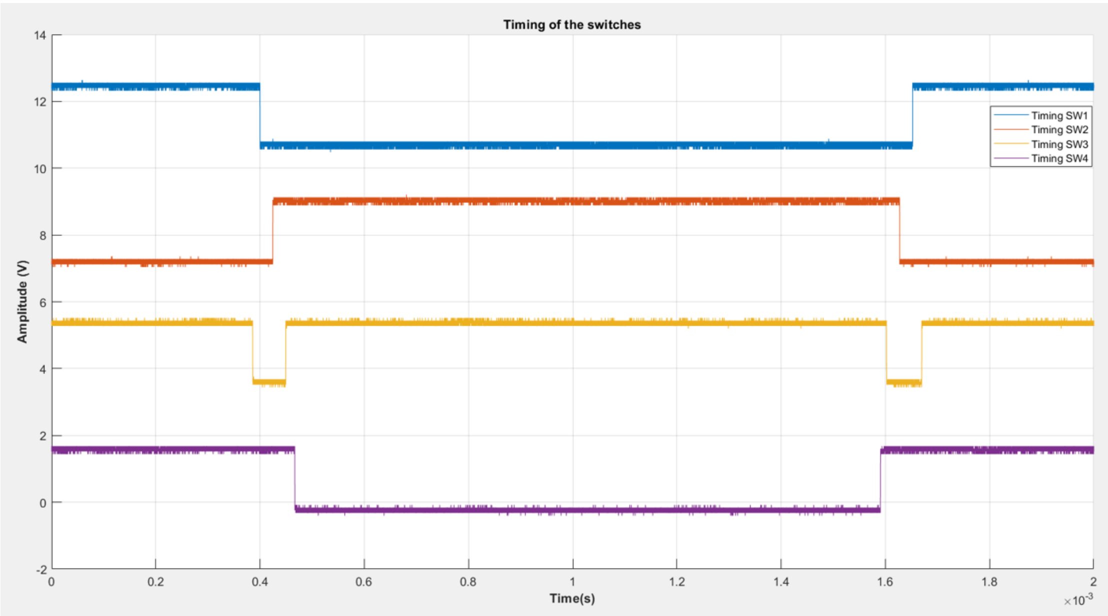

Figure 4.34: Timing of switch command signals

The results obtained continue to present voltage spikes at the instants in which the switches commutate, since the switching intervals are very short at the output of the circuit there is a single spike with a duration of about 25ms and a high amplitude close to the upper limit of dynamics accepted by the circuit.

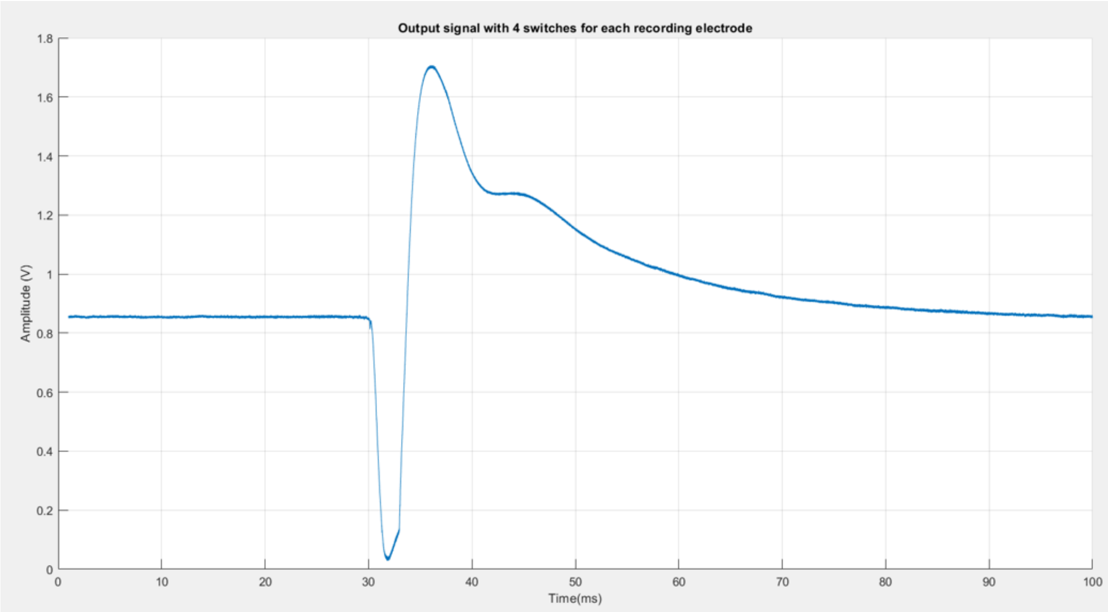

Figure 4.35: Simulation results of test performed by using four switches for each recording electrode

4.8.4 Conclusions on the origin of the spikes

Having excluded all other causes, the most reasonable hypothesis on the origin of these voltage spikes is that they are caused by the considerable and sudden decrease in the impedance seen at the input when the body is disconnected. Since eliminating this type of voltage spike would have meant making a substantial change to the hardware before going down this path, it was preferred to try software removal of the stimulation artifact.

Chapter 5

Software Stimulation Artifact Suppression

For the software removal of the stimulation artifact, the electromyographic signal was not taken directly from the electrostimulated muscle but, in the case of the arm, from the antagonist muscle, again using the Apollux acquisition board. The choice turned out to be convenient since the duration of the artifact is about 10 times shorter than the one detected on the electrostimulated muscle.

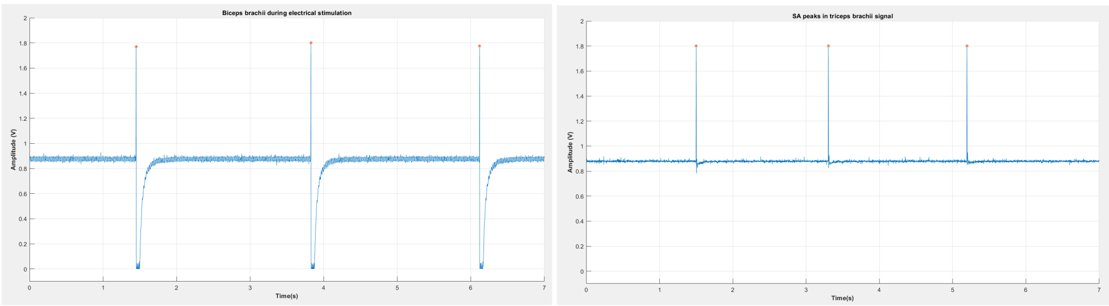

(a) SA detected on stimulated muscle (biceps brachii) **(b)** SA detected on antagonist muscle, not directly stimulated (triceps brachii)

Figure 5.1: Comparison between SA recorded from directly stimulated and not directly stimulated muscle

The technique used for software removal in post-processing is based on the subtraction of a model of the artifact, obtained previously, and notch-type filtering to eliminate any disturbances correlated to stimulation frequency and the components present in the second and third harmonic.
Finally, the ATC technique was applied (see section [1.2.4]) to detect the periods

of voluntary muscle activation during stimulation.

The ATC technique was also applied to the signal taken directly out of the acquisition device and not processed in order to compare the results and have an objective comparison on the usefulness of signal processing.

5.1 Signal processing algorithm

The signal was taken 5 times for each current intensity used starting from 2mA and reaching up to 10mA increasing in 2mA steps, in order to obtain a good sample of signals and to verify the reliability of the results.
Each signal lasts about 20s and is composed of two phases: a first phase of stimulation only and a second in which, during the stimulation, a voluntary contraction of the brachial biceps muscle is performed which leads to complete flexion of the arm.

The signal processing was performed on Matlab and the first step was to bring the baseline of the signal back to zero by subtracting the average value of the baseline from the signal itself. Subsequently, the part containing the recording of the stimulation only and the one containing both the stimulation and the voluntary activation were separated in such a way as to have two separate vectors and to be able to proceed with the extraction of two different SA templates: a generic one of a stimulation signal and a more specific one of muscle activation added to stimulation.

In both cases, the artifact model was calculated as follows: all the peaks present in the signal were identified using the appropriate function of Matlab *findpeaks()* by setting a minimum height to detect only the peaks due to electrical stimulation. After identifying the peaks, 5 samples were taken before the peak and 20 after it and in this way it was possible to take the entire range of samples containing the peak and the tailing part of the stimulation artifact.

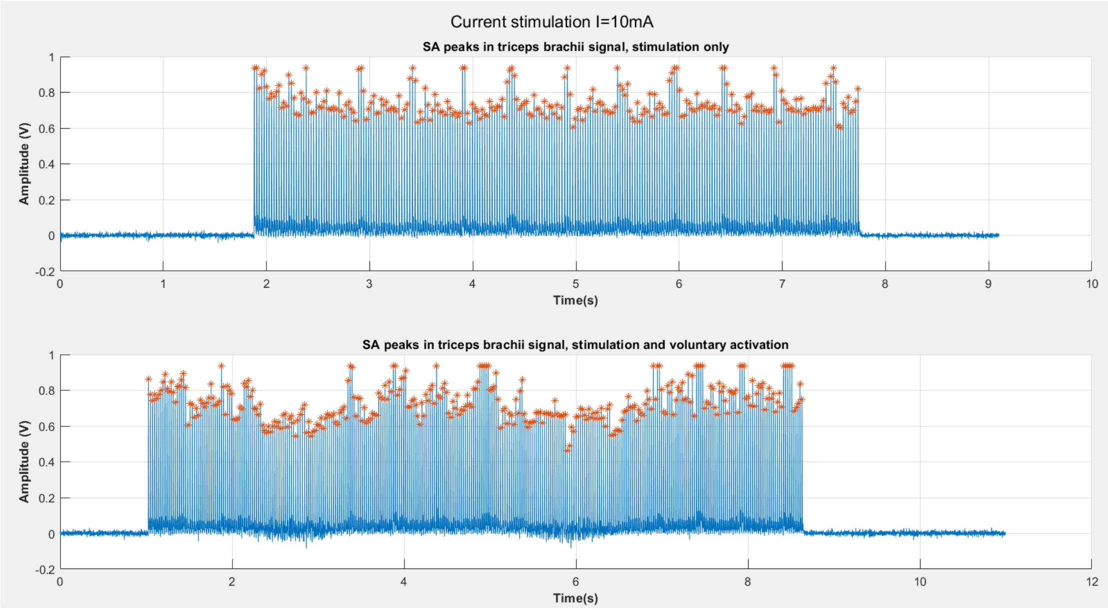

(a) Detection of SA peaks in the raw signals

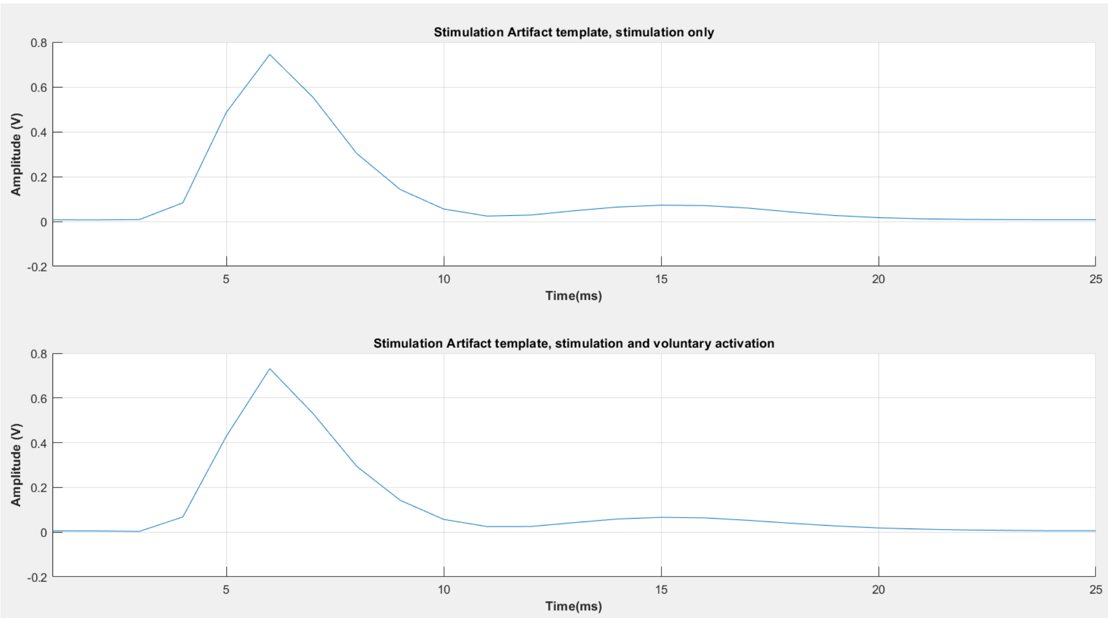

(b) Evaluated SA template both from generic stimulation signal and from signal with stimulation and voluntary activation

Figure 5.2: Evaluation of SA template starting from raw signals

Once the generic or specific model was calculated, it was subtracted from both the stimulation-only signal and the signal also containing the voluntary activation, identifying the intervals in which to subtract it in the same way in which they were identified to evaluate the model, i.e. starting from the identification of the peak point, 5 samples were taken before and 20 after. Of the two types of templates removed, the one that proved to be more effective is the one calculated from the simple stimulation signal even if the differences with the other type of model are minimal.

The next step was to apply three II-order IIR notch filters at 40Hz, 80Hz and 120Hz in order to eliminate disturbances at the stimulation frequency (40Hz) and at the first two harmonics. Finally, the signal obtained was squared and so rectified to have only positive values and to make the use of the ATC technique more effective.

Finally, the ATC technique described in section [1.2.4] was applied, the threshold value was obtained by adding three times its standard deviation to the mean value of the baseline. This choice for the threshold value was made to make all the calculations automatic and not left to arbitrary decisions that could be less accurate.
The ATC technique was applied to both signals separately, the final result was obtained by subtracting from the ATC values of the signal with stimulation and voluntary activation of the muscle, the ATC values obtained from the stimulation signal alone.
The entire signal processing algorithm is reported in figure below:

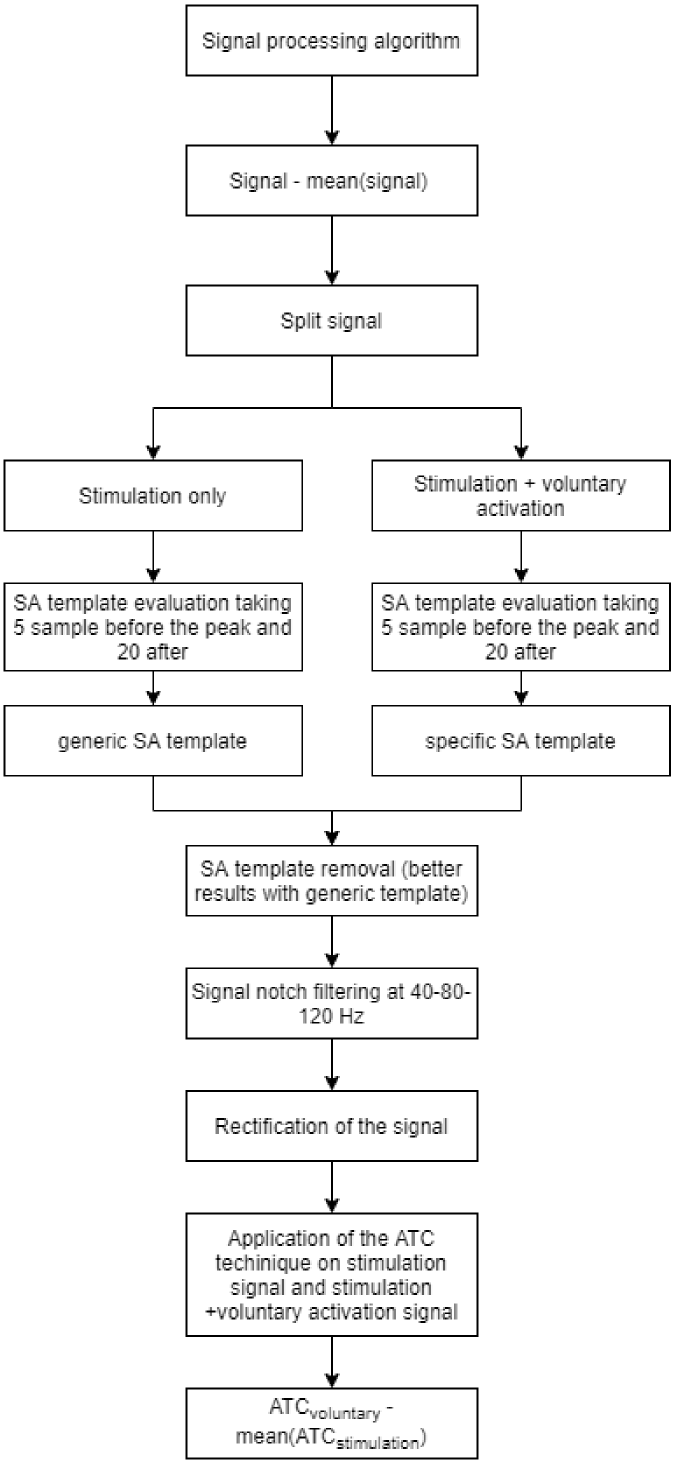

Figure 5.3: Flowchart of signal processing algorithm implemented for software SA removal

To confirm the usefulness of this software removal, the ATC technique was also applied to the signal taken directly out of the Apollux board without undergoing any type of further software manipulation.

5.2 Results

The results obtained both on the processed signal and on the raw signal were grouped by current intensity and compared the 5 tests carried out, so in the images [5.4],[5.5],[5.6],[5.7],[5.8] it is possible to observe the ATC values of the processed signal on the right column and the ATC values of the raw signal on the central column.

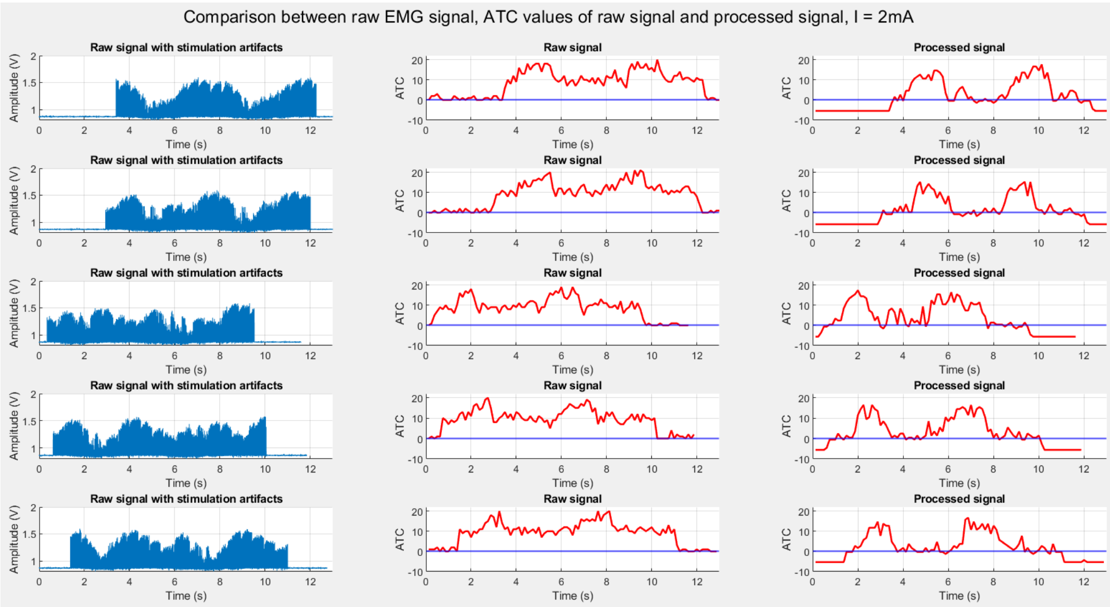

Figure 5.4: Comparison between ATC values obtained from the processed signal and from raw signal, I = 2mA

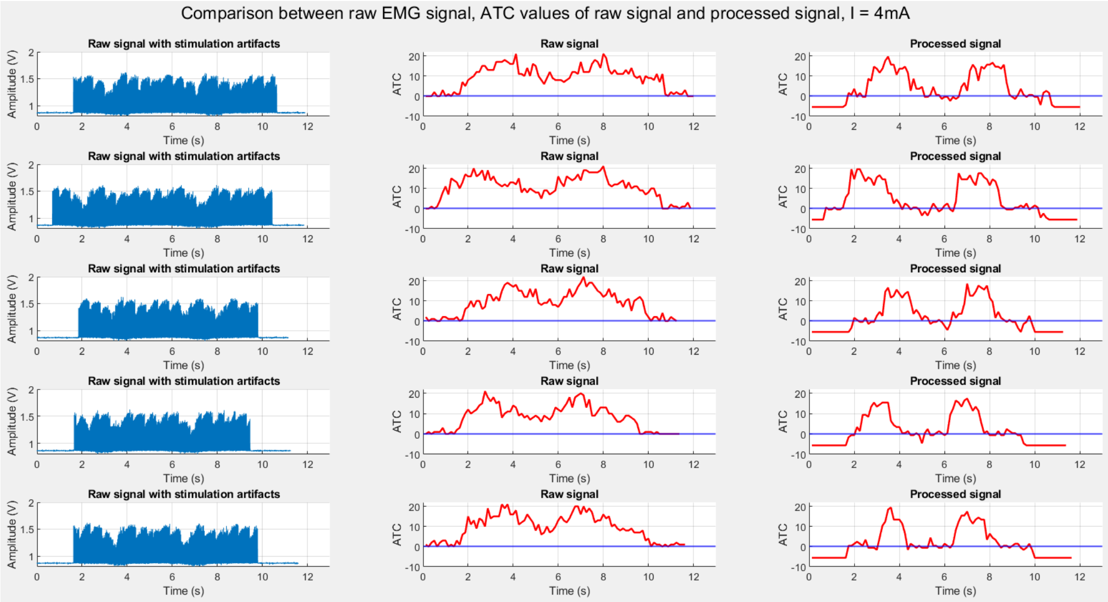

Figure 5.5: Comparison between ATC values obtained from the processed signal and from raw signal, I = 4mA

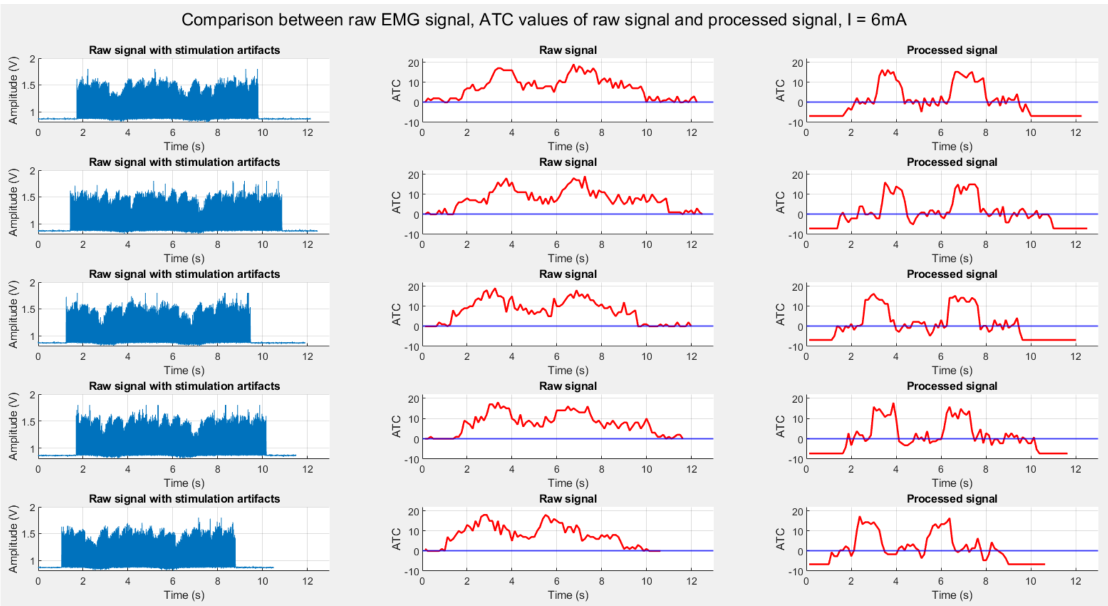

Figure 5.6: Comparison between ATC values obtained from the processed signal and from raw signal, I = 6mA

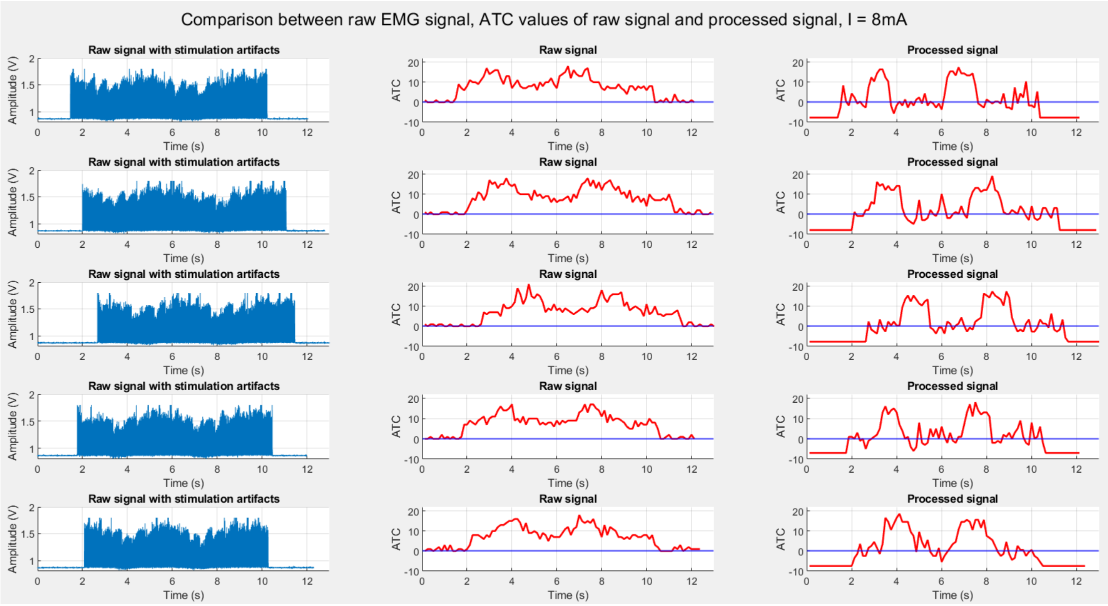

Figure 5.7: Comparison between ATC values obtained from the processed signal and from raw signal, I = 8A

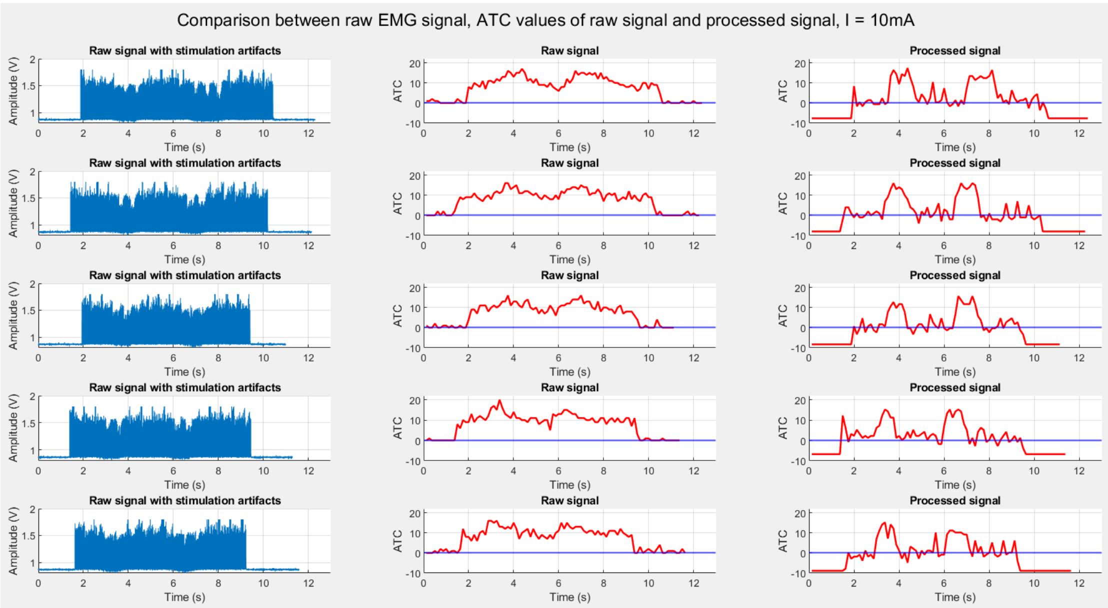

Figure 5.8: Comparison between ATC values obtained from the processed signal and from raw signal, I = 10mA

From these results, it is possible to make some observations: the first is that

signal processing is actually useful to more clearly distinguish the moments of voluntary activation from those intervals in which there is only electrical stimulation. Furthermore, applying the ATC technique on the raw signal it is not always possible to detect something while with the processed signal the results have constant repeatability.
The second observation concerns the ATC values, in fact for the processed signals there are on average higher values, which reach peaks equal to 20, compared to those of the raw signals whose peaks do not reach 15.

Finally, the third observation relates to the stimulation current intensity values, from the image [5.9] it can be seen that as the stimulation current increases, the reduction of the ATC values of the stimulation in the signal also containing the voluntary activation, subtracting the average value of the ATC values of the stimulation alone, it is less effective so that there are quite high peaks even when there is no voluntary activation. However, this does not significantly compromise the distinction of the periods of voluntary activation from those of electrical stimulation alone, since the peaks relating to voluntary movement have a longer duration.

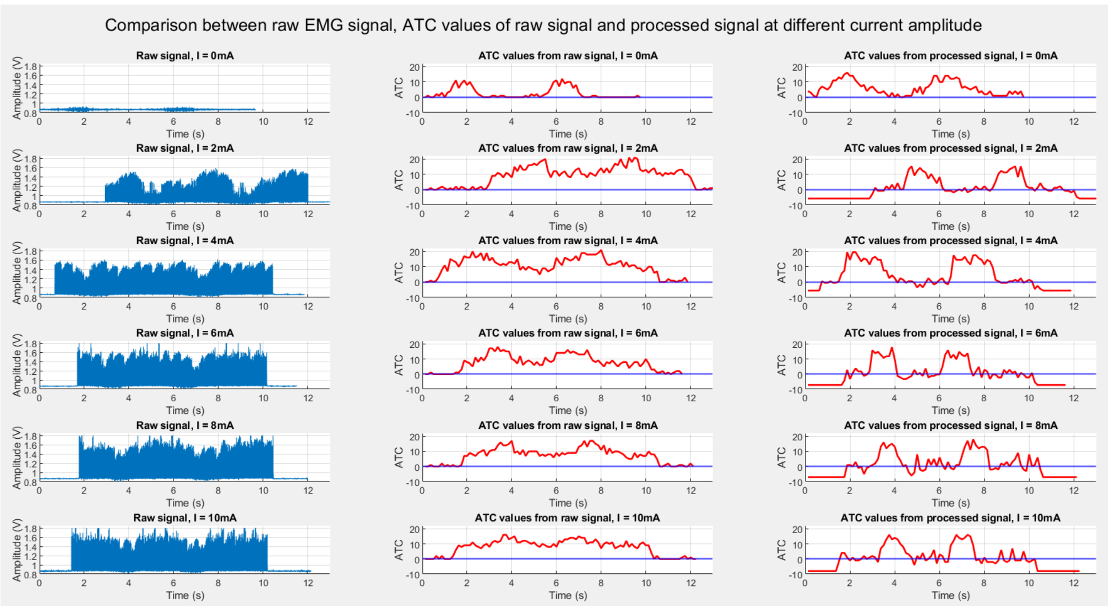

Figure 5.9: Comparison between ATC values evaluated at different stimulation-current intensity

To study the robustness of the ATC technique, all the signal processing was also applied to sEMG signals always taken from the triceps brachii but without electrostimulating the biceps. The results shown in figure [5.10] display that despite all the processing undergone by the sEMG signal, the ATC profiles can still be extracted quite precisely, in fact the highest values of ATC occur in correspondence with muscle activations.

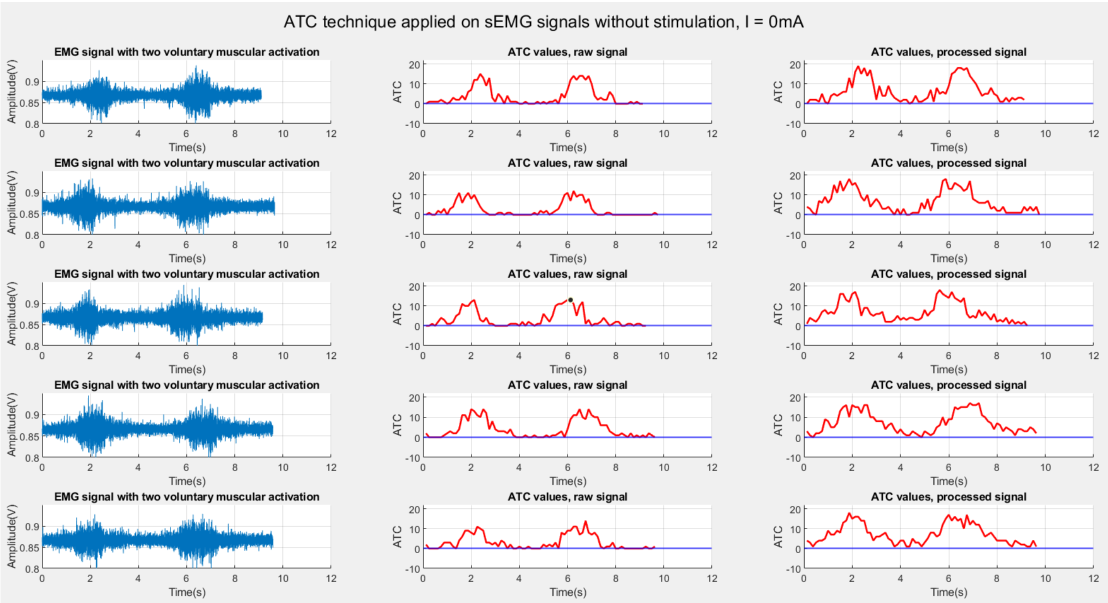

Figure 5.10: ATC evaluated from pure sEMG signal without stimulation

All this software removal process has proved to be particularly useful combined with the ATC technique as it allows to have a distinction between voluntary activation and activation caused by stimulation, which is not visible if the ATC technique is applied directly on the signal recorded by the stimulated muscle using the switches described in the section [4.7] and then applying hardware signal blanking.
From the graphs below ([5.11],[5.12], [5.13]) it is evident how, in addition to the noises due to stimulation, the voltage spikes due to the impedance variation are added (see section[4.8.4]) which do not allow a useful visualization for the study of the voluntary response of the muscle.

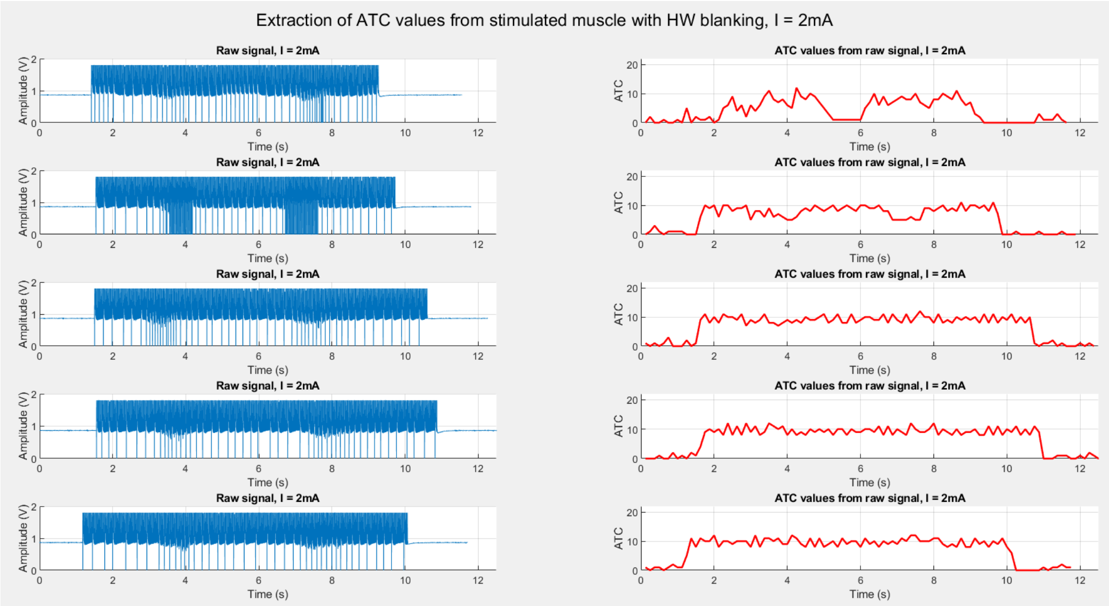

Figure 5.11: ATC evaluated from stimulated muscle after hardware blanking technique, current applied I = 2mA

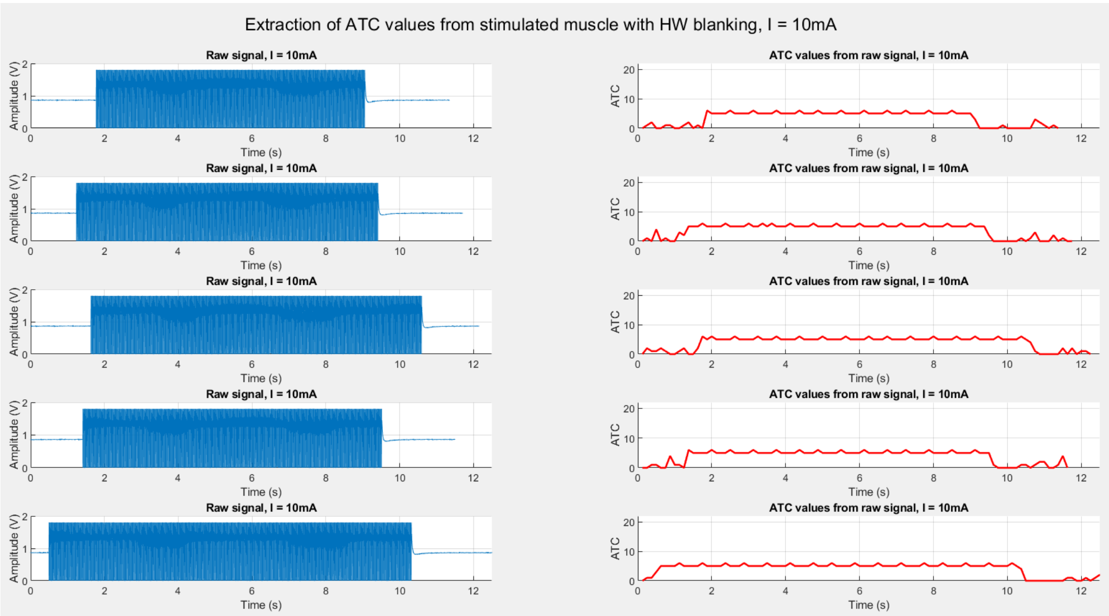

Figure 5.12: ATC evaluated from stimulated muscle after hardware blanking technique, current applied I = 10mA

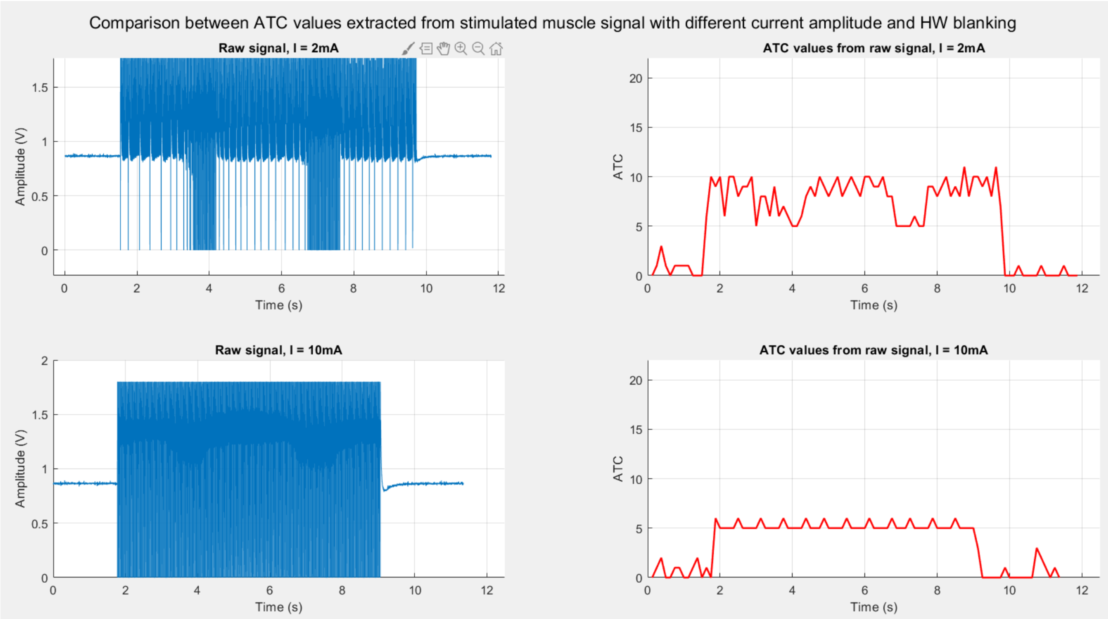

Figure 5.13: ATC evaluated from stimulated muscle after hardware blanking technique, comparison between two different current intensity

Chapter 6

Conclusions and future perspective

The main purposes of this thesis were the optimization of the board and the improvement of the front-end acquisition leading to closed-loop applications, which includes the need to record the sEMG signal even during electrical stimulation.

The first part of the thesis focused on the optimization of the sEMG acquisition board to reach a definitive version, for this reason, the DRL circuit present on the feedback branch of the device was taken into consideration and its performance in terms of signal to noise ratio (SNR) was evaluated. At the end of the analyzes, given the results, it was decided to keep this circuit by modifying the output resistance by increasing its value up to 4.7kΩ.
This decision was made based on the SNR values obtained which, in conditions of movement of the subject and not only of the limb, were greater if the DRL circuit was present.

The second part of the work, on the other hand, was dedicated to improving the front-end acquisition and, specifically, the acquisition of the sEMG signal during muscle stimulation.
First of all, the hardware techniques of signal blanking were tested in order not to record the SA which, however, introduced new disturbances due to the change in impedance that occurs when the electrodes are disconnected from the body.Reducing this new type of noise would have meant making substantial changes to the circuit, so to avoid revolutionizing the hardware, software removal techniques for the SA were tried.
The SA removal technique based on the subtractive method and signal filtering has proved effective when combined with the ATC technique and has provided

good results regarding the distinction between the stimulation signal alone and the voluntary activation signal of the muscle at which the stimulation signal is superimposed on.

Despite the good results achieved there are several studies that can still be done to further improve the device.
The first step could be to improve the signal processing in such a way as to be able to detect voluntary muscle responses in paralyzed patients who could therefore have particularly low amplitudes.
Moreover could be useful to improve the threshold setting technique used for the extraction of ATC values.
Being a rehabilitation device, one of the most interesting studies to be carried out is certainly the one relating to the assessment of muscle fatigue that could occur after a certain number of stimulation sessions. To do this, it might be interesting to study the variation in ATC profiles at the beginning of the rehabilitation session, in the middle and at the end in order to observe, if present, the variation in ATC values.

In this thesis work, as regards the study for the removal of SA, the muscle signals were taken from the antagonist muscle (triceps brachii) and not directly from the stimulated muscle (biceps brachii) as the SA appears to have a duration decidedly minor. In this regard, if one wishes to evaluate the response of the directly stimulated muscle, it would be particularly useful to study and numerically evaluate the correlation that exists between two adjacent muscles and, in this case, antagonists.

Bibliography

[1] Susan E. Mulroney and Adam K. Myers. *Netter's Essential Physiology*. Second. Philadelphia, PA: Elsevier, 2016 (cit. on pp. 2, 3, 5–7).

[2] Roberto Merletti and Dario Farina., eds. *Surface Electromyography: Physiology, Engineering, and Applications*. First. Hoboken, New Jersey: The Institute of Electrical and Electronics Engineers, Inc, John Wiley Sons, Inc, 2016 (cit. on pp. 9, 10).

[3] Ying Dong Yulin Fu Jingjing Zhao and Xiaohao Wang. «Dry Electrodes for Human Bioelectrical Signal Monitoring». In: (2020). DOI: 10.3390/s20133651 (cit. on pp. 12, 14).

[4] Marco Crepaldi, Marco Paleari, Alberto Bonanno, Alessandro Sanginario, Paolo Ariano, Duc Hoa Tran, and Danilo Demarchi. «A quasi-digital radio system for muscle force transmission based on event-driven IR-UWB». In: (2012), pp. 116–119. DOI: 10.1109/BioCAS.2012.6418406 (cit. on pp. 14, 15).

[5] Paolo Motto Ros, Marco Paleari, Nicoló Celadon, Alessandro Sanginario, Alberto Bonanno, Marco Crepaldi, Paolo Ariano, and Danilo Demarchi. «A wireless address-event representation system for ATC-based multi-channel force wireless transmission». In: (2013), pp. 51–56. DOI: 10.1109/IWASI.2013.6576061 (cit. on p. 14).

[6] Stefano Sapienza, Marco Crepaldi, Paolo Motto Ros, Alberto Bonanno, and Danilo Demarchi. «On Integration and Validation of a Very Low Complexity ATC UWB System for Muscle Force Transmission». In: *IEEE Transactions on Biomedical Circuits and Systems* 10.2 (2016), pp. 497–506. DOI: 10.1109/TBCAS.2015.2416918 (cit. on p. 14).

[7] Fabio Rossi, Paolo Motto Ros, Ricardo Maximiliano Rosales, and Danilo Demarchi. «Embedded Bio-Mimetic System for Functional Electrical Stimulation Controlled by Event-Driven sEMG». In: *Sensors* 20.5 (2020). ISSN: 1424-8220. DOI: 10.3390/s20051535. URL: https://www.mdpi.com/1424-8220/20/5/1535 (cit. on pp. 14, 23–25, 27, 33).

[8] Sofia Milanese. «MEMS Microphones for Muscle Fatigue Monitoring: a Tool for Spinal Cord Injury Rehabilitation.» 2017-2018 (cit. on p. 16).

[9] Jerome Bickenbach, Alana Officer, Tom Shakespeare, Per von Groote, World Health Organization, and The International Spinal Cord Society. *International perspectives on spinal cord injury / edited by Jerome Bickenbach ... [et al].* World Health Organization, 2013, xiii, 231 p. (Cit. on pp. 19, 20).

[10] Popovic M.R. Masani K. *Functional Electrical Stimulation in Rehabilitation and Neurorehabilitation.* Springer, Berlin, Heidelberg, 2011, pp. 877–896. DOI: 10.1007/978-3-540-74658-4_44 (cit. on pp. 21, 24).

[11] Cesar Marquez-Chin and Milos R. Popovic. «Functional electrical stimulation therapy for restoration of motor function after spinal cord injury and stroke: a review». In: *BioMedical Engineering OnLine* 19 (2020) (cit. on pp. 22, 23).

[12] Li-Wei Chou, Samuel C. Lee, Therese E. Johnston, and Stuart A. Binder-Macleod. «The Effectiveness of Progressively Increasing Stimulation Frequency and Intensity to Maintain Paralyzed Muscle Force During Repetitive Activation in Persons With Spinal Cord Injury». In: *Archives of Physical Medicine and Rehabilitation* 89.5 (2008), pp. 856–864. ISSN: 0003-9993. DOI: https://doi.org/10.1016/j.apmr.2007.10.027. URL: https://www.sciencedirect.com/science/article/pii/S0003999308001111 (cit. on p. 24).

[13] M. Ilic, D. Vasiljevic, and D.B. Popovic. «A programmable electronic stimulator for FES systems». In: *IEEE Transactions on Rehabilitation Engineering* 2.4 (1994), pp. 234–239. DOI: 10.1109/86.340875 (cit. on pp. 29–32).

[14] Bruce B. Winter and John G. Webster. «Driven-right-leg circuit design». In: *IEEE Transactions on Biomedical Engineering* BME-30.1 (1983), pp. 62–66. DOI: 10.1109/TBME.1983.325168 (cit. on pp. 34, 35, 37).

[15] URL: https://en.wikipedia.org/wiki/Driven_right_leg_circuit (cit. on p. 35).

[16] E.M. Spinelli, N.H. Martinez, and M.A. Mayosky. «A transconductance driven-right-leg circuit». In: *IEEE Transactions on Biomedical Engineering* 46.12 (1999), pp. 1466–1470. DOI: 10.1109/10.804574 (cit. on pp. 35, 37).

[17] Enrique M Spinelli, Nolberto H Martinez, and Miguel Angel Mayosky. «A single supply biopotential amplifier». In: *Medical Engineering Physics* 23.3 (2001), pp. 235–238. ISSN: 1350-4533. DOI: https://doi.org/10.1016/S1350-4533(01)00040-6. URL: https://www.sciencedirect.com/science/article/pii/S1350453301000406 (cit. on pp. 37, 38).

[18] Yurong Li, Jun Chen, and Yuan Yang. «A Method for Suppressing Electrical Stimulation Artifacts from Electromyography». In: *International Journal of Neural Systems* 29.06 (2019). PMID: 30646793, p. 1850054. DOI: `10.1142/S0129065718500545`. eprint: `https://doi.org/10.1142/S0129065718500545`. URL: `https://doi.org/10.1142/S0129065718500545` (cit. on pp. 46, 48, 49, 52).

[19] Dario Farina, Andrea Blanchietti, Marco Pozzo, and Roberto Merletti. «M-wave properties during progressive motor unit activation by transcutaneous stimulation». In: *Journal of Applied Physiology* 97.2 (2004). PMID: 15121744, pp. 545–555. DOI: `10.1152/japplphysiol.00064.2004`. eprint: `https://doi.org/10.1152/japplphysiol.00064.2004`. URL: `https://doi.org/10.1152/japplphysiol.00064.2004` (cit. on p. 47).

[20] Zheng-Yang Bi, Chen-Xi Xie, Yu-Xuan Zhou, Hai-Peng Wang, Xiao-Ying Lü, and Zhi-Gong Wang. «An Anti Stimulation Artifacts and M-waves Surface Electromyography Detector with a Short Blanking Time[*]». In: *2020 42nd Annual International Conference of the IEEE Engineering in Medicine Biology Society (EMBC)*. 2020, pp. 4126–4129. DOI: `10.1109/EMBC44109.2020.9176373` (cit. on pp. 49, 50, 56, 62).

[21] Andrea Crema. «Progettazione e sviluppo di un sistema per la rilevazione del segnale elettromiografico volontario e indotto dalla stimolazione elettrica per la valtazione dell’affaticamento muscolare». 2005-2006 (cit. on pp. 49–51).

[22] R. Thorsen. «An artefact suppressing fast-recovery myoelectric amplifier». In: *IEEE Transactions on Biomedical Engineering* 46.6 (1999), pp. 764–766. DOI: `10.1109/10.764955` (cit. on p. 50).

[23] Thierry Keller and Milos Popovic. «REAL-TIME STIMULATION ARTIFACT REMOVAL IN EMG SIGNALS FOR NEUROPROSTHESIS CONTROL APPLICATIONS». In: (Jan. 2001) (cit. on p. 52).